The effect of push-pull rod on the dynamic behavior of movable bridges

Georgios Tzanidakis

Delft University of Technology

TU Delft Delft University of Technology

Rijkswaterstaat
Ministerie van Infrastructuur en Milieu

Challenge the future

The effect of push-pull rod on the dynamic behavior of movable bridges

by

Georgios Tzanidakis

in partial fulfillment of the requirement for the degree of

Master of Science

in Civil Engineering

at Delft University of Technology

to be defended publicly on the 7th of May 2018

Thesis Committee:	Prof. dr. A.V. Metrikine,	TU Delft
	Dr. Ir. A. Tsouvalas,	TU Delft
	Ir. K. Sektani,	TU Delft
	Ing. J. den Toom,	Rijkswaterstaat

An electronic version of this thesis is available at http://repository.tudelft.nl/

TU Delft

Rijkswaterstaat
Ministerie van Infrastructuur en Milieu

Preface

This master's thesis contains the research regarding the effect of the push-pull rod on the decisive dynamic loads generating at the machinery part of a movable bridge during motion. It has been devised for the fulfillment of the master's degree in Structural Engineering at Delft University of Technology. This project was carried out at the Dutch Ministry of Infrastructure and the Environment (Rijkswaterstaat), section Bridges and Viaducts (afd. Bruggen and Viaducten), where I undertook an internship. For the completion of this study I was supported from people I would like to thank.

To start with, I would like to express my sincere gratitude to Ir. K. Sektani, Ing. J. den Toom, and Dr. Ir. A. Tsouvalas who have entrusted me with this research project. I thank Ir. K. Sektani, my daily supervisor from TU Delft, for his guidance throughout this period along with the time that he spent in our weekly meetings. I am also grateful to Ing. J. den Toom, my supervisor at Rijkswaterstaat, for sharing his experience as well as the available technical documents from the archives of the Ministry, concerning this topic. At this point I would like to mention that it was an honor to have my first working experience in the Netherlands at Rijkswaterstaat, were I was provided with all the necessary facilities to work for this project. A special thanks to all the colleagues of the section Bridges and Viaducts for their exemplary behavior and support. Moreover, I would like to thank Dr. Ir. A. Tsouvalas for his commenting and advising as far as the dynamics of the topic are concerned. Furthermore, I am thankful to Prof. dr. A. V. Metrikine for his critical feedback and comments he provided me in our meetings.

Additionally, I would like to express my deep gratitude to Mr. Robert Baay of the Dutch company De Gidts & Feldman BV (exclusive distributor of the German manufacturer of the disc springs Christian Bauer GmbH) for his quick response and willingness for providing me with technical knowledge regarding the behavior of the disc springs.

I could never forget to thank all my friends who assisted, supported and sometime tolerated me.

Last but not least, I would like to thank my family for their encouragement, sustained support, trust and understanding through all these years of my studies

Georgios Tzanidakis

Delft, May 2018

Abstract

In the Netherlands the design of a movable bridge and machinery part is based on the design standard NEN 6786:2001 (2001). When the bridge is in motion the calculations for the machinery part focus on the dynamic loads (torque) generating at the motor shaft. The calculation of these loads is carried out using tabulated formulas of the standard, which have been derived via a 2-DoF linear dynamic model. In this model the linear spring represents the total stiffness of the machinery part. For the calculation of the spring stiffness the push-pull rod component is excluded, assuming it as a rigid component of the system during the movement cycle of the bridge. The push-pull rod (also known as the buffer) is a component of the machinery of several bascule bridges that connects the leaf of the bridge with the drive mechanism. It consists of stacked disc springs and its stiffness varies based on the load acting on it.

The main objectives of this thesis are to model the force deformation behavior of the buffer component, incorporate it in an update set of equations of motion of the bridge-machinery system, and study its effect on the decisive dynamic loads generated at the motor shaft during motion. First, the generalized force deformation diagram of the buffer is formulated with a piecewise function that is based on the force-deflection function for a stack of disc springs according to the standard DIN 2092:2006:03 (2006). Second, the damping of the buffer is modeled as Coulomb friction type, since friction is generated in various position in the stack of disc springs and is the main source of energy dissipation of the buffer component. The validity of the proposed modeling of the buffer component is evaluated via a SDoF model of it, performing a series of dynamic analyses and interpreting the results. Afterwards, the model of the buffer component is introduced in a new set of equations of motion for the bridge-machinery system, derived with the Lagrangian formalism technique. The resulting highly nonlinear set of equations of motion is implemented in the bascule bridge of the new Ramspol bridge located on N50. The analyses aim to the calculation of the torque generated at the motor shaft during an emergency stop at full speed. This loading case is the most decisive with respect to loads generating at the motor shaft.

The resulted maximum torque from the dynamic analyses is compared with the torque calculated with the formulas of the standard NEN 6786:2001 (2001). The state of the buffer determines by which formula of the standard the comparison is carried out. A series of dynamic analyses is performed varying, the type of brake (constant or bilinear), the time the brake is applied, the duration of the emergency stop and the friction coefficient of the buffer. In case the buffer is not fully compressed, the calculations with the dynamic model result in lower maximum torque compared with the one according to the standard. In case the buffer is fully compressed the magnitude of the resulting maximum torque depends on the aforementioned variables, whilst the one calculated with the standard is independent of them. In general, the resulting maximum torque derived from the dynamic model decreases with the increase of the friction coefficient of the buffer and the bilinear modeling of the braking.

Contents

Preface i
Abstract iii
Contents v
1. Introduction 1
1.1. Background 1
1.2. The Research Problem 3
1.3. Scope 5
1.4. Research Objectives 5
1.5. Research Questions 6
1.6. Thesis Outline 7
2. Existing standard and design rules 9
2.1. Introduction 9
2.2. Existing Standard 9
2.3. Background of the standard 11
2.3.1. External loads 12
2.3.2. Undamped system 13
2.3.3. Damped system 17
2.4. Sensitivity analysis regarding the number of DoF taken into account 26
2.4.1. 2-DoF model versus SDoF model 28
2.4.2. 3-DoF & 4-DoF model versus 2-DoF model 31
3. Behavior of the buffer 37
3.1. Introduction 37
3.2. State of the art in disc springs 37
3.3. Individual disc springs 39
3.4. Stacks of disc springs 42
3.4.1. Disc springs in series 42
3.4.2. Disc Springs in parallel 43
3.4.3. Disc springs in parallel and in series 44
3.5. Buffer-force function 45
3.6. Example of formula application 48

3.7. Hysteresis in disc springs 49
4. Buffer force evaluation 53
4.1. Introduction 53
4.2. Dynamic analysis 54
4.2.1. Influence of the amplitude of the external force 57
4.2.2. Influence of friction 58
4.2.3. Influence of mass 59
4.2.4. Influence of the excitation frequency 62
5. Dynamic model of the bridge-machinery system 65
5.1. Introduction 65
5.2. New lumped mass model 65
5.2.1. Energy of the system 66
5.2.2. Geometry between the bridge and the Panama wheel 67
5.2.3. Generalized forces acting on the system 68
5.2.4. Equations of motion 71
6. Application and results 73
6.1. Introduction 73
6.2. Inputs for the analyses 73
6.3. External loads and sign conventions 77
6.4. Stages of the analysis 79
6.5. Preliminary analysis 80
6.6. Updated dynamic model of the bridge-machinery system 82
6.7. Results and comparison with existing standard 88
7. Conclusions and recommendations 97
7.1. Conclusions 97
7.2. Recommendations 98
8. Bibliography 101

1. Introduction

1.1. Background

Bridges can be constructed, either fixed or movable, depending on the circumstances and specifications of the area where they are designed (Brolsma & Roelse, 2011). In situations where the required clearance with respect to the waterway passage cannot be achieved with a fixed bridge, a movable bridge can be used instead (Brolsma & Roelse, 2011). For instance, in conditions where both short span and high clearance are required, a fixed bridge would need very high piers and steep grades. This, in turn would result in an expensive design and could also cause serviceability struggles regarding the passage of heavy vehicles over the steep grades (Koglin, 2003). Given this case, a movable bridge may be the least costly and the most practical alternative, providing crossing of a (navigable) waterway (Koglin, 2003).

The first instances of movable bridges can be found in Egypt back in the fourteenth century B.C. (Koglin, 2003). Several other applications of movable bridges are reported back to the fifth century B.C. (Koglin, 2003). However, the outbreak of using movable bridges takes place in the Middle Ages, where “drawbridges” are commonly used as a protective conformation over the moats of medieval castles (Koglin, 2003). A variety of movable bridges and associated bridge mechanisms have been designed and constructed over the last century (Coelman, 1992). The type of bridge that is most widely used in the main road network of the Netherlands by Rijkswaterstaat, is the bascule bridge. This can be explained by the fact that the bascule bridge opens quickly, provides unlimited clearance while open and requires less energy during operation (Koglin, 2003). The word bascule means seesaw in French. The design of the bascule bridge is based on the drawbridge. The deck of the bridge is balanced with a counterweight, so that its center of gravity is near the axis of rotation. The deck balancing is frequently not precise resulting in a residual overweight moment around the pivot of the bridge. In the majority of the applications the bascule bridge rotates around a fixed trunnion and consists of a deck with a counterweight integrated at the rear portion of the main beams, located in the basement of the structure (Figure 1.1). This type of bridge according to Rijkswaterstaat projects, works often with a straight rack or with a Panama wheel operating system (Figure 1.2). The latter is named after the Panama Canal, where it was first used as part of the locks. In this system, an electric motor drives a pinion, geared to the Panama wheel, at a constant speed, via a gearbox (Figure 1.2).(Coelman, 1992)

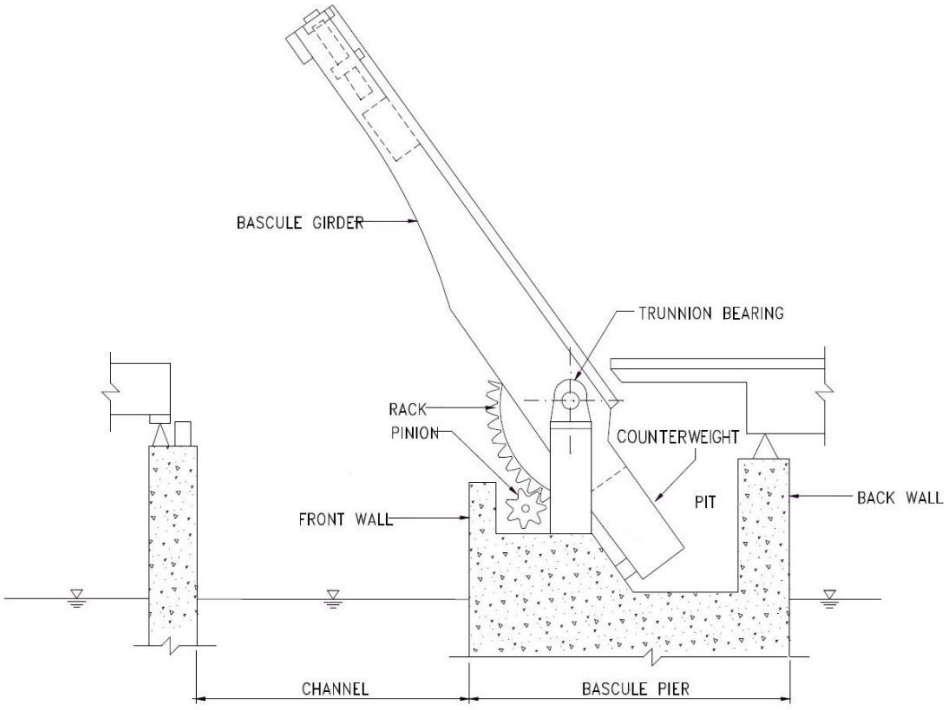

Figure 1.1: Side view of single leaf bascule bridge with fixed trunnion (Wisconsin Department of Transportation, 2017)

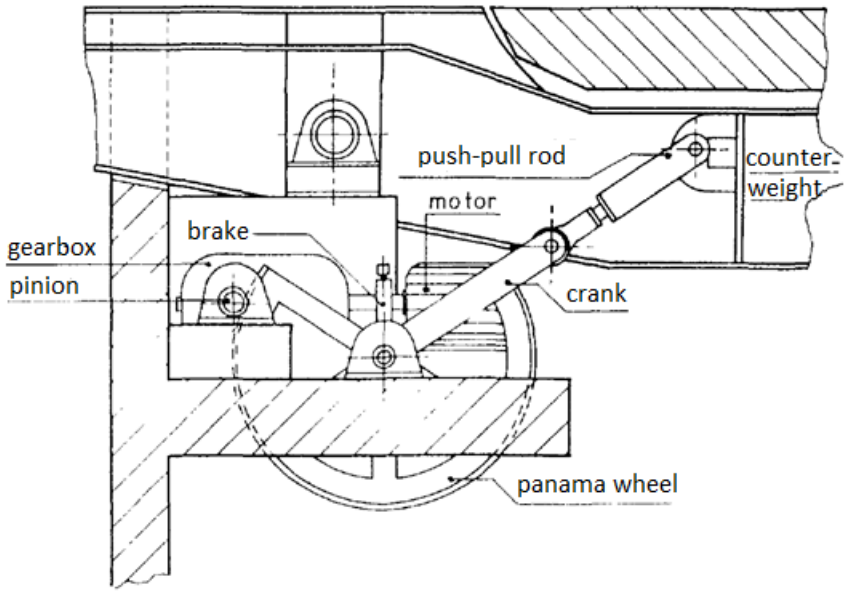

Figure 1.2: Panama wheel drive mechanism of a bascule bridge, side view (Coelman, 1992) (modified)

In all Panama wheel operating mechanisms, a key component is the so-called push-pull rod also known as buffer. This is placed between the bridge deck and the Panama wheel and is hinged at both ends provided that it takes only axial forces (Figure 1.2).

The buffer serves multiple functions. To start with, when it is in closed position it guarantees that the bridge deck is secured, preventing flapping due to the passage of traffic or suction due to wind forces (NEN 6786:2001 (2001), p134). Moreover, it accommodates any imposed deformation by temperature or trucks that can influence the machinery (NEN 6786:2001 (2001)). On the contrary, high dynamic loads can occur at the machinery of a movable bridge with a buffer component, during motion of the system and depending on the loading case; for instance, during an emergency stop. (NEN 6786:2001 (2001), p.134).

In the Netherlands, the design of a movable bridge and machinery part is based on the design standard NEN 6786:2001 (2001). When the bridge is in motion the calculations for the machinery part focus on the loads (torque) acting at the motor shaft. This shaft connects the motor with the gearbox and it is on this position that the brake of the system is also applied (Figure 1.2). For the sake of simplicity and ease of calculations, the design standard contains tabulated formulas to calculate the decisive loads in different loading cases of motion. These formulas are derived from dynamic analyses carried out on a linear dynamic model that describes the rotational motion of the system (Figure 1.3).

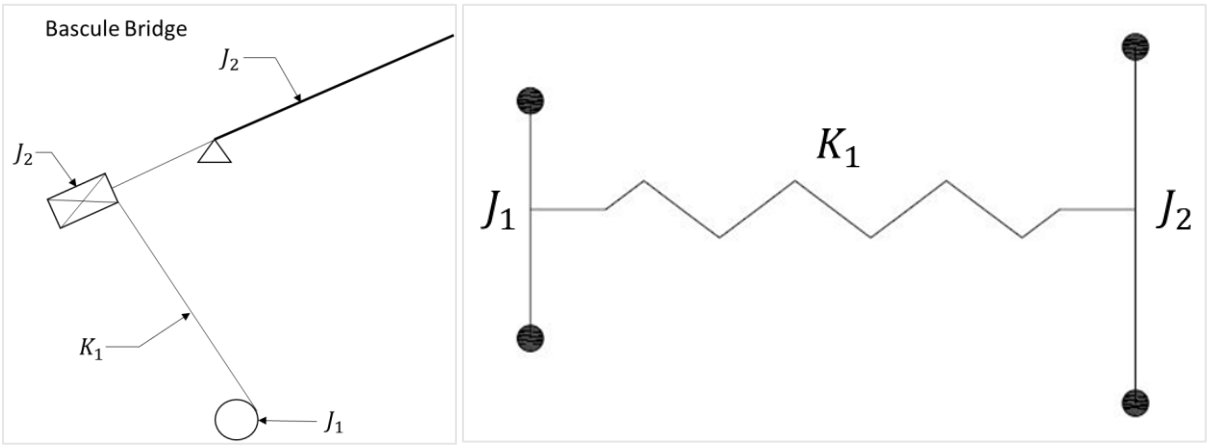

Figure 1.3: Proposed dynamic model according to the standard NEN 6786:2001 (2001)

The proposed dynamic model according to the existing standard NEN 6786:2001 (2001) consists of two degrees of freedom, one represents the motor (J_1) and the other the bridge (J_2). The two degrees of freedom are interconnected with a torsional spring which represents the total stiffness of the machinery (K_1).

1.2. The Research Problem

In the current design standard NEN 6786:2001 (2001) the buffer is assumed as a rigid component of the system. Hence, the stiffness of the buffer is not taken into account in the total stiffness of the machinery (K_1) in the proposed dynamic model (Figure 1.3).

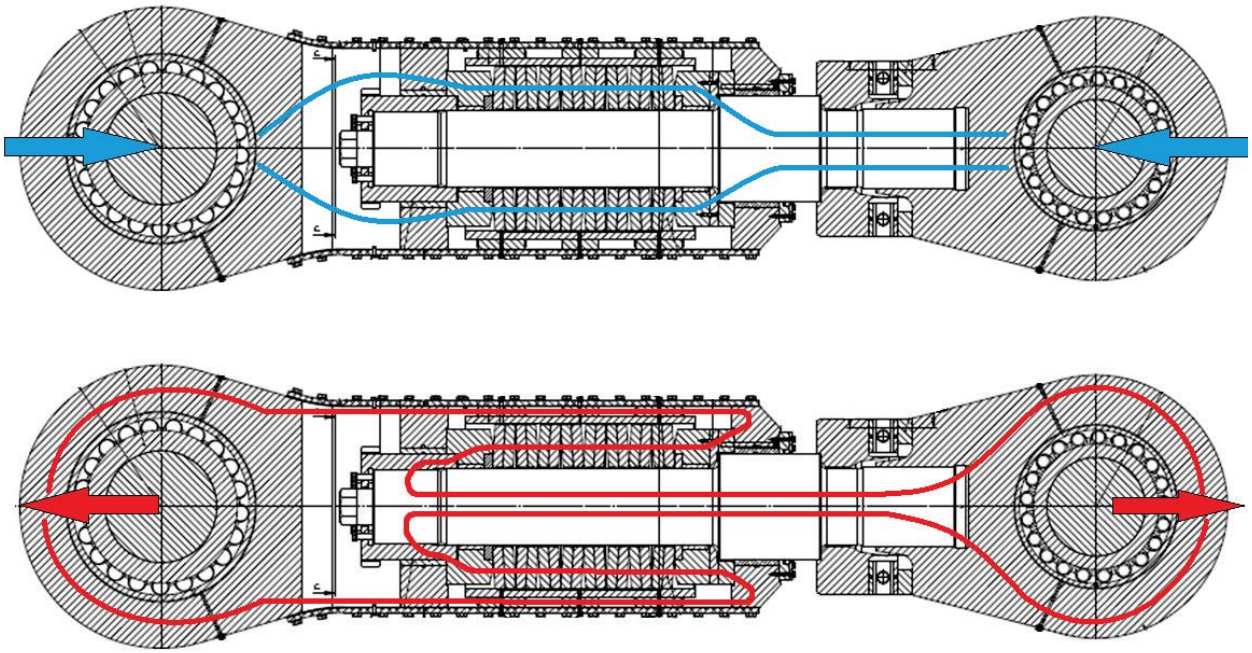

Figure 1.4: Push-pull rod cross section and force flow for external force equal to prestress: Rod in compression (top), Rod in tension (bottom) (Van Zantvliet, 2015)

The buffer contains double acting disc springs that allow elongation or shortening, depending on its axial force. According to the buffer's design, the disc springs always work in compression, regardless the loading state of the buffer; whether in tension or compression (Figure 1.4). The force deformation behavior of the buffer is shown in Figure 1.5.

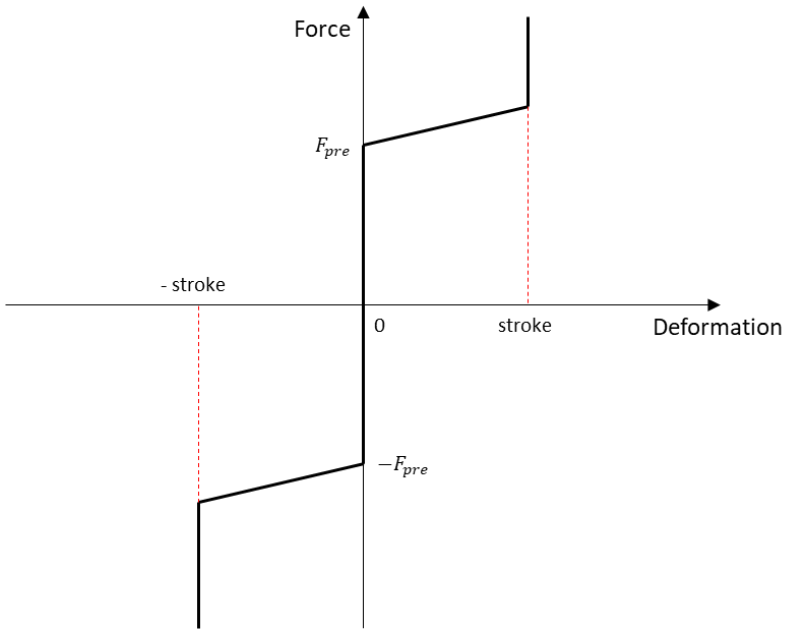

Figure 1.5: Force deformation behavior of the push-pull rod

Up to a certain loading level the buffer is rigid. This is achieved by pre-compressing (prestressing) the stack of disc springs. Therefore, the stack does not deform until the loading of the buffer reaches the force associated to its prestressing (F_{pre}). Once the buffer is loaded above this threshold, the disc springs become active and the buffer can elongate or compress. The design of the buffer limits its deformation, with introduced stop in the arrangement of the stack of disc springs. The maximum deformation that the buffer can undergo is called the stroke of the buffer. The buffer behaves rigid again after reaching the stroke.

Unlike the assumption in the standard NEN 6786:2001 (2001) the behavior of the buffer is not always rigid, it depends on the acting load (Figure 1.5). The load acting on the buffer varies during motion of the bridge.

The exclusion of the buffer from the proposed dynamic model (Figure 1.3) poses the question whether the formulas in the standard are conservative or not. Thus, it is desired to include the buffer in a dynamic model of the movable bridge and perform dynamic analyses to examine its influence on the decisive dynamic loads generated at the machinery part of the system during motion.

1.3. Scope

The scope of this thesis mainly focuses on carrying out analyses in a dynamic model of a movable bridge, while including the buffer in the equations of motion. The dynamic analyses are restricted to bascule bridges with Panama wheel drive. The analyses aim at the calculation of the decisive dynamic loads generated at the machinery part of the system during motion, meaning the torque generated at the motor shaft. The loading case considered for the analyses is an emergency stop at full speed, since this is the most decisive loading case with respect to the torque generated at the motor shaft. The resulting torque based on the dynamic analyses, is compared to the torque calculated with the corresponding formulas of the standard NEN 6786:2001 (2001). Since the focus of this study is in the operating mechanism of the system, the enhancement of the bridge modeling is out of the research objectives of this thesis.

1.4. Research Objectives

This thesis aims to integrate the buffer in a dynamic model of the system and study its influence on the decisive dynamic loads that occur on the bridge's machinery during motion. The five main objectives of this thesis are listed below:

- Formulate the force deformation behavior of the buffer;
- Explore the hysteresis of the buffer force due to friction;
- Incorporate the model of the buffer into the equations of motion of the bridge;
- Calculate the determining dynamic loads at the machinery of the system during motion;
- Compare the calculated loads resulted from the dynamic model with the loads calculated according to the existing standards.

1.5. Research Questions

In respect to the above objectives, the main research question of this thesis is:

How to model the dynamic behavior of a movable bridge driven by a mechanism including push-pull rod, in order to predict the decisive dynamic loads generated at the machinery part during motion?

In order to pursue this question, a set of sub-questions has also been put forth. The answer to each sub-question will be a step towards the answer of the main one.

Sub-questions

1. How do the number of degrees of freedom influence the system movable bridge-machinery in terms of the decisive dynamic loads that occur at the machinery of the system during motion?

The system movable bridge – machinery consists of a number of components which add stiffness, inertia and damping to the system. In the proposed dynamic model of the standard NEN 6786:2001 (2001) (recently replaced by NEN 6786:2017 with design formulas remaining largely the same) only the inertias of the motor and the bridge are considered as degrees of freedom. Regarding the machinery components, it is only their torsional stiffness that is taken into account. The answer to this question will allow to understand whether the proposed linear dynamic model (Figure 1.3) is a valid approximation of the system or not. Moreover, the increase in the degrees of freedom within the dynamic model will, in turn, help explain the influence of the additional inertia term to the decisive dynamic loads generated at the machinery of the system during motion.

2. What are the equations of motion related to the system of bascule bridge with Panama wheel drive?

This sub-question gives birth to the following questions:

- How can the force deformation behavior of a buffer be formulated?
- How can the hysteretic behavior of the buffer be formulated?

To answer this set of questions, it is essential to carry out an assessment of the behavior of the disc springs which are the main components that influence the behavior of the buffer. This is crucial, since the outcome will serve as the input in the new equations of motion.

- How can the model concerning buffer's behavior be incorporated in the equations of motion?

Answering this will allow to answer the second sub-question.

3. What is the response of the new set of equations of motion in terms of decisive dynamic loads generated at the machinery of the system, in comparison with the design rules of the existing standard NEN 6786:2001 (2001)?

The new derived equations of motion are examined in an existing bridge and a series of analyses is performed to estimate the decisive dynamic loads of the system that occur at the motor shaft. The resulting maximum torque is compared with the torque calculated according to the existing standard NEN 6786:2001 (2001).

1.6. Thesis Outline

In order to answer the above research questions and fulfill the objectives of this thesis, a research strategy is drawn as illustrated in Figure 1.6. In the first place, the existing standard is reviewed in regard to the design guidelines for the dynamic analysis of the structure under consideration (see Ch. 2). To get a better insight into the assumptions on which the design formulas of the existing standard are based, it is decided to reproduce them, performing dynamic analyses on the proposed linear dynamic model (Figure 1.3). Furthermore, the influence of the number of degrees of freedom of the dynamic model in the resulting torque at the motor shaft during motion is examined.

The subsequent chapter has two main purposes; to review the existing literature on the behavior of the disc springs and to model the performance of the buffer. The manufacturer of the disc springs has kindly provided information about technical specifications of the springs under research.

The outcome of chapter 3 is evaluated performing dynamic analyses in a single degree of freedom system. The purpose of these analyses is to check the accuracy of the proposed modeling concerning the performance of the buffer.

Finally, the model of the buffer's behavior is incorporated in the dynamic model of the system, deriving a new set of equations of motion (see Ch. 5). These are implemented on the moving part of Ramspol bridge located on N50 with the sole purpose of calculating the dynamic loads at the motor shaft during motion and compare them with the loads calculated according to the formulas of the existing standards (see Ch. 6). The concluding remarks are presented in chapter 7.

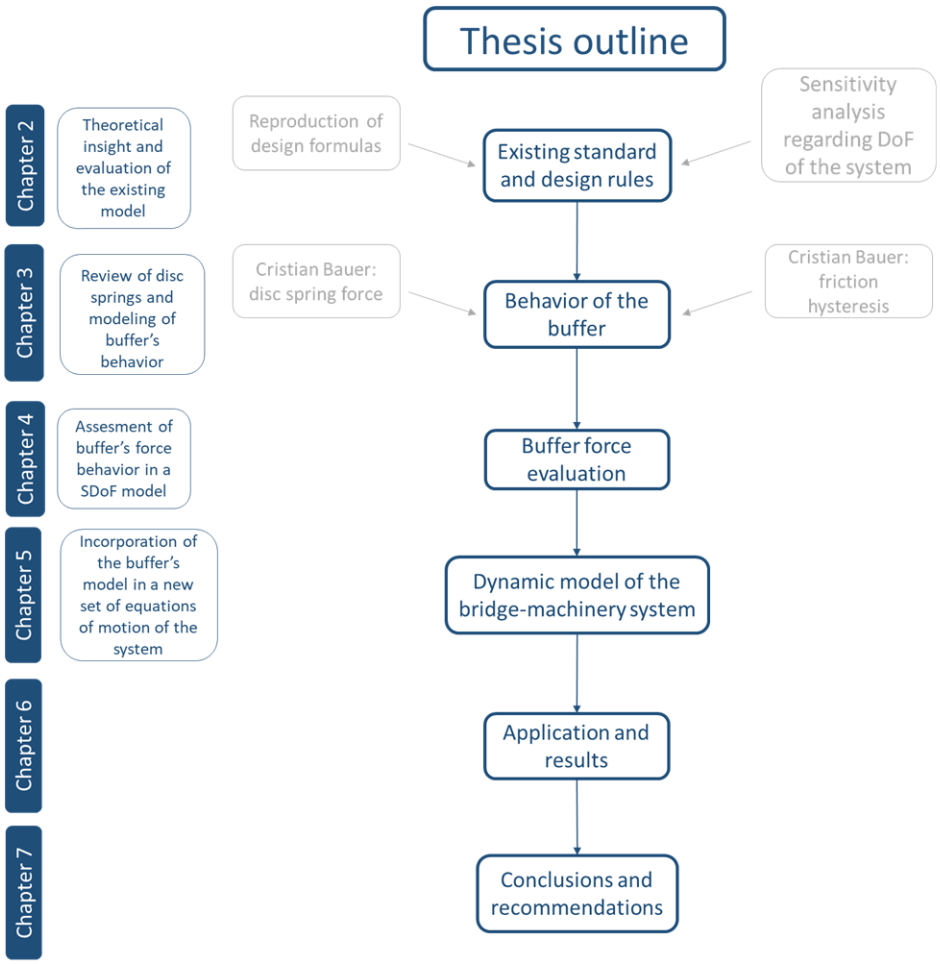

Figure 1.6: Layout of the report

2. Existing standard and design rules

2.1. Introduction

This chapter summarizes the knowledge and information collected during the first months of this thesis. First, the current analysis according to the existing standard is introduced. Afterwards, the design formulas associated with the loading cases of interest of this thesis are reproduced. In the end of this chapter, a sensitivity analysis is performed in the dynamic model increasing the degrees of freedom taken into account, observing their influence on the torque generated at the motor shaft.

2.2. Existing Standard

In the Netherlands, the design of a movable bridge is based on the Dutch standard NEN 6786 "Voorschriften voor het ontwerpen van beweegbare bruggen (Vobb)" which contains the rules for the design of movable bridges. The calculations of the design loads for both the steel structure and the mechanical equipment are distinguished in the following operating states:

- Bridge closed
- Bridge open
- During the movement cycle
- Outside the movement cycle

The relationship between the four different operating states is indicated in the matrix bellow.

Table 2.1: Relationship between the four different operating states of a movable bridge

	During the movement cycle	Outside the movement cycle
Bridge closed	-	x
Bridge open	x	x

During the movement cycle the design loads on the mechanical equipment are spited into two main categories:

- Normal operation
- Emergency operation

The emergency operation refers to driving of the bridge different than during the normal operation. Every movable bridge must be equipped with emergency operation mechanism. The emergency operation mechanism can make use of bridge's machinery parts of the normal one. The calculations in the case of emergency operation are determined in accordance with the case of normal operations. The duration of

movement in emergency operation may be considerably greater than the duration of movement in normal operation.

The calculations for the design loads on the mechanical equipment in a moving cycle are categorized depending on the type of the drive mechanism, namely:

- Electromechanical drive
- Electrohydraulic drive
- With hand driven

The design loads on the mechanical equipment of a bascule bridge with Panama wheel drive belong to the category “Electromechanical drive” with the associated formulas collected in Table 11 of the standard NEN 6786:2001 (2001).

The design formulas related to the research of this thesis are quoted below:

Table 2.2: Design formulas applicable for the loading case of emergency stop

Application of brake	$\varphi_a \cdot \varepsilon \cdot M_{br;d} + \lvert 1 - \varphi_a \cdot \varepsilon \rvert \cdot M_{s;d}$	(2.1)
Recoil after brake	$M_{s;d} + \varphi_{br} \cdot \varepsilon \cdot (M_{s;d} + M_{br;d})$	(2.2)
Spring buffer fully compressed	$M_{s;d} + 0{,}4 \cdot 0{,}9 \cdot \gamma_0 \cdot \sqrt{\omega^2 \cdot \mathrm{K}_1 \cdot J_2}$	(2.3)

where:

$M_{s;d}$ is the design torque due to the external loading, reduced at the motor shaft;

φ_a is the dynamic magnification factor in the case “Application of brake” and is equal to 1,9;

φ_{br} is the dynamic magnification factor in the case “Recoil after brake” and is equal to 1,5;

ε is the mass factor and is equal to: $\varepsilon = \frac{J_2}{J_1 + J_2}$;

J_1 and J_2 are the mass moment of inertias of the motor and the bridge respectively, reduced at the motor shaft;

$M_{br;d}$ is the braking torque and is equal to: $M_{br;d} = M_{s;d} + M_{a;d}$;

$M_{a;d}$ is the torque generated by the brake and is equal to: $M_{a;d} = \gamma_0 \cdot (J_1 + J_2/\eta) \cdot \frac{d\omega}{dt}$;

η is the efficiency factor for internal losses of the transmission and is equal to 1 in the two aforementioned cases;

$\frac{d\omega}{dt}$ is the deceleration caused by the application of the brake;

K_1 is the torsional stiffness of the machinery reduced at the motor shaft. The stiffness of the spring buffer should not be included in the calculation of K_1;

γ_0 is a load magnification factor.

The situation “Application of brake” refers to the maximum torque acting at the motor shaft during braking of the bridge. The situation “Recoil after brake” refers to the maximum torque at the motor shaft when the speed of the bridge is zero for the first time after application of the brake, while the wind direction stays the same.

Formula (2.3) of situation “Spring buffer fully compressed” is stated in the code that it is a rule of thumb (NEN 6786:2001, p, 134). The origin of the factor 0,4 in this formula is not known. It is one of the main tasks of this research to compare the results of this formula with the results of analyses performed in a dynamic model including the buffer, and evaluate the use of this factor (0,4) whether it is conservative or not.

With a first review of the code, it is not clear what the damping ratio is, which is taken into account for the derivation of the tabulated formulas.

To get a better insight of the dynamic model of this system and understand the background of the tabulated formulas, it is decided to reproduce formulas (2.1) and (2.2). The derivation of formula (2.1) is also applicable to the formula for acceleration/deceleration, since from dynamic point of view the braking of the system is a deceleration in a relatively short time.

2.3. Background of the standard

In the standard it is stated that, the rotational motion of the system bridge-machinery during the movement cycle is described with a linear 2-DoF dynamic model. That model as illustrated in the code is shown in the first chapter (Figure 1.3). In Figure 2.1 the same dynamic model is illustrated again in a more apparent schematization. All stiffnesses, mass moment of inertias and loads must be reduced to the motor shaft using the associated transmission factors, since the analysis is performed at that level.

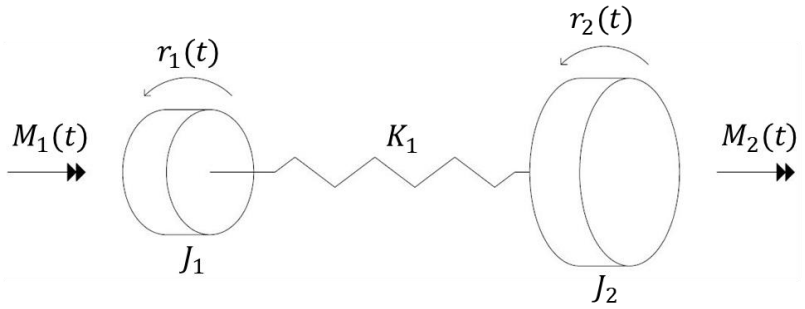

Figure 2.1: 2-DoF linear rotational model for the movable bridge-machinery system, defined in the standard NEN 6786:2001 (2001)

Transmissions in mechanical systems (gearboxes, gear trains) provide speed and torque conversions from the driving source (motor) to the driven body (i.e. the movable bridge in the system under consideration). The transmissions convert the high engine speed and low engine torque, into low driving speed and high driving torque and vice versa. Therefore, large bodies can be driven by relatively small driving sources.

The equations of motion related to the system of Figure 2.1 are:

$$\begin{pmatrix} J_1 & 0 \\ 0 & J_2 \end{pmatrix} \cdot \begin{pmatrix} \ddot{r}_1(t) \\ \ddot{r}_2(t) \end{pmatrix} + \begin{pmatrix} K_1 & -K_1 \\ -K_1 & K_1 \end{pmatrix} \cdot \begin{pmatrix} r_1(t) \\ r_2(t) \end{pmatrix} = \begin{pmatrix} M_1(t) \\ M_2(t) \end{pmatrix} \quad (2.4)$$

in which:

$r_1(t)$ and $r_2(t)$ are the rotational degrees of freedom of the motor and the bridge respectively;

$M_1(t)$ and $M_2(t)$ are the external torques acting on the motor and the bridge respectively;

K_1 is total stiffness of the machinery reduced at the motor shaft. In the code it is denoted as C_1. However, in this report it is given the letter K to distinguish from the terms of the damping.

The system of Figure 2.1 is updated with the addition of viscous damping resulting to the updated set of equations of motion:

$$\begin{pmatrix} J_1 & 0 \\ 0 & J_2 \end{pmatrix} \cdot \begin{pmatrix} \ddot{r}_1(t) \\ \ddot{r}_2(t) \end{pmatrix} + \begin{pmatrix} C_d & -C_d \\ -C_d & C_d \end{pmatrix} \cdot \begin{pmatrix} \dot{r}_1(t) \\ \dot{r}_2(t) \end{pmatrix} + \begin{pmatrix} K_1 & -K_1 \\ -K_1 & K_1 \end{pmatrix} \cdot \begin{pmatrix} r_1(t) \\ r_2(t) \end{pmatrix} = \begin{pmatrix} M_1(t) \\ M_2(t) \end{pmatrix} \quad (2.5)$$

in which:

C_d is the viscous damping of the machinery;

$\dot{r}_1(t)$ and $\dot{r}_2(t)$ are the angular velocities of the motor and the bridge respectively.

First, a dynamic analysis is performed in the undamped case (2.4) and then in the damped system (2.5). It must be mentioned at this stage that all the calculations in the upcoming analyses will be performed without the use of any load magnification factors. The purpose of this thesis is intended to examine the validity of the primary formulas of the code and the associated proposed dynamic model. The load magnification factors are the outcome of statistical analysis regarding the probability of occurrence in two loading scenarios and also to account for the distribution of the loading. These are additional factors based on probabilistic analysis which is out of the scope of this thesis.

2.3.1. External loads

One of the important inputs of the upcoming analysis is the external loading of the system before, during and after an emergency stop. The proposed linear dynamic model of the standard NEN 6786:2001 (2001) is a statically indetermined one, since it is not attached to a boundary. This implies that the application of

a load at one of the degrees of freedom will give motion to the system that will not damped out when the load is removed. The system will perform a rigid body rotation. However, not all the loads acting on the system put it into motion. For instance, the loads action on the bridge side. Therefore, the external loads on the side of the bridge, have to be balanced with loads of the same magnitude and opposite direction on the motor side during the whole motion.

The analysis is focused to the loading case of an emergency stop. Before applying the brake, the system is rotating with a constant speed, namely the nominal rotational velocity of the motor. Both degrees of freedom have the same constant velocity before the brake is applied. At this stage the external load acting on the motor has the same magnitude as the load acting on the bridge with a different sign. Afterwards, when the brake is applied the load acting on the motor is equal to M_{br}. Furthermore, when the system is halt, the external load acting on the motor has again the same magnitude as the external load on the bridge with a different sign. To make it clear the described set of loading is depicted in formulas (2.6) and (2.7).

$$\begin{pmatrix} M_1(t) \\ M_2(t) \end{pmatrix} \tag{2.6}$$

in which:

$M_2(t)$ is the external torque acting on the bridge, reduced at the motor shaft;

$M_1(t)$ is the external torque acting on the motor described by the piecewise function:

$$M_1(t) = \begin{Bmatrix} -M_2(t), & t < t_1 \\ M_{br}, & t_1 \leq t \leq t_2 \\ -M_2(t), & t > t_2 \end{Bmatrix} \tag{2.7}$$

in which:

t_1 is the time when the brake is applied;

t_2 is the time when the bridge stops.

In the upcoming analyses the external torque $M_2(t)$ is referred simply as M_2 for the shake of simplicity in the formulas.

2.3.2. Undamped system

The equations of motion and the associated initial conditions of the undamped system are:

$$\begin{pmatrix} J_1 & 0 \\ 0 & J_2 \end{pmatrix} \cdot \begin{pmatrix} \ddot{r}_1(t) \\ \ddot{r}_2(t) \end{pmatrix} + \begin{pmatrix} K_1 & -K_1 \\ -K_1 & K_1 \end{pmatrix} \cdot \begin{pmatrix} r_1(t) \\ r_2(t) \end{pmatrix} = \begin{pmatrix} M_1(t) \\ M_2 \end{pmatrix} \tag{2.8}$$

with initial conditions:

$$r_1(0) = r_{1ini}\,, r_2(0) = r_{2ini} \tag{2.9}$$

$$\dot{r}_1(0) = \omega_{nom}\,, \dot{r}_2(0) = \omega_{nom} \tag{2.10}$$

The system is described by two coupled equations of motion. Hence, the solution of the set of equations (2.8-2.10) is obtained using the modal analysis technique. Modal analysis is a mathematical technique which makes use of the orthogonality property of the mode shapes in linear dynamics to decouple a coupled system of equations. With this technique one switches the system of coupled equations in the real domain, to uncoupled equations in the modal domain in the absence of damping. Afterwards, in the modal domain, each equation is solved separately, regarding the corresponding modal degree of freedom. Finally, the solution of the unknown degrees of freedom, in the real domain, is obtained by using the superposition of the modes of vibrations. This is achieved with the following formula:

$$\{r\} = [E] \cdot \{r^*\} \tag{2.11}$$

in which:

$\{r\}$ is the vector of the unknown degrees of freedom in the real domain, in this case:

$$\{r\} = \begin{pmatrix} r_1(t) \\ r_2(t) \end{pmatrix} \tag{2.12}$$

$[E]$ is the eigenvector matrix of the system under consideration;

$\{r^*\}$ is the vector of the degrees of freedom in the modal domain, and is equal to:

$$\{r^*\} = \begin{pmatrix} r_1^*(t) \\ r_2^*(t) \end{pmatrix} \tag{2.13}$$

The modal analysis is performed in the system and the torque on the torsional spring of the system is calculated using formula:

$$T(t) = K_1 \cdot (r_1(t) - r_2(t)) \tag{2.14}$$

The torque during the application of the brake is described with formula:

$$\begin{aligned} T(t) = \frac{J_2}{J_1 + J_2} \cdot M_{br} - \frac{J_1}{J_1 + J_2} \cdot M_2 - \frac{J_2}{J_1 + J_2} (M_{br} + M_2) \cdot \cos\big(\omega_n \cdot (t - t_1)\big) \\ + (M_2 + K_1 \cdot r_{1ini} - K_1 \cdot r_{2ini}) \cdot \cos(\omega_n \cdot t) \end{aligned} \tag{2.15}$$

which is valid in the timespan $t_1 < t \leq t_2$.

In formula (2.15) ω_n is the natural frequency of the system with value:

$$\omega_n = \frac{\sqrt{J_1 + J_2} \cdot \sqrt{K_1}}{\sqrt{J_1} \cdot \sqrt{J_2}} \tag{2.16}$$

The system has two natural frequencies because it is composed of two masses. However, the first natural frequency is zero and describes the rigid body rotation of the system since the two masses are not connected to a boundary. Thus, it is practical to mention the second natural frequency of the system just as the natural frequency of it.

The maximum torque at this phase of motion is:

$$T_{max} = \frac{J_2}{J_1 + J_2} \cdot M_{br} - \frac{J_1}{J_1 + J_2} \cdot M_2 + \frac{J_2}{J_1 + J_2}(M_{br} + M_2) + (M_2 + K_1 \cdot r_{1ini} - K_1 \cdot r_{2ini}) \cdot \cos(\omega_n \cdot t_{max}) \tag{2.17}$$

with

t_{max} the time of the maximum of equation (2.15) which is calculated by solving equation in terms of t:

$$\cos\big(\omega_n \cdot (t - t_1)\big) = -1 \tag{2.18}$$

The solution of equation (2.18) is:

$$t_{max} = t = \frac{\pi}{\omega_n} + t_1 \tag{2.19}$$

On the right-hand side of formula (2.17) the term $(\frac{J_2}{J_1+J_2} \cdot M_2)$ is added and subtracted.

$$T_{max} = \frac{J_2}{J_1 + J_2} \cdot M_{br} - \frac{J_1}{J_1 + J_2} \cdot M_2 + \frac{J_2}{J_1 + J_2} \cdot M_2 - \frac{J_2}{J_1 + J_2} \cdot M_2 + \frac{J_2}{J_1 + J_2}(M_{br} - M_2) + (M_2 + K_1 \cdot r_{1ini} - K_1 \cdot r_{2ini}) \cdot \cos(\omega_n \cdot t_{max}) \tag{2.20}$$

The summation of the terms $(-\frac{J_1}{J_1+J_2} \cdot M_2)$ and $(-\frac{J_2}{J_1+J_2} \cdot M_2)$ gives $(-M_2)$ which substituted in the equation (2.20) gives:

$$T_{max} = \frac{J_2}{J_1 + J_2} \cdot M_{br} + \frac{J_2}{J_1 + J_2} \cdot M_2 - M_2 + \frac{J_2}{J_1 + J_2}(M_{br} + M_2) + (M_2 + K_1 \cdot r_{1ini} - K_1 \cdot r_{2ini}) \cdot \cos(\omega_n \cdot t_{max}) \tag{2.21}$$

Formula (2.21) is simplified into:

$$T_{max} = \frac{2 \cdot J_2}{J_1 + J_2} \cdot M_{br} + \frac{2 \cdot J_2}{J_1 + J_2} \cdot M_2 - M_2 + (M_2 + K_1 \cdot r_{1ini} - K_1 \cdot r_{2ini}) \cdot \cos(\omega_n \cdot t_{max}) \quad (2.22)$$

Introducing the factor $\varepsilon = \frac{J_2}{J_1 + J_2}$ formula (2.22) becomes:

$$T_{max} = 2 \cdot \varepsilon \cdot M_{br} + 2 \cdot \varepsilon \cdot M_2 - M_2 + (M_2 + K_1 \cdot r_{1ini} - K_1 \cdot r_{2ini}) \cdot \cos(\omega_n \cdot t_{max}) \quad (2.23)$$

The harmonic term of equation (2.23) is the influence of the initial conditions. The maximum value of the harmonic part is when $\cos(\omega_n \cdot t_{max}) = 1$ which leads in:

$$T_{max} = 2 \cdot \varepsilon \cdot M_{br} + 2 \cdot \varepsilon \cdot M_2 + (K_1 \cdot r_{1ini} - K_1 \cdot r_{2ini}) \quad (2.24)$$

The last term of equation (2.24) is the spring force at the beginning of the dynamic analysis of the system. The external forces at that state are M_2 at the side of the bridge and $-M_2$ at the side of the motor. In addition, the two masses are rotating with constant speed. Given these conditions the spring force $K_1 \cdot (r_{2ini} - r_{1ini})$ is equal to M_2 according to the 1st Newtons law. Therefore, formula (2.24) is rewritten in the form:

$$T_{max} = 2 \cdot \varepsilon \cdot M_{br} + 2 \cdot \varepsilon \cdot M_2 - M_2 \quad (2.25)$$

Formula (2.25) gives the maximum torque at the motor shaft during the application of the brake with the assumption that the brake torque and the external load act on the same direction. In case the brake torque and the external load act on opposite directions the maximum torque is then:

$$T_{max} = 2 \cdot \varepsilon \cdot M_{br} - 2 \cdot \varepsilon \cdot M_2 + M_2 \quad (2.26)$$

To cover both cases in one formula equations (2.25) and (2.26) result in:

$$T_{max} = 2 \cdot \varepsilon \cdot M_{br} \pm 2 \cdot \varepsilon \cdot M_2 \mp M_2 \quad (2.27)$$

With the use of the absolute value function, formula (2.27) can be simplified into:

$$T_{max} = 2 \cdot \varepsilon \cdot M_{br} + |1 - 2 \cdot \varepsilon| \cdot M_2 \quad (2.28)$$

Formula (2.28) seems to be almost the same as the one according to the standards (2.1) with the only difference that the dynamic factor in formula (2.28) is equal to 2 whereas in formula (2.1) is 1,9.

The torque after the bridge is stop is described with formula:

$$T(t) = M_2 - \frac{J_2}{J_1 + J_2}(M_{br} + M_2) \cdot \cos\big(\omega_n \cdot (t - t_1)\big) + \frac{J_2}{J_1 + J_2}(M_{br} + M_2) \cdot \cos\big(\omega_n \cdot (t - t_2)\big) + (M_2 + K_1 \cdot r_{1ini} - K_1 \cdot r_{2ini}) \cdot \cos(\omega_n \cdot t) \tag{2.29}$$

which is valid in the timespan $t > t_2$

The last term of formula (2.29) as explained previously stepping forward from formula (2.24) to (2.25) reduces to zero. In addition, the factor $\varepsilon = \frac{J_2}{J_1 + J_2}$ is introduced in formula (2.29) which yields:

$$T(t) = M_2 - \varepsilon \cdot (M_{br} + M_2) \cdot \cos\big(\omega_n \cdot (t - t_1)\big) + \varepsilon \cdot (M_{br} + M_2) \cdot \cos\big(\omega_n \cdot (t - t_2)\big) \tag{2.30}$$

The worst-case scenario takes place when the peaks of the two harmonic parts coincide, which result in:

$$T_{max} = 2 \cdot \varepsilon \cdot M_{br} + 2 \cdot \varepsilon \cdot M_2 + M_2 \tag{2.31}$$

Through comparison of formulas (2.31) and (2.2) a strong correlation is observed, with the only difference in the dynamic factor, which in case of the undamped dynamic system is 2 whereas in the formula of the standard is 1,5.

The contrast in the dynamic factors of the derived formulas (2.28), (2.31) and the corresponding ones stated in the standard (2.1), (2.2), generates the idea to perform the same analysis in a system with viscous damping so as to achieve the same formula as the one mentioned in the standard.

2.3.3. Damped system

The analysis as carried out previously is followed also in this chapter with the only difference that the equations of motion contain terms accounting for the damping of the system. This damping is assumed to be of viscous type. The damping coefficient of the system is defined as linearly proportional to the natural frequency of the system. When, switching from the real domain to the modal domain each equation of motion has one natural frequency and is decoupled of the others. At this stage the modal damping matrix can be derived in the following manner:

$$C^* = M^* \cdot 2 \cdot \xi \cdot \begin{pmatrix} \omega_1 \\ \omega_2 \end{pmatrix} = \begin{pmatrix} m_{11}^* & 0 \\ 0 & m_{22}^* \end{pmatrix} \cdot 2 \cdot \xi \cdot \begin{pmatrix} \omega_1 \\ \omega_2 \end{pmatrix} \tag{2.32}$$

in which:

ξ is the damping ratio;

ω_1 and ω_2 are the natural frequencies of the system;

M^* is the modal mass matrix of the system.

The assumption of the same damping ratio at each mode is scientifically acceptable. Since the analysis is at the stage of the modal domain and the equations of motion are decoupled the modal mass matrix is diagonal and also the modal damping matrix. The damping coefficients in the real domain are obtained using the inverse process switching from modal domain to the real one (Eq. (2.33)).

$$C = (E^T)^{-1} \cdot C^* \cdot E^{-1} \tag{2.33}$$

The assumptions regarding the modal damping matrix do not conclude all of the times in realistic results in real domain. Only after evaluation, one can interpret if the damping coefficients in the real domain have a reasonable physical meaning. For the system under consideration and the assumptions made previously the damping matrix in the real domain yields:

$$C = \begin{pmatrix} \frac{2 \cdot \sqrt{J_1 + J_2} \cdot (J_2 + \frac{J_2^{\,2}}{J_1}) \cdot \sqrt{K_1} \cdot \xi}{\sqrt{J_1} \cdot \sqrt{J_2} \cdot (1 + \frac{J_2}{J_1})^2} & -\frac{2 \cdot \sqrt{J_1 + J_2} \cdot (J_2 + \frac{J_2^{\,2}}{J_1}) \cdot \sqrt{K_1} \cdot \xi}{\sqrt{J_1} \cdot \sqrt{J_2} \cdot (1 + \frac{J_2}{J_1})^2} \\ -\frac{2 \cdot \sqrt{J_1 + J_2} \cdot (J_2 + \frac{J_2^{\,2}}{J_1}) \cdot \sqrt{K_1} \cdot \xi}{\sqrt{J_1} \cdot \sqrt{J_2} \cdot (1 + \frac{J_2}{J_1})^2} & \frac{2 \cdot \sqrt{J_1 + J_2} \cdot (J_2 + \frac{J_2^{\,2}}{J_1}) \cdot \sqrt{K_1} \cdot \xi}{\sqrt{J_1} \cdot \sqrt{J_2} \cdot (1 + \frac{J_2}{J_1})^2} \end{pmatrix} \tag{2.34}$$

The resulting damping matrix is symmetric and it is according to the assumed form in the equations of motion (2.5). Therefore, it is verified that the assumptions made previously are valid for the system under consideration. The entries of the damping matrix can be simplified in a more compact form after evaluation. The first entry of the matrix is called C_d and is rewritten below:

$$C_d = \frac{2 \cdot \sqrt{J_1 + J_2} \cdot (J_2 + \frac{J_2^{\,2}}{J_1}) \cdot \sqrt{K_1} \cdot \xi}{\sqrt{J_1} \cdot \sqrt{J_2} \cdot (1 + \frac{J_2}{J_1})^2} \tag{2.35}$$

The fraction $\frac{\sqrt{J_1+J_2} \cdot \sqrt{C_1}}{\sqrt{J_1} \cdot \sqrt{J_2}}$ is collected in formula (2.35) and is substituted with ω_n according to formula (2.16). Therefore, (2.35) becomes:

$$C_d = \frac{2 \cdot \omega_n \cdot (J_2 + \frac{J_2^{\,2}}{J_1}) \cdot \xi}{(1 + \frac{J_2}{J_1})^2} \tag{2.36}$$

The mass moment of inertia of the bridge J_2 can be collected out of the bracket in the numerator of (2.36) as a common factor.

$$C_d = \frac{2 \cdot \omega_n \cdot J_2 \cdot (1 + \frac{J_2}{J_1}) \cdot \xi}{(1 + \frac{J_2}{J_1})^2} \tag{2.37}$$

The term $(1 + \frac{J_2}{J_1})$ cancels the square of the bracket in the denominator in (2.37) and then the damping coefficient turns into:

$$C_d = \frac{2 \cdot \omega_n \cdot J_2 \cdot \xi}{(1 + \frac{J_2}{J_1})} \tag{2.38}$$

The nominator and the denominator of (2.38) are multiplied with the term $(J_1 \cdot K_1)$:

$$C_d = \frac{J_1 \cdot K_1 \cdot 2 \cdot \omega_n \cdot J_2 \cdot \xi}{J_1 \cdot K_1 \cdot (1 + \frac{J_2}{J_1})} = \frac{2 \cdot \omega_n \cdot J_1 \cdot J_2 \cdot K_1 \cdot \xi}{K_1 \cdot (J_1 + J_2)} \tag{2.39}$$

The fraction $\frac{J_1 \cdot J_2}{K_1 \cdot (J_1 + J_2)}$ in (2.39) is equal to $\frac{1}{{\omega_n}^2}$ based on the definition of the natural frequency of the system (2.16). Substituting it in (2.39) yields:

$$C_d = \frac{2 \cdot \omega_n \cdot K_1 \cdot \xi}{{\omega_n}^2} = \frac{2 \cdot K_1 \cdot \xi}{\omega_n} \tag{2.40}$$

The equations of motion and the associated initial conditions of the system with viscus damping taken into account are:

$$\begin{pmatrix} J_1 & 0 \\ 0 & J_2 \end{pmatrix} \cdot \begin{pmatrix} \ddot{r}_1(t) \\ \ddot{r}_2(t) \end{pmatrix} + \begin{pmatrix} \frac{2 \cdot K_1 \cdot \xi}{\omega_n} & -\frac{2 \cdot K_1 \cdot \xi}{\omega_n} \\ -\frac{2 \cdot K_1 \cdot \xi}{\omega_n} & \frac{2 \cdot K_1 \cdot \xi}{\omega_n} \end{pmatrix} \cdot \begin{pmatrix} \dot{r}_1(t) \\ \dot{r}_2(t) \end{pmatrix} + \begin{pmatrix} K_1 & -K_1 \\ -K_1 & K_1 \end{pmatrix} \cdot \begin{pmatrix} r_1(t) \\ r_2(t) \end{pmatrix} = \begin{pmatrix} M_1(t) \\ M_2 \end{pmatrix} \tag{2.41}$$

with initial conditions:

$$r_1(0) = r_{1ini}\,, r_2(0) = r_{2ini} \tag{2.42}$$

$$\dot{r}_1(0) = \omega_{nom}\,, \dot{r}_2(0) = \omega_{nom} \tag{2.43}$$

where $M_1(t)$ is the same as indicated in (2.7).

The modal analysis technique is again implemented and the torque on the torsional spring of the system is calculated using formula:

$$T(t) = K_1 \cdot (r_1(t) - r_2(t)) + C_d \cdot (\dot{r}_1(t) - \dot{r}_2(t)) \tag{2.44}$$

The torque during the application of the brake is described with formula:

$$\begin{aligned} T(t) = \frac{J_2}{J_1 + J_2} \cdot M_{br} - \frac{J_1}{J_1 + J_2} \cdot M_2 + e^{-\omega_n \cdot \xi \cdot (t - t_1)} (A_1 \cdot \cos(\omega_1 \cdot (t - t_1)) + B_1 \\ \cdot \sin(\omega_1 \cdot (t - t_1))) + e^{-\omega_n \cdot \xi \cdot t} (A_2 \cdot \cos(\omega_1 \cdot t) + B_2 \\ \cdot \sin(\omega_1 \cdot t)) \end{aligned} \tag{2.45}$$

with:

$$t_1 < t \leq t_2 \tag{2.46}$$

$$\omega_1 = \omega_n \cdot \sqrt{1 - \xi^2} \tag{2.47}$$

$$A_1 = -\varepsilon(M_{br} + M_2) \cdot (1 + \frac{C_d \cdot \xi \cdot \omega_1}{C_1 \cdot \sqrt{1 - \xi^2}} - \frac{C_d \cdot \xi \cdot \omega_n}{C_1}) \tag{2.48}$$

$$B_1 = -\varepsilon(M_{br} + M_2) \cdot (\frac{\xi}{\sqrt{1 - \xi^2}} - \frac{C_d \cdot \omega_1}{C_1} - \frac{C_d \cdot \xi^2 \cdot \omega_n}{C_1 \cdot \sqrt{1 - \xi^2}}) \tag{2.49}$$

$$A_2 = (M_2 + K_1 \cdot r_{1ini} - K_2 \cdot r_{2ini}) \cdot (1 + \frac{C_d \cdot \xi \cdot \omega_1}{C_1 \cdot \sqrt{1 - \xi^2}} - \frac{C_d \cdot \xi \cdot \omega_n}{C_1}) \tag{2.50}$$

$$B_2 = (M_2 + K_1 \cdot r_{1ini} - K_2 \cdot r_{2ini}) \cdot (\frac{\xi}{\sqrt{1 - \xi^2}} - \frac{C_d \cdot \omega_1}{C_1} - \frac{C_d \cdot \xi^2 \cdot \omega_n}{C_1 \cdot \sqrt{1 - \xi^2}}) \tag{2.51}$$

In formula (2.45) the terms that compose it can be grouped into three categories:

1. Time independent terms;
2. Decay oscillating part with respect to t=0;
3. Decay oscillating part with respect to t=t_1.

Under the assumption that the brake is applied quite some time after $t = 0$, it can be assumed that the terms multiplied with $e^{-\omega_n \cdot \xi \cdot t}$ are fully damped. This implies that these terms in formula (2.45) are disregarded for t ≥ t_1.

The constants A_1 and B_1 in formulas (2.48, 2.49) are simplified in a more compact form. Substituting ω_1 according to (2.47) into (2.48) the right hand-side bracket becomes:

$$\left(1+\frac{C_d\cdot\xi\cdot\omega_1}{C_1\cdot\sqrt{1-\xi^2}}-\frac{C_d\cdot\xi\cdot\omega_n}{C_1}\right)=\left(1+\frac{C_d\cdot\xi\cdot\omega_n}{C_1}-\frac{C_d\cdot\xi\cdot\omega_n}{C_1}\right)=1 \tag{2.52}$$

The result of formula (2.52) yields that constant A_1 in formula (2.48) turns into:

$$A_1=-\varepsilon(M_{br}+M_2) \tag{2.53}$$

Furthermore, formula (2.47) is substituted in the right-hand side bracket of formula (2.49):

$$\begin{aligned}&\left(\frac{\xi}{\sqrt{1-\xi^2}}-\frac{C_d\cdot\omega_1}{C_1}-\frac{C_d\cdot\xi^2\cdot\omega_n}{C_1\cdot\sqrt{1-\xi^2}}\right)\\&\quad=\left(\frac{\xi}{\sqrt{1-\xi^2}}-\frac{C_d\cdot\omega_n\cdot\sqrt{1-\xi^2}}{C_1}-\frac{C_d\cdot\xi^2\cdot\omega_n}{C_1\cdot\sqrt{1-\xi^2}}\right)\end{aligned} \tag{2.54}$$

The term $\sqrt{1-\xi^2}$ is multiplied in both nominator and the denominator of the middle fraction in formula (2.54) and it is evaluated further:

$$\left(\frac{\xi}{\sqrt{1-\xi^2}}-\frac{C_d\cdot\omega_n\cdot\sqrt{1-\xi^2}\cdot\sqrt{1-\xi^2}}{C_1\cdot\sqrt{1-\xi^2}}-\frac{C_d\cdot\xi^2\cdot\omega_n}{C_1\cdot\sqrt{1-\xi^2}}\right) \tag{2.55}$$

$$\left(\frac{\xi}{\sqrt{1-\xi^2}}-\frac{C_d\cdot\omega_n\cdot(1-\xi^2)}{C_1\cdot\sqrt{1-\xi^2}}-\frac{C_d\cdot\xi^2\cdot\omega_n}{C_1\cdot\sqrt{1-\xi^2}}\right) \tag{2.56}$$

The distributive property at the middle fraction in formula (2.56) is performed and the counter terms are canceled resulting in:

$$\begin{aligned}&\left(\frac{\xi}{\sqrt{1-\xi^2}}-\frac{C_d\cdot\omega_n}{C_1\cdot\sqrt{1-\xi^2}}+\frac{C_d\cdot\xi^2\cdot\omega_n}{C_1\cdot\sqrt{1-\xi^2}}-\frac{C_d\cdot\xi^2\cdot\omega_n}{C_1\cdot\sqrt{1-\xi^2}}\right)\\&\quad=\left(\frac{\xi}{\sqrt{1-\xi^2}}-\frac{C_d\cdot\omega_n}{C_1\cdot\sqrt{1-\xi^2}}\right)\end{aligned} \tag{2.57}$$

In the right hand-side of equation (2.57) the damping coefficient C_d is substituted according to the formula (2.40) and is simplified further:

$$\left(\frac{\xi}{\sqrt{1-\xi^2}} - \frac{\frac{2\cdot C_1\cdot\xi}{\omega_n}\cdot\omega_n}{C_1\cdot\sqrt{1-\xi^2}}\right) \tag{2.58}$$

$$\left(\frac{\xi}{\sqrt{1-\xi^2}} - \frac{2\cdot\xi}{\sqrt{1-\xi^2}}\right) = -\frac{\xi}{\sqrt{1-\xi^2}} \tag{2.59}$$

Following the evaluation performed in formulas (2.54-2.59) the bracket on the right hand-side in formula (2.49) is turn into the fraction depicted in formula (2.59). Hence the coefficient B_1 in formula (2.49) has turn into:

$$B_1 = -\varepsilon(M_{br}+M_2)\cdot(-\frac{\xi}{\sqrt{1-\xi^2}}) \tag{2.60}$$

The constant part of equation (2.45) is:

$$\frac{J_2}{J_1+J_2}\cdot M_{br} - \frac{J_1}{J_1+J_2}\cdot M_2 \tag{2.61}$$

The term $\frac{J_2}{J_1+J_2}\cdot M_2$ is added and subtracted in (2.61)

$$\frac{J_2}{J_1+J_2}\cdot M_{br} - \frac{J_1}{J_1+J_2}\cdot M_2 - \frac{J_2}{J_1+J_2}\cdot M_2 + \frac{J_2}{J_1+J_2}\cdot M_2 \tag{2.62}$$

The summation $-\frac{J_1}{J_1+J_2}\cdot M_2 - \frac{J_2}{J_1+J_2}\cdot M_2$ is equal to $-M_2$. Substituting it into (2.62) and also introducing the factor $\varepsilon = \frac{J_2}{J_1+J_2}$, it yields:

$$\varepsilon\cdot M_{br} + \varepsilon\cdot M_2 - M_2 \tag{2.63}$$

To sum up, the resulting torque on the torsional spring of the system during the application of the brake is rewritten and updated based on the evaluation performed in equations (2.52-2.63):

$$\begin{aligned} T(t) = \varepsilon\cdot M_{br} + \varepsilon\cdot M_2 - M_2 + e^{-\omega_n\cdot\xi\cdot(t-t_1)}(-\varepsilon(M_{br}+M_2)\cdot\cos\big(\omega_1\cdot(t-t_1)\big) \\ + -\varepsilon(M_{br}+M_2)\cdot(-\frac{\xi}{\sqrt{1-\xi^2}})\cdot\sin\big(\omega_1\cdot(t-t_1)\big)) \end{aligned} \tag{2.64}$$

The factor $\varepsilon(M_{br}+M_2)$ is taken out of the bracket in (2.64) as common:

$$T(t)=\varepsilon\cdot M_{br}+\varepsilon\cdot M_2-M_2-\varepsilon(M_{br}+M_2)\cdot e^{-\omega_n\cdot\xi\cdot(t-t_1)}\left(\cos\left(\omega_1\cdot(t-t_1)\right)-\frac{\xi}{\sqrt{1-\xi^2}}\cdot\sin\left(\omega_1\cdot(t-t_1)\right)\right) \tag{2.65}$$

The summation of the harmonic functions in the bracket of formula (2.65) can be compacted more introducing a phase shift and an amplitude based on the following mathematical relationships:

$$A\cdot\cos(\omega\cdot t)+B\cdot\sin(\omega\cdot t)=A_0\cdot\cos(\omega\cdot t-\varphi_1) \tag{2.66}$$

with

$$A_0=\sqrt{A^2+B^2} \tag{2.67}$$

$$\varphi_1=\tan^{-1}\left(\frac{B}{A}\right) \tag{2.68}$$

Then formula (2.65) yields:

$$T(t)=\varepsilon\cdot M_{br}+\varepsilon\cdot M_2-M_2-\varepsilon(M_{br}+M_2)\cdot e^{-\omega_n\cdot\xi\cdot(t-t_1)}\cdot\sqrt{\frac{1+\xi^2}{1-\xi^2}}\cdot\cos(\omega_1\cdot(t-t_1)-\varphi_1) \tag{2.69}$$

with

$$\varphi_1=\tan^{-1}\left(-\frac{\xi}{\sqrt{1-\xi^2}}\right) \tag{2.70}$$

The maximum value of equations (2.69) is obtained when:

$$\cos(\omega_1\cdot(t-t_1)-\varphi_1)=-1 \tag{2.71}$$

Introducing the new unknown $t_{new}=t-t_1$ in the equation (2.71) and solving for it, it is obtained:

$$t_{new}=\frac{\pi+\varphi_1}{\omega_1} \tag{2.72}$$

Substituting formula (2.72) into (2.69) the maximum torque during brake at the motor shaft is:

$$T_{max} = \varepsilon \cdot M_{br} + \varepsilon \cdot M_2 - M_2 + \varepsilon(M_{br} + M_2) \cdot e^{-\omega_n \cdot \xi \cdot \frac{\pi+\varphi_1}{\omega_1}} \cdot \sqrt{\frac{1+\xi^2}{1-\xi^2}} \tag{2.73}$$

For $\xi = 0{,}0344$ the multiplication $e^{-\omega_n \cdot \xi \cdot \frac{\pi+\varphi_1}{\omega_1}} \cdot \sqrt{\frac{1+\xi^2}{1-\xi^2}} = 0{,}901 \cong 0{,}9$ and the equation (2.73) turns into:

$$T_{max} = \varepsilon \cdot M_{br} + \varepsilon \cdot M_2 - M_2 + \varepsilon(M_{br} + M_2) \cdot 0{,}9 \tag{2.74}$$

$$T_{max} = 1{,}9 \cdot \varepsilon \cdot M_{br} + 1{,}9 \cdot \varepsilon \cdot M_2 - M_2 \tag{2.75}$$

In case the wind and the brake act on different direction equation (2.75) becomes:

$$T_{max} = 1{,}9 \cdot \varepsilon \cdot M_{br} - 1{,}9 \cdot \varepsilon \cdot M_2 + M_2 \tag{2.76}$$

Both cases in equations (2.75) and (2.76) are included in one formula:

$$T_{max} = 1{,}9 \cdot \varepsilon \cdot M_{br} \pm 1{,}9 \cdot \varepsilon \cdot M_2 \mp M_2 \tag{2.77}$$

With the use of the absolute value function, formula (2.77) can be simplified into:

$$T_{max} = 1{,}9 \cdot \varepsilon \cdot M_{br} + |1 - 1{,}9 \cdot \varepsilon| \cdot M_2 \tag{2.78}$$

The aforementioned analysis ended up in the same formula as the one stated in the standards (2.1) for the maximum torque at the motor shaft during braking of the system. Moreover, with this analysis it is discovered the damping ratio assumed by the standards.

In the damped system the analysis regarding the load case “Recoil after brake” is also performed. The torque at the motor shaft regarding this situation is given by:

$$\begin{aligned} T(t) = M_2 + e^{-\omega_n \cdot \xi \cdot (t-t_1)}\big(A_1 \cdot \cos\big(\omega_1 \cdot (t-t_1)\big) + B_1 \cdot \sin\big(\omega_1 \cdot (t-t_1)\big)\big) \\ + e^{-\omega_n \cdot \xi \cdot t}(A_2 \cdot \cos(\omega_1 \cdot t) + B_2 \cdot \sin(\omega_1 \cdot t)) + e^{-\omega_n \cdot \xi \cdot (t-t_2)}(A_3 \\ \cdot \cos\big(\omega_1 \cdot (t-t_2)\big) + B_3 \cdot \sin\big(\omega_1 \cdot (t-t_2)\big)) \end{aligned} \tag{2.79}$$

with:

$$t > t_2 \tag{2.80}$$

$$A_3 = \varepsilon(M_{br} + M_2) \cdot (1 + \frac{C_d \cdot \xi \cdot \omega_1}{C_1 \cdot \sqrt{1-\xi^2}} - \frac{C_d \cdot \xi \cdot \omega_n}{C_1}) \tag{2.81}$$

$$B_3 = \varepsilon(M_{br} + M_2) \cdot (\frac{\xi}{\sqrt{1-\xi^2}} - \frac{C_d \cdot \omega_1}{C_1} - \frac{C_d \cdot \xi^2 \cdot \omega_n}{C_1 \cdot \sqrt{1-\xi^2}}) \tag{2.82}$$

The coefficients A_1, B_1, A_2, B_2 are the same as determined in equations (2.48-2.51), while ω_1 is introduced in (2.47). Following the same methodology as depicted through formulas (2.52-2.69), the equation (2.79) can be simplified into:

$$\begin{aligned} T(t) = M_2 - \varepsilon(M_{br} + M_2) \cdot e^{-\omega_n \cdot \xi \cdot (t-t_1)} \cdot \sqrt{\frac{1+\xi^2}{1-\xi^2}} \cdot \cos(\omega_1 \cdot (t-t_1) - \varphi_1) \\ + \varepsilon(M_{br} + M_2) \cdot e^{-\omega_n \cdot \xi \cdot (t-t_2)} \cdot \sqrt{\frac{1+\xi^2}{1-\xi^2}} \cdot \cos(\omega_1 \cdot (t-t_2) - \varphi_1) \end{aligned} \tag{2.83}$$

The time dependent parts of formula (2.83) follows the same decay oscillation which is illustrated in Figure 2.2.

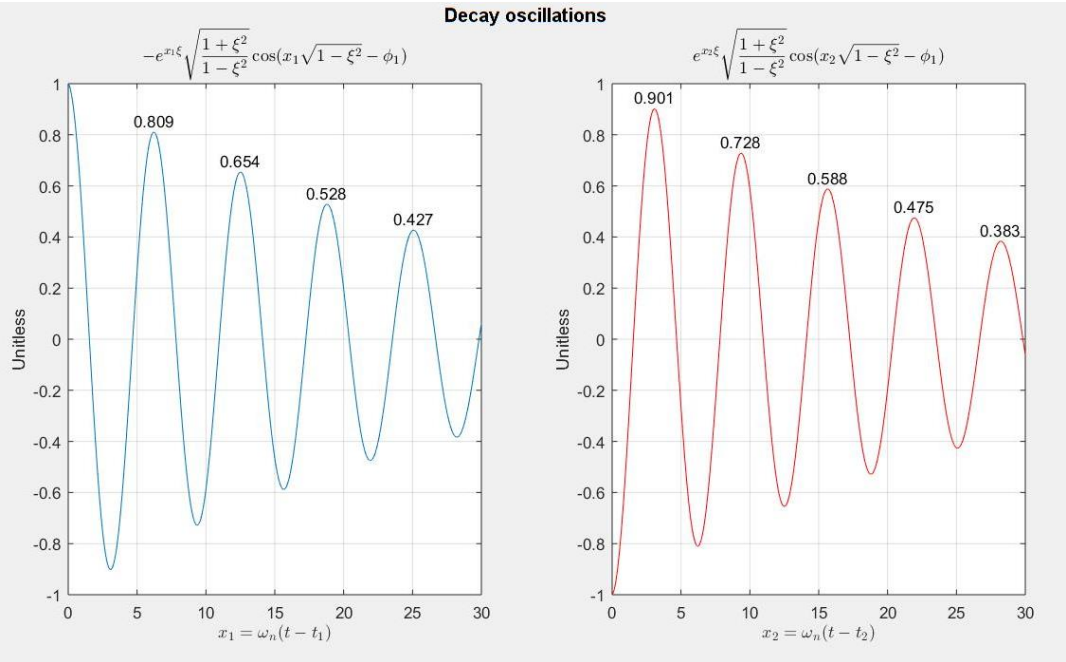

Figure 2.2: Decay oscillatory parts of Eq. (2.83) with damping ratio 3,44%

In order to elaborate the decay oscillations, the multiplications $\omega_n \cdot (t - t_1)$ and $\omega_n \cdot (t - t_2)$ are substituted with the variables x_1 and x_2 respectively. The most unfavorable scenario, which results to the highest torque at the motor shaft in this phase of motion, is when the first maximum of each of the two time-dependent parts coincide. This results in:

$$T_{max} = M_2 + 0{,}809 \cdot \varepsilon(M_{br} + M_2) + 0{,}901 \cdot \varepsilon(M_{br} + M_2) \quad (2.84)$$

$$T_{max} = 1{,}709 \cdot \varepsilon \cdot M_{br} + 1{,}709 \cdot \varepsilon \cdot M_2 + M_2 \quad (2.85)$$

Through comparison of formula (2.85) with formula (2.2) it is seen that the derived one is more conservative than the one of the standards, resulting to higher torque. However, the occurrence of the scenario where formula (2.85) is based has a very low probability of occurrence, since the peaks of the two time-dependent parts have to be coincide. In all other cases where the peak of the second time depend part does not coincide with the peak of the first one in equation (2.83) results in dynamic factors that go closer to 1,5 or lower than that one. Thus, due to the very low probability of the scenario behind formula (2.85) it can be concluded that the formula of the standards (2.2) is a very good approximation of the loading case “Recoil after brake”.

2.4. Sensitivity analysis regarding the number of DoF taken into account

The aforementioned study carried out in the basis of the existing standard and the reproduction of the design formulas provides insight regarding the dynamic model of the system movable bridge-machinery. This is achieved in terms of input parameters such as modeling of external loading, the assumed damping ratio and the resulting decisive dynamic loads on the system. It is also important to examine the influence of the number of degrees of freedom taken into account in the dynamic model.

First, it is compared the response of a 2-DoF dynamic model to that of a single degree of freedom (SDoF) one. In reality the velocity of the electric motor can be programmed and predefined. Hence, taking the integral of the velocity, the angle of the motor can be calculated. In this case the first degree of freedom of the system is already defined. Therefore, the first mass can be removed and substituted by a boundary with prescribed rotation and rotational velocity. Then, the system of equations from two degrees is reduced to one resulting into a SDoF system.

Afterwards, it is decided to explore the influence of increasing the degrees of freedom by adding inertia terms and associated degrees of freedom in the system and split the stiffness of the machinery into sub parts.

The major input parameters of the upcoming analysis are depicted in Table 2.3.

Table 2.3: Input parameters for the sensitivity analysis

Mass moment of inertia of the motor	J_1	0.837
Mass moment of inertia of the bridge reduced at the motor shaft	J_2	0.443
Total stiffness of the machinery reduced at the motor shaft	K_1	7.111
Nominal speed of the motor	ω_{nom}	99.82
Damping ratio of the system	ξ	0,0344

The time the motor needs to reach its nominal speed is assumed to be **14 sec**. Therefore, the acceleration of the motor can be determined as:

$$a_{ac} = \frac{\omega_{nom}}{14} \tag{2.86}$$

The **brake** in the system is **applied at 60sec**. The **braking duration varies**. The deceleration of the system due to application of the brake is determined in the same manner as the acceleration. The formula to determine the deceleration is:

$$a_{br} = -\frac{\omega_{nom}}{t_{br}} \tag{2.87}$$

where t_{br} is the time required the bridge to stop.

The external torque on the bridge is not calculated in detail in these analyses, since the main attention is paid at the effect of the degrees of freedom on the decisive loads and not their exact value. However, the order of magnitude of the maximum wind load is based on realistic wind values. The upcoming analyses are carried out for wind under the bridge and the maximum value of the torque due to wind is assumed -250 Nm. Moreover, it is assumed that the wind torque increases linear from t=0s to t=30s to reach its maximum value and then is kept constant. The behavior of the torque acting on the bridge due to wind load is illustrated in Figure 2.3.

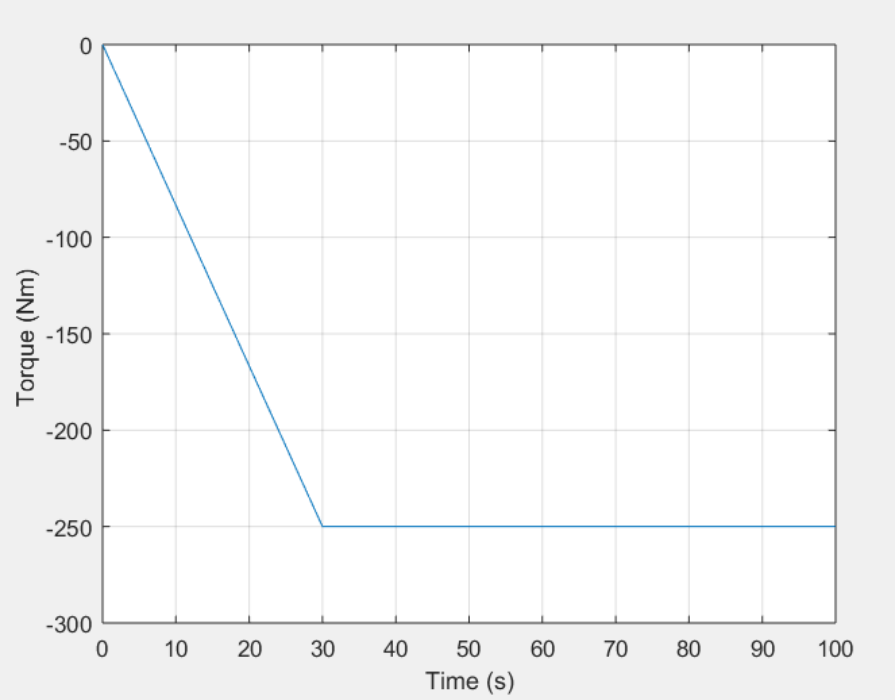

Figure 2.3: External torque due to wind $M_2(t)$

2.4.1. 2-DoF model versus SDoF model

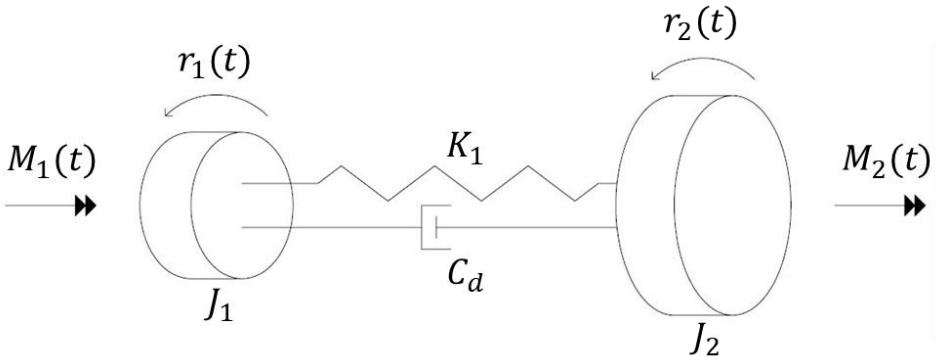

Figure 2.4: 2-Dof rotational dynamic model with viscous damping

The equations of motion for the **2-DoF** dynamic model (Figure 2.4) of the system are:

$$\begin{pmatrix} J_1 & 0 \\ 0 & J_2 \end{pmatrix} \cdot \begin{pmatrix} \ddot{r}_1(t) \\ \ddot{r}_2(t) \end{pmatrix} + \begin{pmatrix} C_d & -C_d \\ -C_d & C_d \end{pmatrix} \cdot \begin{pmatrix} \dot{r}_1(t) \\ \dot{r}_2(t) \end{pmatrix} + \begin{pmatrix} K_1 & -K_1 \\ -K_1 & K_1 \end{pmatrix} \cdot \begin{pmatrix} r_1(t) \\ r_2(t) \end{pmatrix} = \begin{pmatrix} M_1(t) \\ M_2(t) \end{pmatrix} \quad (2.88)$$

with

C_d calculated according to formula (2.40).

The external torque at the motor side is:

$$M_1(t) = \begin{cases} a_{ac} \cdot (J_1 + J_2) - M_2(t), & 0 \le t \le 14s \\ -M_2(t), & 14s < t \le 60s \\ a_{br} \cdot (J_1 + J_2) - M_2(t), & 60s < t \le 60s + t_{br} \\ -M_2(t), & t > 60s + t_{br} \end{cases} \quad (2.89)$$

The external torque at the bridge side is already depicted in Figure 2.3 and its function is:

$$M_2(t) = \begin{cases} -\frac{250 \cdot t}{30}, & 0 \le t \le 30s \\ -250, & t > 30s \end{cases} \quad (2.90)$$

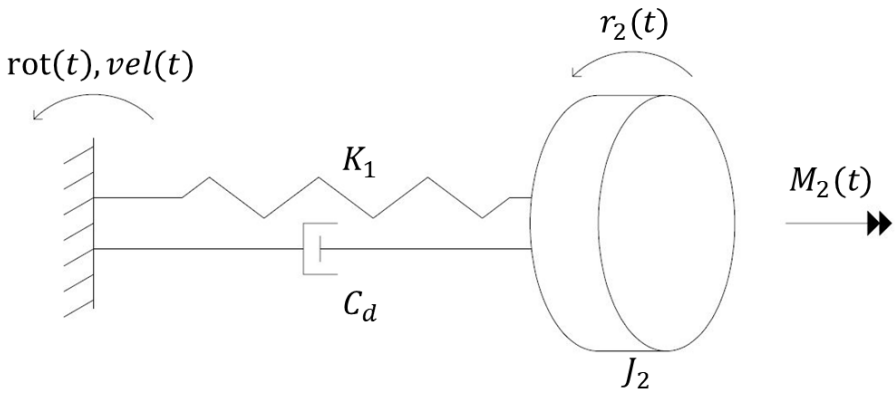

Figure 2.5: SDoF rotational dynamic model

The equation of motion of the **SDoF** dynamic model in Figure 2.5 is:

$$J_2 \cdot \ddot{r}_2 + \acute{C}_d \cdot (\dot{r}_2 - vel(t)) + K_1 \cdot (r_2 - rot(t)) = M_2(t) \quad (2.91)$$

with

$$\acute{C}_d = 2 \cdot \xi \cdot \sqrt{\frac{K_1}{J_2}} \cdot J_2 \quad (2.92)$$

$$vel(t) = \int \begin{cases} a_{ac}, & 0 \le t \le 14s \\ a_{br}, & 60s < t \le 60s + t_{br} \end{cases} dt \quad (2.93)$$

$$rot(t) = \int vel(t)\, dt \quad (2.94)$$

Sign convention of the analysis

The coordinate system of the analysis is as shown in Figure 2.6.

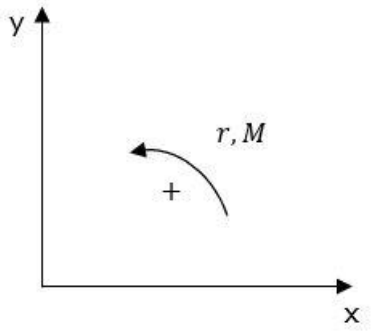

Figure 2.6: Assumed coordinate system of the analyses

The arrangement of the bridge with wind load under while opens is depicted in Figure 2.7.

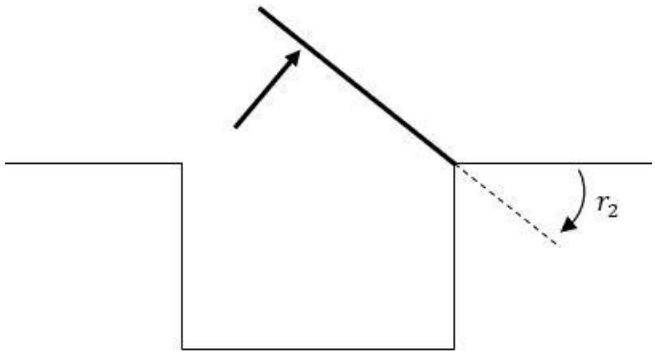

Figure 2.7: Assumed bridge configuration while opens and external wind load

According to the assumed coordinate system and the bridge configuration in Figure 2.6 and Figure 2.7 the angle of the bridge while it opens and the external torque due to wind have a negative sign. In addition, the angular velocity of the motor and its associated angle have a negative sign too, during the opening of the bridge. To explain the signs of external loads, the 2-DoF system with the assumed coordinate system is sketched in different phases of motion.

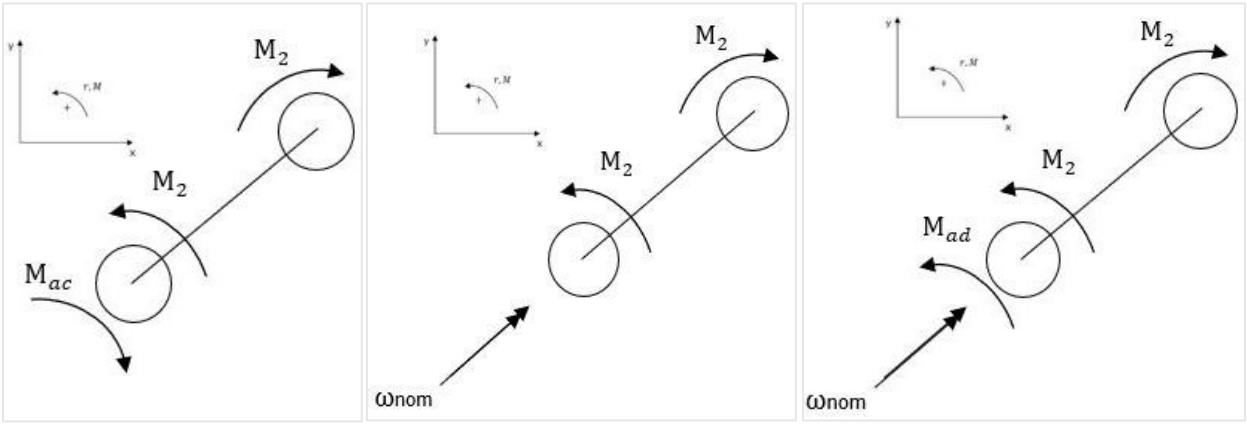

Figure 2.8: Coordinate system and external loading at different phases of motion. Left: Acceleration of the system. Middle: System rotating with constant speed. Right: Braking of the system

The analysis is performed for several braking durations. The maximum torque during the application of the brake is calculated in the two dynamic models and it is compared with the outcome of formula (2.1) of the existing standard. The results of the analyses are summarized in the following table.

Table 2.4: Results of analyses carried out in 2-DoF, SDoF model and formula (2.1) of the standard NEN 6786:2001 (2001)

Braking duration (t_{br})	Max Torque 2-DoF	Max Torque SDoF	Vobb formula
1s	334,009Nm	333,982Nm	334,018Nm
2s	292,008Nm	291,981Nm	292,009Nm
3s	278,007Nm	277,981Nm	278,006Nm
5s	266,807Nm	266,78Nm	266,804Nm

The results of Table 2.4 indicate that both 2-DoF and SDoF dynamic models can be used to calculate the maximum torque at the motor shaft during brake. Therefore, it depends on the discretion of the engineer which of these two alternatives will be used for the dynamic analysis of the system.

2.4.2. 3-DoF & 4-DoF model versus 2-DoF model

The possibility of increasing the degrees of freedom in the system is considered in this sub-section. As it is already mentioned the proposed dynamic model consists of two degrees of freedom, the electric motor and the bridge, connected with a torsional spring which represents the total stiffness of the machinery. The analyses are performed at the level of the motor shaft. Therefore, all input parameters are reduced at that level using the associated transmission factors.

The proposed dynamic model seems to be a simplification of the real structure, since there are lots of elements in the system with associated inertias which are not taken into account. Thus, it is decided to perform analyses in linear models with increasing number of degrees of freedom that are taken into account. Prerequisite of these analyses is to study the order magnitude of these additional intermediate inertias. The review that is carried out is based on technical drawings, and the inertias of the intermediate shafts are calculated roughly and then reduced at the level of the motor shaft. It is concluded that the

intermediate inertias of the system are in the order of magnitude of 0,1% compared to inertia of the motor or the reduced one of the bridge.

The order of magnitude of the intermediate inertias of the system is so small, and the reason of discarding them from the equations of motion is obvious. However, for the validation of this impression, dynamic analyses are performed in dynamic models of three and four degrees of freedom. In these models, additional intermediate inertia terms are considered, with magnitudes varying in the range of $(0{,}1\% \cdot J_2 \div 2\% \cdot J_2)$.

In addition, since these additional degrees of freedom are placed intermediate of the two major ones, the stiffness and the damping of the machinery have to be split up. To do so, the formula regarding springs in series is implemented. The total stiffness of the machinery, as calculated in the 2-DoF dynamic model, is split into two or three springs in series according to:

$$\frac{1}{K_{1,2d}} = \frac{1}{K_{1,3d}} + \frac{1}{K_{2,3d}} \tag{2.95}$$

$$\frac{1}{K_{1,2d}} = \frac{1}{K_{1,4d}} + \frac{1}{K_{2,4d}} + \frac{1}{K_{3,4d}} \tag{2.96}$$

In formulas (2.95) and (2.96) the following relations are held:

$$\frac{1}{K_{1,3d}} = fact_{1,3d} \cdot \frac{1}{K_{1,2d}} \tag{2.97}$$

$$\frac{1}{K_{2,3d}} = \frac{1}{K_{1,2d}} - \frac{1}{K_{1,3d}} \tag{2.98}$$

$$\frac{1}{K_{1,4d}} = fact_{1,4d} \cdot \frac{1}{K_{1,2d}} \tag{2.99}$$

$$\frac{1}{K_{2,4d}} = fact_{2,4d} \cdot \frac{1}{K_{1,2d}} \tag{2.100}$$

$$\frac{1}{K_{3,4d}} = \frac{1}{K_{1,2d}} - \frac{1}{K_{1,4d}} - \frac{1}{K_{2,4d}} \tag{2.101}$$

where

$fact_{1,3d}$ is the percentage of the total stiffness of the machinery ($K_{1,2d}$) that is assigned to the stiffness of the first spring of the three degrees of freedom model;

$fact_{1,4d}$ is the percentage of the total stiffness of the machinery ($K_{1,2d}$) that is assigned to the stiffness of the first spring of the four degrees of freedom model;

$fact_{2,4d}$ is the percentage of the total stiffness of the machinery ($K_{1,2d}$) that is assigned to the stiffness of the second spring of the four degrees of freedom model.

In the same manner, the damping coefficient of the 2-DoF model is split. Varying the percentages in formulas (2.97, 2.99, 2.100), the division of the initial spring stiffness changes, which results in diverse possible positions of the additional degrees of freedom in the system. To make it clear in Figure 2.9 is illustrated what is mentioned before. At the top of each figure the 2-DoF dynamic model is drawn. At the bottom different configurations of the 3-DoF model are drawn.

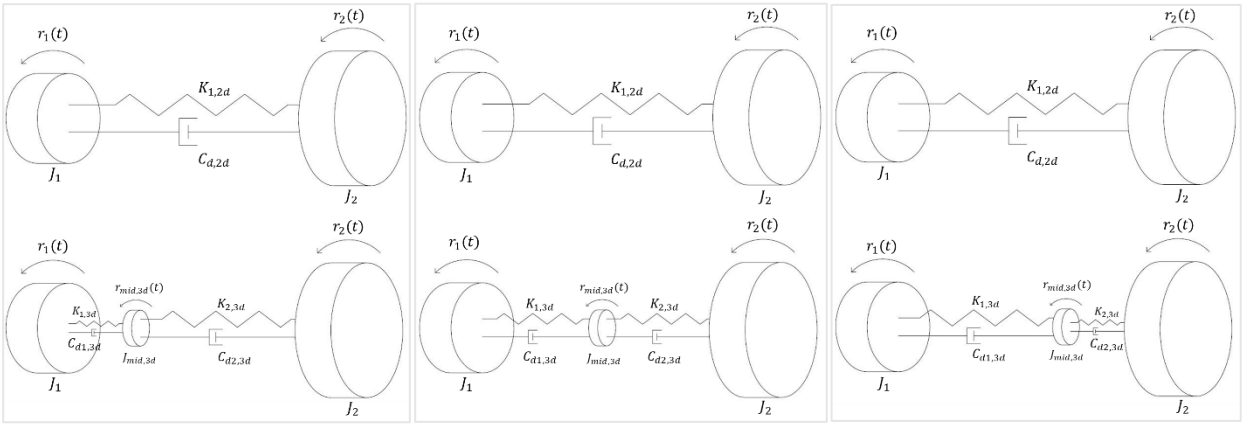

Figure 2.9: Impression of machinery stiffness division in 3-DoF model (bottom) in comparison with 2-DoF model (top).

Left:$\text{fact}_{1,3\text{d}} = 0{,}25$;Middle: $\text{fact}_{1,3\text{d}} = 0{,}5$;Right: $\text{fact}_{1,3\text{d}} = 0{,}75$

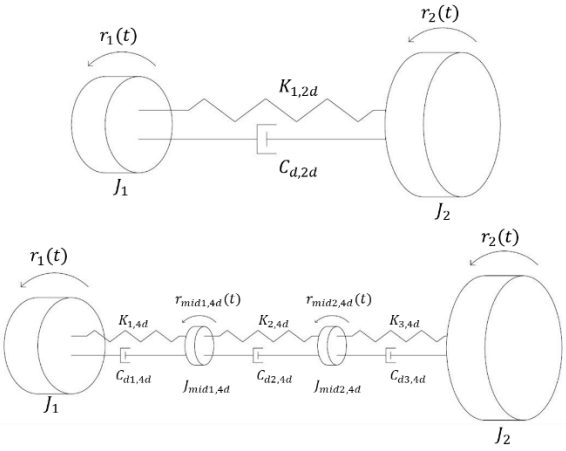

Figure 2.10: Impression of machinery stiffness division in 4-DoF model (bottom) in comparison with 2-DoF model (top).

$(\text{fact}_{1,4\text{d}} = 0{,}33;\ \text{fact}_{2,4\text{d}} = 0{,}33)$

The results of the analyses are summarized in Table 2.6 and Table 2.7. The analyses are performed with external loading such as depicted in formulas (2.89,2.90) with **braking duration (t_{br})** equal to **1s**. The results of these analyses are compared with the outcome of the 2-DoF dynamic model (2.88) in the Table 2.5.

Table 2.5: 2-DoF model, brake at 60s with duration $t_{br} = 1s$

2-DoF model	
Maximum Torque (Nm)	334,009

Table 2.6: 3-DoF model, calculated maximum torque at the motor shaft during brake applied at 60s with duration $t_{br} = 1s$

3-DoF model: Maximum Torque at the motor shaft (Nm)					
Stiffness & damping distribution as percentage of the 2-DoF ones	**Additional mass, percentage of J_2**				
	0,1%	**0,5%**	**1%**	**1,5%**	**2%**
5%-95%	334,009	334,010	334,012	334,014	334,016
10%-90%	334,015	334,038	334,067	334,096	334,125
25%-75%	334,030	334,112	334,216	334,318	334,420
50%-50%	334,049	334,208	334,406	334,604	334,801
75%-25%	334,061	334,266	334,523	334,779	335,035
90%-10%	334,064	334,284	334,558	334,831	335,103
95%-5%	334,065	334,287	334,564	334,840	335,115

Table 2.7: 4-DoF model, calculated maximum torque at the motor shaft during brake applied at 60s with duration $t_{br} = 1s$

4-DoF model: Maximum Torque at the motor shaft (Nm)					
Stiffness & damping distribution as percentage of the 2-DoF ones	**Additional masses, percentage of J_2**				
	0,1%-0,1%	**0,5%-0,5%**	**1%-1%**	**1,5%-1,5%**	**2%-2%**
5%-5%-90%	334,015	334,040	334,071	334,102	334,133
10%-10%-80%	334,031	334,118	334,226	334,333	334,440
20%-20%-60%	334,058	334,254	334,496	334,737	334,976
33,33%-33,33%-%-33,33%	334,085	334,390	334,768	335,144	335,518
60%-20%-20%	334,107	334,500	334,988	335,473	335,956
80%-10%-10%	334,117	334,548	335,083	335,615	336,143
90%-5%-5%	334,120	334,561	335,109	335,653	336,193

Through comparison of the results in Table 2.6 and Table 2.7 with that of Table 2.5, it is perceived that the influence of the intermediate additional degrees of freedom (with inertias in the order of magnitude $0{,}1\% \cdot J_2 \div 2\% \cdot J_2$) on the maximum torque at the motor shaft is negligible. On the other hand, even if the influence of the additional degrees of freedom is negligible, in general the division of the stiffness and damping influences the result. The correlation of the position of the additional inertia and the division of stiffness and damping is illustrated in Figure 2.9 and Figure 2.10. Therefore, it can be concluded that the closer the additional inertias are to the inertia of the bridge, the higher the influence of it is in the maximum torque at the motor shaft.

It is decided to perform one last sensitivity analysis adding an inertia term in the system at the position of the bridge and connect this new mass with the bridge with a new linear spring with very high stiffness Figure 2.11. The stiff spring is drawn with thick line.

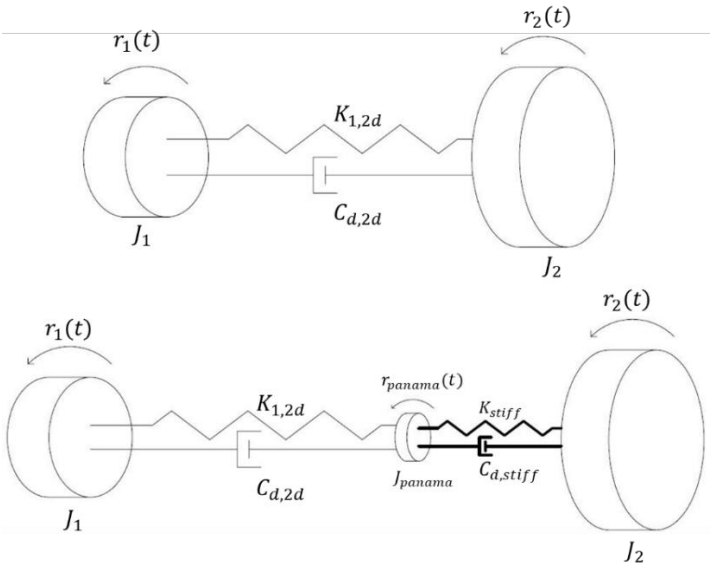

Figure 2.11: Linear modeling of the system bascule bridge with Panama wheel (bottom) in comparison with the 2-DoF one

With this modeling a linear approximation of the structure with the Panama wheel and the buffer is accomplished. The buffer is already assumed as a rigid component in the design code, so it is modeled roughly here as a linear spring with very high stiffness. In addition, the mass moment of inertia of the Panama wheel is estimated in the order of magnitude of $1\% \cdot J_2 \div 10\% \cdot J_2$. These analyses are performed again for external loading as depicted in formulas (2.89,2.90) with **braking duration (t_{br})** equal to **1s**. The results are compared with the outcome of the 2-DoF dynamic model (2.88). The results of the analyses are summarized in Table 2.8.

Table 2.8: Maximum torque at the motor shaft of the model with the Panama wheel for brake applied at 60s with duration $t_{br} = 1\text{s}$

Inertia of the Panama wheel	Maximum torque (Nm)
$1\% \cdot J_2$	334,567
$2\% \cdot J_2$	335,120
$5\% \cdot J_2$	336,758
$10\% \cdot J_2$	339,451

The outcome of the analyses in Table 2.8 compared with that of Table 2.5, indicates that the addition of a Panama wheel will increase the calculated maximum torque at the motor shaft. However, for inertia terms of the Panama wheel in the order of magnitude less than $5\% \cdot J_2$, the increase at the maximum torque is less than 1%. Therefore, the influence of the addition of a Panama wheel in the system is negligible. In the existing analyses, the mass moment of inertia of the Panama wheel is not calculated. A study is carried out tracing back to technical drawings of bascule bridges with Panama wheel drive. A rough estimation of the Panama wheel mass moment of inertia results in an order of magnitude of 2%-5% of the inertia of the bridge.

The last analysis is very important for the upcoming research, since it is decided to add the Panama wheel in the equations of motion of the system so as to incorporate the buffer in the equations of motion.

3. Behavior of the buffer

3.1. Introduction

The purpose of this chapter is to establish a generic formula which describes the generalized force-displacement diagram of the buffer component. First, a literature review is carried out regarding the performance of the disc springs, which are the most important components of the buffer. Second, the generalized force-displacement diagram of the buffer component is built up based on the disc springs' performance. Finally, the influence of friction on a stack of disc springs is explored.

3.2. State of the art in disc springs

According to the existing literature, the torque-angle behavior of the drive mechanism, when the buffer is taken into account, is illustrated in the following diagram.

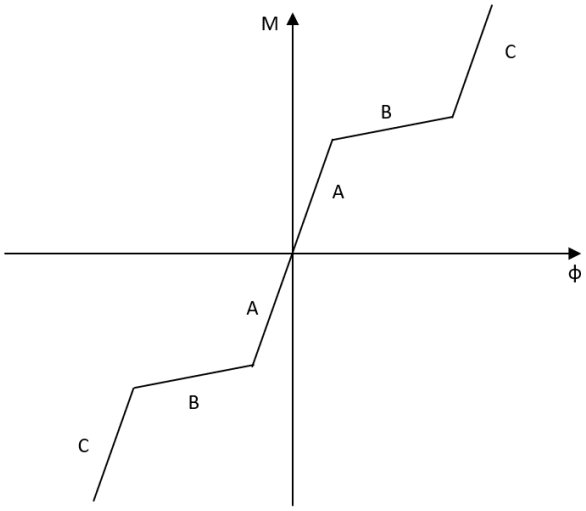

Figure 3.1: Torque-angle diagram of the drive mechanism

In branches A and C the buffer is assumed infinitely stiff, thus the total stiffness is calculated based on the torsional stiffness of the machinery alone. In branch B, however, the stack of disc springs in the buffer is active and their behavior is taken into account influencing the total stiffness of the system.

Focusing on the buffer itself, its force deformation behavior is described in chapter 1 and is indicated in Figure 1.5.

Figure 1.5 and Figure 3.1 illustrate that the disc springs in the buffer have a linear force deformation behavior. On the contrary according to (Christian Bauer (3), 2006) the disc spring characteristic force deflection curve is nonlinear and it is depicted in the following diagram (Figure 3.2).

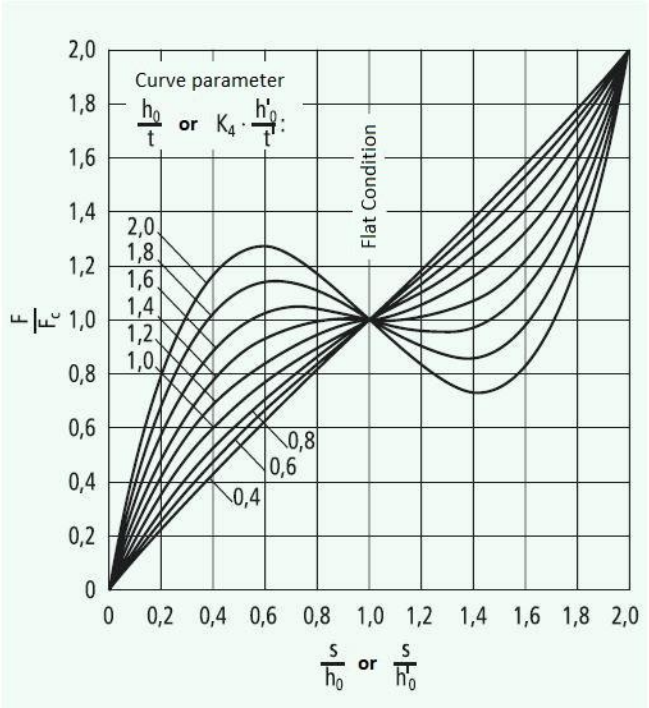

Figure 3.2: Calculated force-deflection characteristics of individual disc springs depending in their curve parameter $\frac{h_0}{t}$. or $K_4 \cdot \frac{h_0'}{t'}$ (Christian Bauer (3), 2006)

The disc springs are grouped into two main categories, disc springs with contact surface and disc springs without contact surface. The difference is illustrated in Figure 3.3. On the left, the edges of the disc spring are rounded (no contact surface), whilst on the right one these corresponding edges are horizontal (contact surface).

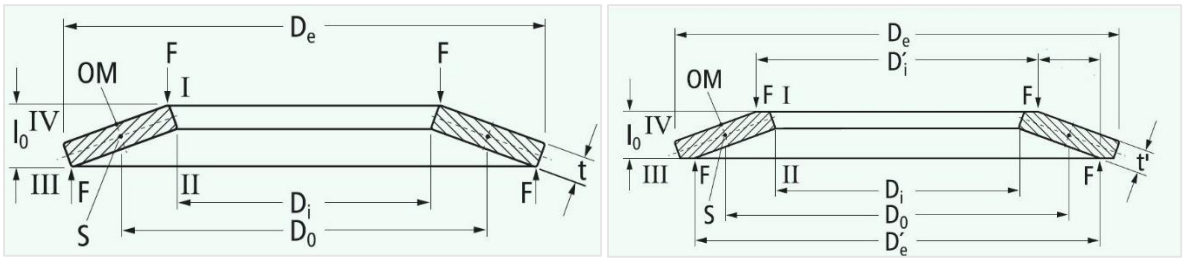

Figure 3.3: Cross section of individual disc spring without contact surface (Left). Cross section of individual disc spring with contact surface (Right) (Christian Bauer (3), 2006)

The curve parameter of a disc spring is calculated with the following equation:

$$\kappa = K_4 \cdot \frac{h_0}{t} \tag{3.1}$$

in which:

$h_0 = l_0 - t$ is an auxiliary variable which is equal to the deflection of the disc spring in flat condition;

l_0 is the overall height of the disc spring in the unloaded condition;

t is the thickness of the disc spring;

K_4 is a coefficient used for the calculation of disc springs (Christian Bauer (3), 2006) & (standard DIN 2092:2006:03 (2006)).

For disc springs without contact surfaces $K_4 = 1$ and the curve parameter κ reduces to $\frac{h_0}{t}$. For disc springs with contact surface the parameters h_0 and $\kappa = K_4 \cdot \frac{h_0}{t}$ are substitute with h_0' and $\kappa = K_4 \cdot \frac{h_0'}{t'}$ respectively. In general, the curve parameter of a disc spring does not need to be calculated by the engineer because it is given directly by the manufacturer as one of the properties of the spring (Christian Bauer (4), 2006).

The effect of nonlinearity depends on the curve parameter of the disc spring. The higher the numerator (the variable h_0 or h_0') the more nonlinear the performance of a disc spring. The nonlinearity of the disc springs shows a snap-through behavior. The same behavior is observed in case of two oblique springs loaded out of plane (Brennan, Mace, & Kovacic, 2010). This type of nonlinearity is of geometric nature since the geometry of the initial undisturbed system changes considerably with loading.

In Figure 3.2 the characteristic force-deflection curve of a number disc springs with different curve parameter can be observed. The horizontal axis is the normalized deflection and the vertical axis is the normalized applied force. The deflection is normalized by the height of the disc spring. The applied force is normalized by the force of the disc spring in flat condition.

3.3. Individual disc springs

In (Christian Bauer (3), 2006) the spring force F is given as a function of the disc spring deflection s. This equation is defined according to the standard DIN 2092:2006:03 (2006) and is mentioned below.

$$F[s] = \frac{4 \cdot E}{1 - \mu^2} \cdot \frac{t^4}{K_1 \cdot D_e^2} \cdot {K_4}^2 \cdot \frac{s}{t} \cdot \left[{K_4}^2 \cdot \left(\frac{h_0}{t} - \frac{s}{t}\right) \cdot \left(\frac{h_0}{t} - \frac{s}{2 \cdot t}\right) + 1\right] \tag{3.2}$$

in which:

$E = 206.000 \ \frac{N}{mm^2}$ is the elastic modulus of the material according to the standard DIN 2092:2006:03 (2006);

$\mu = 0{,}3$ is the Poisson ratio of the material according to the standard DIN 2092:2006:03 (2006);

D_e is the outside diameter of the disc spring (Figure 3.3);

K_1, K_4 are coefficients used for the calculations of the disc springs (Christian Bauer (3), 2006) & (standard DIN 2092:2006:03 (2006));

s is the variable of the formula concerning the deflection of the disc spring.

Equation (3.2) is evaluated so as to get rid of the coefficients K_1 and K_4 and simplify it. In the first place, according to (Christian Bauer (3), 2006) and the standard DIN 2092:2006:03 (2006) the term $\frac{4\cdot E}{1-\mu^2}\cdot\frac{t^3\cdot h_0}{K_1\cdot D_e^2}\cdot {K_4}^2$ in equation (3.2) can be substituted by the factor F_c which refers to the calculated spring force of an individual disc spring in flat condition ($s = h_0$). To reveal that term the right-hand side of equation (3.2) is multiplied with $\frac{h_0}{h_0}$ (Eq. (3.3)). Afterwards, the terms out of the bracket in (3.3) are reordered so as to display clearly the aforementioned term (Eq. (3.4)). Finally, the factor F_c is introduced in the equation of the spring force in (3.5).

$$F[s] = \frac{h_0}{h_0}\cdot\frac{4\cdot E}{1-\mu^2}\cdot\frac{t^4}{K_1\cdot D_e^2}\cdot {K_4}^2\cdot\frac{s}{t}\cdot\left[{K_4}^2\cdot\left(\frac{h_0}{t}-\frac{s}{t}\right)\cdot\left(\frac{h_0}{t}-\frac{s}{2\cdot t}\right)+1\right] \tag{3.3}$$

$$F[s] = \frac{4\cdot E}{1-\mu^2}\cdot\frac{t^3\cdot h_0}{K_1\cdot D_e^2}\cdot {K_4}^2\cdot\frac{s}{h_0}\cdot\left[{K_4}^2\cdot\left(\frac{h_0}{t}-\frac{s}{t}\right)\cdot\left(\frac{h_0}{t}-\frac{s}{2\cdot t}\right)+1\right] \tag{3.4}$$

$$F[s] = F_c\cdot\frac{s}{h_0}\cdot\left[{K_4}^2\cdot\left(\frac{h_0}{t}-\frac{s}{t}\right)\cdot\left(\frac{h_0}{t}-\frac{s}{2\cdot t}\right)+1\right] \tag{3.5}$$

The terms $\frac{s}{t}$ and $\frac{s}{2\cdot t}$ in equation (3.5) are multiplied both with $(\frac{h_0}{t}\cdot\frac{t}{h_0})$ (Eq. (3.6)) in order to introduce the fraction $\frac{h_0}{t}$ in every term in the brackets (Eq. (3.7)). Subsequently, the coefficient ${K_4}^2$ is split and distributed in each term of the two brackets (Eq.(3.8)).

$$F[s] = F_c\cdot\frac{s}{h_0}\cdot\left[{K_4}^2\cdot\left(\frac{h_0}{t}-\frac{h_0}{t}\cdot\frac{t}{h_0}\cdot\frac{s}{t}\right)\cdot\left(\frac{h_0}{t}-\frac{h_0}{t}\cdot\frac{t}{h_0}\cdot\frac{s}{2\cdot t}\right)+1\right] \tag{3.6}$$

$$F[s] = F_c\cdot\frac{s}{h_0}\cdot\left[{K_4}^2\cdot\left(\frac{h_0}{t}-\frac{h_0}{t}\cdot\frac{s}{h_0}\right)\cdot\left(\frac{h_0}{t}-\frac{h_0}{t}\cdot\frac{s}{2\cdot h_0}\right)+1\right] \tag{3.7}$$

$$F[s] = F_c\cdot\frac{s}{h_0}\cdot\left[\left(K_4\cdot\frac{h_0}{t}-K_4\cdot\frac{h_0}{t}\cdot\frac{s}{h_0}\right)\cdot\left(K_4\cdot\frac{h_0}{t}-K_4\cdot\frac{h_0}{t}\cdot\frac{s}{2\cdot h_0}\right)+1\right] \tag{3.8}$$

Introducing the curve parameter (3.1) in equation (3.8) results in:

$$F[s] = F_c\cdot\frac{s}{h_0}\cdot\left[\left(\kappa-\kappa\cdot\frac{s}{h_0}\right)\cdot\left(\kappa-\frac{\kappa}{2}\cdot\frac{s}{h_0}\right)+1\right] \tag{3.9}$$

The equation (3.9) describes the spring force on an individual disc spring as a function of its deflection (s) with parameters:

- the calculated spring force of an individual disc spring in flat condition ($F_c = F[s = h_0]$)
- the thickness (t) and the initial height of the disc spring in unloaded condition (l_0) merged in one auxiliary variable $h_0 = l_0 - t$
- the curve parameter of the disc spring κ

The aforementioned parameters can be read from the technical document of the manufacturer (Christian Bauer (3), 2006) depending on the disc spring under consideration.

In addition, the normalized force–deflection equation of a disc spring is given in (3.10). To obtain it equation (3.9) is normalized two times. First, the normalized deflection $s_{nl} = \frac{s}{h_0}$ is substituted in (3.9). Second, the whole equation is divided with the force associated to the flat condition of the disc spring $\frac{F[s_{nl}]}{F_c}$

$$F_{nl}[s_{nl}] = \frac{F[s_{nl}]}{F_c} = s_{nl} \cdot [(\kappa - \kappa \cdot s_{nl}) \cdot \left(\kappa - \frac{\kappa}{2} \cdot s_{nl}\right) + 1] \tag{3.10}$$

It must be mentioned that due to the normalization that equation (3.10) is subjected the deflection $s_{nl} = 1$ corresponds to the flat condition of the disc spring with resulting normalized spring force $F_{nl}[s_{nl} = 1] = 1$. Equation (3.10) is used to reproduce the diagram of the manufacturer depicted earlier in Figure 3.2. The curve parameter is given the values in the range $[0{,}4 \div 2{,}0]$ with step $0{,}2$. The desired plot is drawn in the software Matlab and is presented in Figure 3.4.

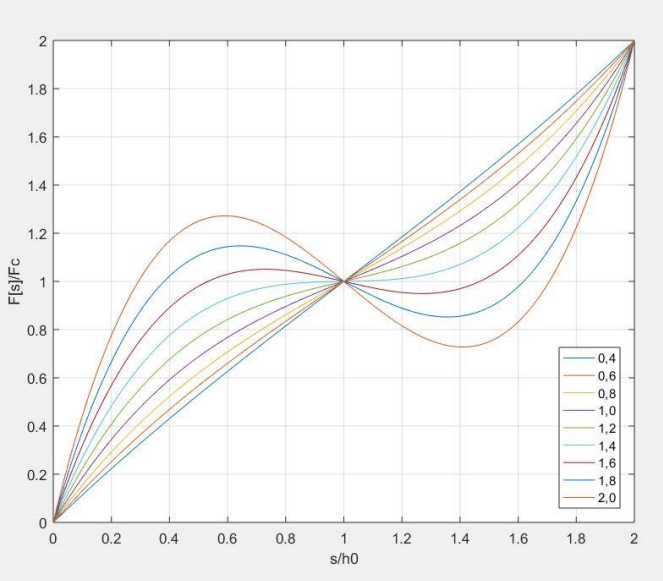

Figure 3.4: Calculated force-deflection characteristics of individual disc springs for different curve parameter κ using equation (3.10)

3.4. Stacks of disc springs

Disc springs can be stacked in different configurations to extend the application range of an individual one and cover higher forces and/or greater deflections.

3.4.1. Disc springs in series

An alternating stack of disc springs is regarded as in series disc spring configuration. In this case:

$$F_{stack} = F_{i=1} \tag{3.11}$$

and

$$s_{stack} = i \cdot s_{i=1} \tag{3.12}$$

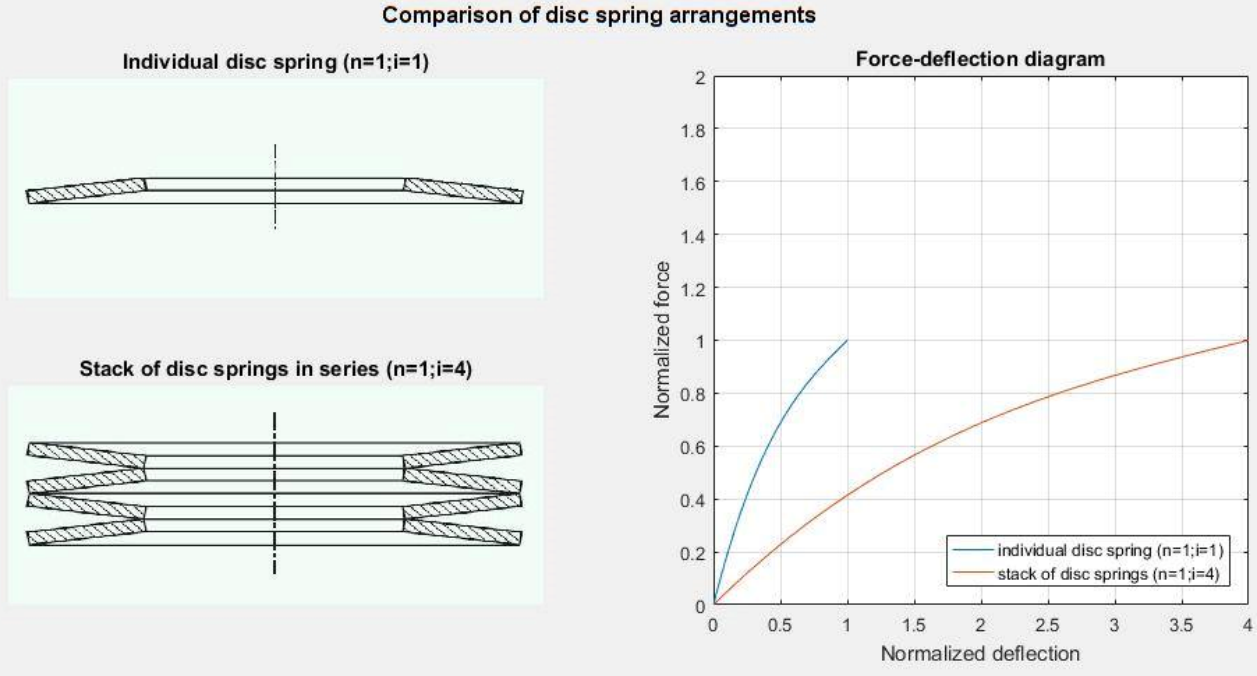

Figure 3.5: Behavior of disc springs in series versus individual disc spring. Left: Cross-sectional impression of individual disc spring (top) and disc springs stacked in series (bottom) (Christian Bauer (3), 2006). Right: Force-deflection diagram of four-disc springs stacked in series, in comparison with the individual one.

The effect of stacking disc springs in series is illustrated in Figure 3.5 (right). The force required to flatten the stack of disc springs is equal to the force required to flatten the individual one, however the deflection of the stack is i times greater than that of the individual one.

3.4.2. Disc Springs in parallel

When disc springs are applied in nested formation are regarded as in parallel configuration. In this case:

$$F_{stack} = n \cdot F_{n=1} \tag{3.13}$$

and

$$s_{stack} = s_{n=1} \tag{3.14}$$

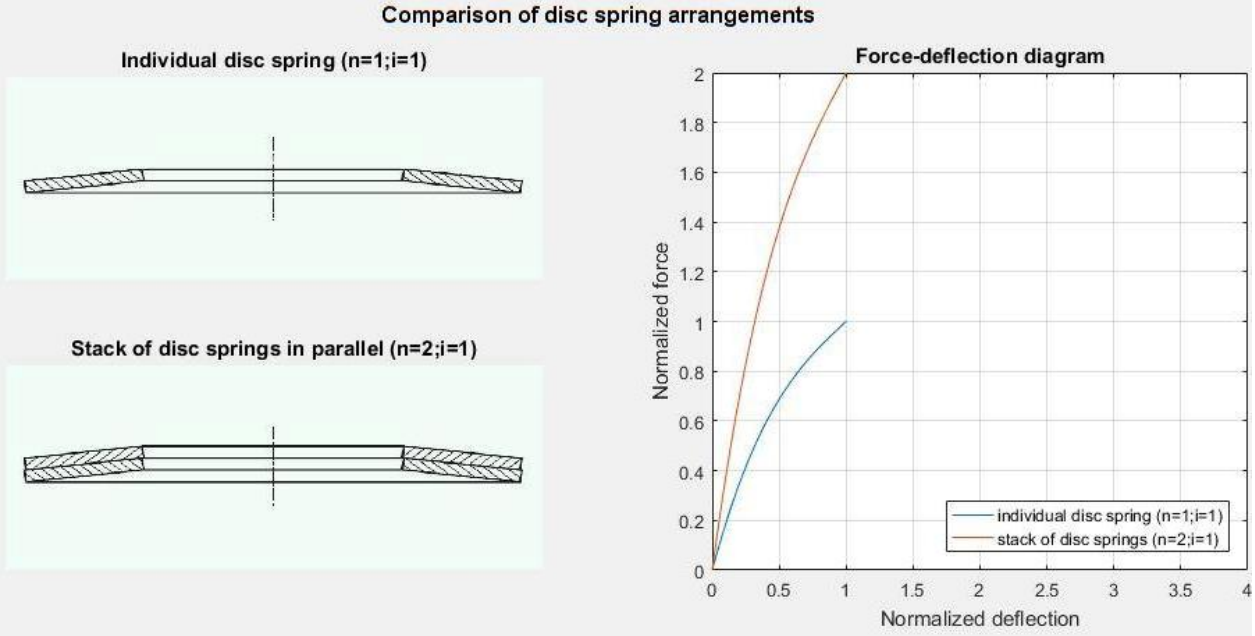

Figure 3.6: Behavior of disc springs in parallel versus individual disc spring. Left: Cross-sectional impression of individual disc spring (top) and disc springs stacked in parallel (bottom) (Christian Bauer (3), 2006). Right: Force-deflection diagram of two-disc springs stacked in parallel in comparison with the individual one.

The effect of stacking disc springs in parallel is illustrated in Figure 3.6(right). The force required to flatten the stack of disc springs is n times greater than the force required to flatten the individual one, however the deflection of the stack is equal to the deflection of the individual one.

3.4.3. Disc springs in parallel and in series

In case i alternating disc springs (in series) made up of n nested ones (in parallel) are stacked, the following applies:

$$F_{stack} = n \cdot F_{i=1,n=1} \tag{3.15}$$

and

$$s_{stack} = i \cdot s_{i=1,n=1} \tag{3.16}$$

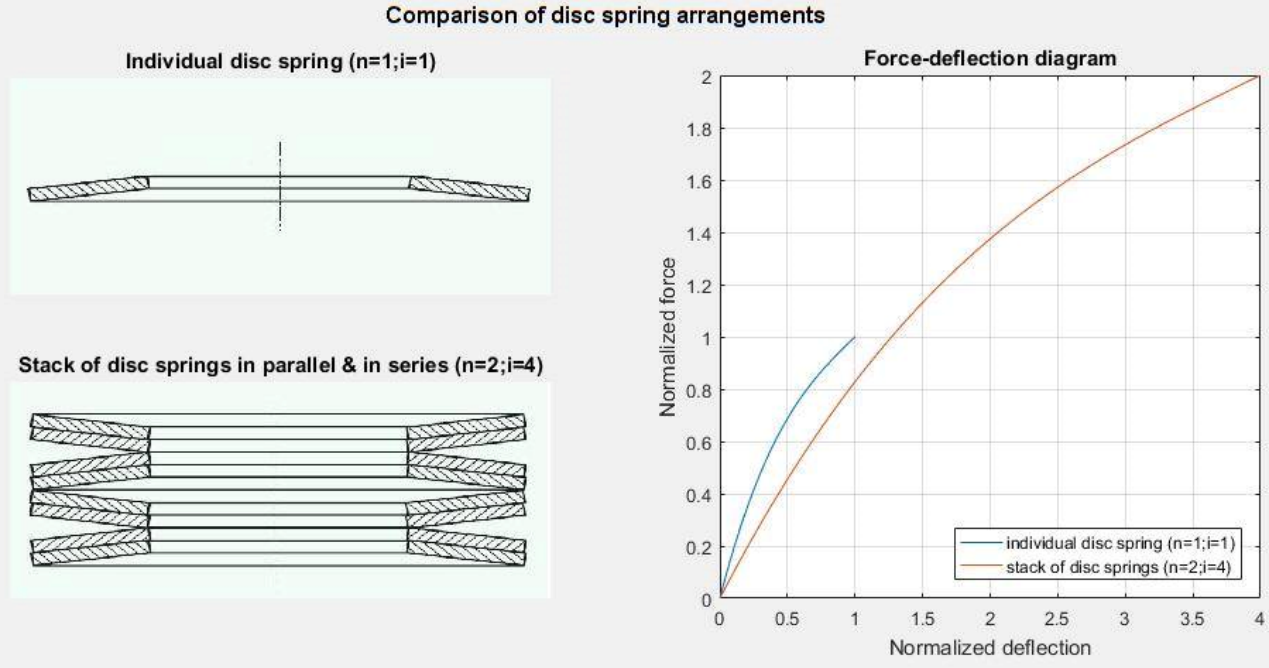

Figure 3.7: Behavior of disc springs stacked both in parallel & in series versus individual disc spring. Left: Cross-sectional impression of individual disc spring (top) and disc springs stacked both in parallel & in series (bottom) (Christian Bauer (3), 2006). Right: Force-deflection diagram of the stack of disc springs in comparison with the individual one.

The effect of stacking disc springs both in series and in parallel is illustrated in Figure 3.7(right). The force required to flatten the stack of disc springs is n times greater than the force required to flatten the individual one and the deflection of the stack is i times greater than that of the individual one.

To sum up the characteristic force-deflection curve of a stack of disc springs can be expressed with equation:

$$F[s] = F_c \cdot n \cdot \frac{s}{i \cdot h_0} \cdot \left[\left(\kappa - \kappa \cdot \frac{s}{i \cdot h_0}\right) \cdot \left(\kappa - \kappa \cdot \frac{s}{2 \cdot i \cdot h_0}\right) + 1\right] \tag{3.17}$$

3.5. Buffer-force function

The force deflection curve of a stack of disc springs has already been formulated. This is the decisive component regarding the force-displacement behavior of the buffer. Based on equation (3.17) the force-displacement diagram of the buffer can be developed.

Since the buffer's performance changes considerably with the applied force (from rigid to non-linear and vice versa), it will be described mathematically with the use of a piecewise function.

Prerequisites to determine the behavior of the buffer are:

- The properties of the disc springs used:
    - Individual disc spring characteristics (κ, h_0,F_c)
    - Disc spring stack configuration (n, i)
- Initial prestress of the buffer (F_p)
- Stroke of the buffer s_{str}

Once the characteristics of the individual disc spring are distinguished, one can refer to the corresponding table in (Christian Bauer (4), 2006) and read the curve parameter ($\kappa = \frac{h_0}{t}$ or $\kappa \cdot \frac{h_0'}{t'}$), the deflection of the disc spring in flat condition (h_0, or h_0') and the spring force in flat condition (F_c). These data in combination with the stacking arrangement info comprise the required inputs of formula (3.17). Hence, the force-deflection curve of the stack of disc springs under consideration can be drawn.

The stack of disc springs is active in a specific region, defined by the initial prestress and the stroke of the buffer. This information in addition to formula (3.17) is used to define the range where the stack of disc springs is active.

In theory, the buffer's force displacement characteristic can be expressed with the following piecewise function:

$$F_{buffer}[s] = \begin{Bmatrix} -\infty\,, & s < -s_{str} \\ -F\left[s_p + |s|\right]\,, & -s_{str} \leq s < 0 \\ \left[-F_p\ F_p\right]\,, & s = 0 \\ F\left[s_p + s\right]\,, & 0 < s \leq s_{str} \\ \infty\,, & s > s_{str} \end{Bmatrix} \tag{3.18}$$

In practice the aforementioned formula is modelled following the subsequent process.

First, the magnitude of initial compression of the stack of disc springs in the buffer is calculated based on the initial prestress. This is achieved by solving the following equation:

$$F[s] = F_p \tag{3.19}$$

The real root of this equation is called s_p ($s_{prestress}$) where $F[s_p] = F_p$. Then, the vertical branch of the force displacement characteristic of the buffer is constructed. The rigid behavior of the buffer, until the prestressing force is reached, is modelled as a linear function of displacement with very high stiffness. A factor l_{dsp} is introduced where:

for $s \in [-l_{dsp},\ l_{dsp}]$

$$F_{buffer}[s] = \frac{F[l_{dsp} + s_p]}{l_{dsp}} \cdot s \tag{3.20}$$

and the resulting buffer force ranges in the interval:

$F_{buffer} \in [-F[l_{dsp} + s_p],\ F[l_{dsp} + s_p]]$

For very small values of l_{dsp}close to zero, the above mention ranges result in:

for $s \in \lim_{l_{dsp}\to 0} [-l_{dsp},\ l_{dsp}] = [0]$ with

$$F_{buffer} \in \left[-\lim_{l_{dsp}\to 0} F[l_{dsp} + s_p],\ \lim_{l_{dsp}\to 0} F[l_{dsp} + s_p]\right] = [-F[s_p],\ F[s_p]]$$

which is the exact force displacement behavior of the buffer around zero displacement as described in the theoretical formula (3.18). Therefore, it is proved that the proposed linear approximation is a good one for very small values of the factor l_{dsp}.

Afterwards, as soon as the prestressing force is exceeded, the stack of disc springs becomes active until the stroke of the buffer is reached. At this range, the force deformation behavior of the buffer is described based on the formula (3.17). The mathematical representation of this branch is the following:

for $s \in (l_{dsp},\ s_{str}]$

$$F_{buffer}[s] = F[s_p + s] \tag{3.21}$$

and for $s \in [-s_{str}, -l_{dsp})$

$$F_{buffer}[s] = -F\left[s_p + |s|\right] \tag{3.22}$$

Finally, once the stroke of the buffer is reached, it behaves again as a rigid component. Hence, at this range the force deformation behavior of the buffer is modelled again as a linear function of displacement with the same high stiffness as in the initial case. The mathematical representation of this branch is the following:

for $s \in (s_{str}, +\infty)$

$$F_{buffer}[s] = \frac{F[l_{dsp} + s_p]}{l_{dsp}} \cdot (s - s_{str}) + F[s_p + |s_{str}|] \tag{3.23}$$

and for $s \in (-\infty, s_{str})$

$$F_{buffer}[s] = \frac{F[l_{dsp} + s_p]}{l_{dsp}} \cdot (s + s_{str}) - F[s_p + s_{str}] \tag{3.24}$$

To conclude, the force displacement characteristic of the buffer is modeled in the code with the following piecewise function:

$$F_{buffer}[s] = \begin{cases} \frac{F[l_{dsp} + s_p]}{l_{dsp}} \cdot (s + s_{str}) - F[s_p + |s_{str}|], & s < -s_{str} \\ -F\left[s_p + |s|\right], & -s_{str} \le s < -l_{dsp} \\ \frac{F[l_{dsp} + s_p]}{l_{dsp}} \cdot s, & -l_{dsp} \le s \le l_{dsp} \\ F\left[s_p + s\right], & l_{dsp} < s \le s_{str} \\ \frac{F\left[l_{dsp} + s_p\right]}{l_{dsp}} \cdot (s - s_{str}) + F\left[s_p + s_{str}\right], & s > s_{str} \end{cases} \tag{3.25}$$

3.6. Example of formula application

The aforementioned process is depicted with the following application. The input parameters of the application are:

Table 3.1: Inputs of the application

κ	1,2	i	10
h_0	0,3 mm	F_p	150 N
F_c	62,6 N	s_{str}	1,5 mm
n	5	l_{dsp}	0,001 mm

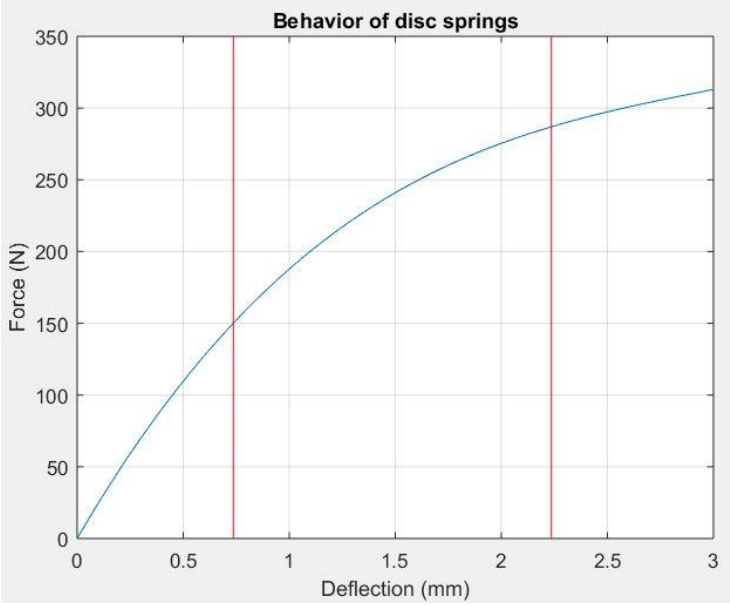

Figure 3.8: Force-deformation behavior of the assumed stack of disc springs

First, the characteristic force deformation curve of the stack of disc springs under consideration is plotted using formula (3.17). In Figure 3.8 it is illustrated with blue. Afterwards, the range where the stack of disc springs is active is defined. Solving equation (3.19) in terms of the unknown deformation, the left vertical red boundary of Figure 3.8 is determined. The right vertical red boundary of Figure 3.8 is in a distance of the left one equal to the stroke of the buffer.

The generalized force-displacement diagram is drawn using formula (3.25) and is depicted in Figure 3.9 (top left). The continuity of this diagram is checked, plotting it closer at the positions where its behavior changes (Figure 3.9).

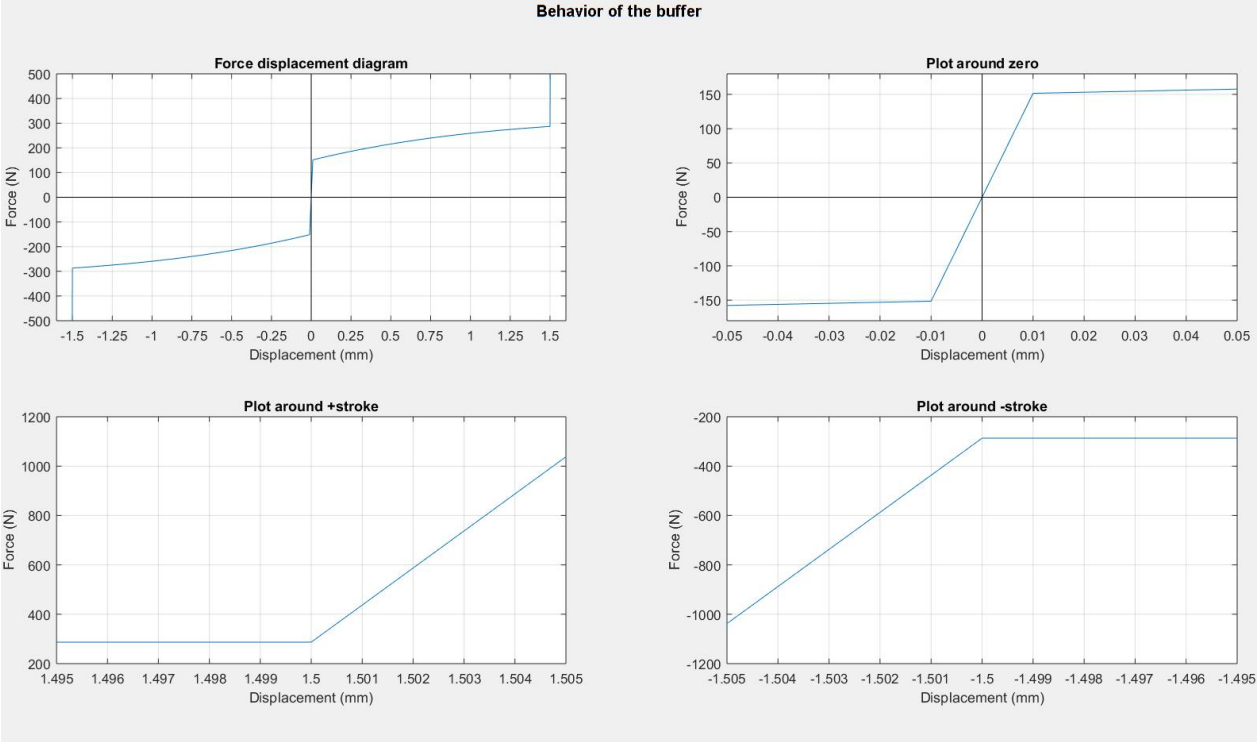

Figure 3.9: Generalized force-displacement diagram of the buffer (top left) and particular plots around zero (top right) and ± stroke (bottom left & right)

3.7. Hysteresis in disc springs

Depending upon the spring arrangement, frictional forces arise during the compression and extension of the springs. There are several positions in a stack of disc springs where friction is generated and are listed below (Figure 3.10):

1. internally in the material (1)
2. at edges of the springs where the load (2)
3. between springs and the guided rod (3)
4. between individual springs (4)

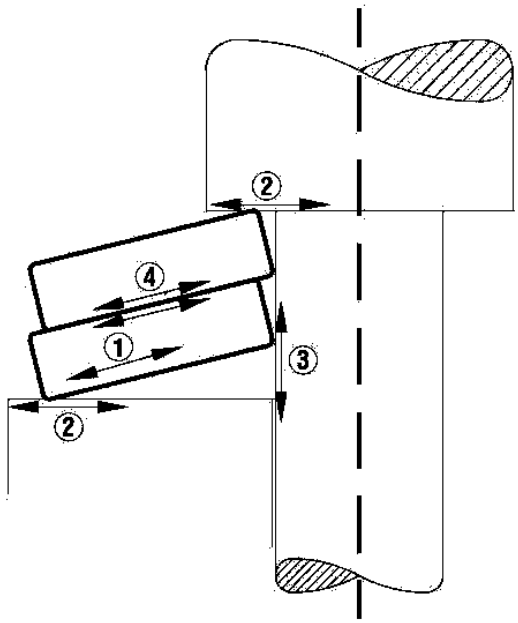

Figure 3.10: Impression of positions where friction is generated in a stack of disc spring (Schnorr, 1997)

The internal friction of the material is not regarded in this analysis. Moreover, according to (Christian Bauer (3), 2006) ,it is mentioned that the amount of friction between the stack of disc springs is not quantified yet in the existing standard DIN 2092:2006:03 (2006).

The effect of friction between adjacent disc springs in the characteristic force-deformation curve of a stack of disc springs is described next. In case of loading, the frictional forces create a moment in the disc spring that counteracts the moment created by the applied load, thus increase the required compressive applied load. When unloading, the moment caused by frictional forces acts in the same direction with that of the applied load, therefore reduces the required retaining force.

The frictional force in a stack of n stacked disc springs can be expressed with the following formula according to the standard DIN 2092:2006:03 (2006):

$$F_{fr} = \pm(w_M \cdot (n-1) + w_R) \cdot F_{stack} \tag{3.26}$$

in which:

w_M is the coefficient of friction between two individual disc springs;

$n-1$ are the numbers contact surfaces between n nested disc springs;

w_R is the coefficient of friction at the edge of a stack of disc springs;

F_{stack} is the vertical applied load at the stack of disc springs.

In case of loading the frictional force, F_{fr} takes a minus sign and in case of unloading F_{fr} becomes positive.

The effect of friction in the force deflection diagram of a stack of disc springs is depicted in Figure 3.11 The hysteresis of the force deflection diagram of a stack of disc springs depends on the number of disc springs in parallel. Increasing the parallel disc springs' formation, the hysteresis effect is more significant.

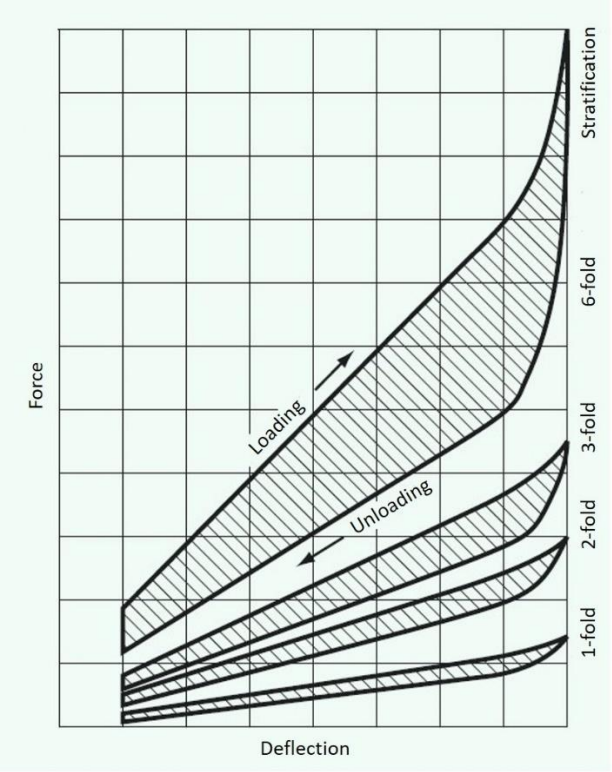

Figure 3.11: Hysteresis of the force deflection diagram of different stack of disc springs due to friction in the interface of adjacent disc springs depending on the number of springs in parallel (Christian Bauer (3), 2006)

In the dynamic model the frictional force is introduced in the form of Coulomb damping force. The Coulomb damping is expressed as:

$$F_{fr} = \mu \cdot N \cdot sign[\dot{x}] \tag{3.27}$$

in which:

$\dot{x}$ is the velocity;

N is the normal reaction force between the sliding surfaces;

μ is the friction coefficient.

Thus, the friction in a stack of the disc springs is then modeled with formula:

$$F_{fr}[s,\dot{s}] = (w_M \cdot (n-1) + w_R) \cdot \left|F_{buffer}[s]\right| \cdot sign[\dot{s}] \tag{3.28}$$

The use of absolute value in formula (3.28) must be underlined. When the buffer is loaded either in tension or compression, the force due to friction must have the same sign with the force of the buffer. In case the buffer is unloaded either in tension or compression the force due to friction must have an opposite sign compared with that of the force of the buffer. These are accomplished with the used of the absolute values in formula (3.28). In the case that the absolute value of the buffer force was not used in formula (3.28), when loading and unloading in compression, the force due to friction would not have the expected sign. The validity of this statement is checked in chapter 4.

In the upcoming analyses, in formula (3.28) a global friction coefficient (μ) is introduced to account for all possible friction coefficients in different positions in a stack of disc springs (Eq. (3.29)).

$$F_{fr}[s,\dot{s}] = \mu \cdot (n-1) \cdot \left|F_{buffer}[s]\right| \cdot sign[\dot{s}] \tag{3.29}$$

This Master's thesis is concerned with the effect of the global disc springs' friction in the force-deformation behavior of the buffer and in the response of the system in terms of decisive dynamic loads. The detailed research on the magnitude of each friction coefficient and its contribution separately comprises a research topic on itself which needs also experiments and additional information. Therefore, it is out of the scope of this thesis.

4. Buffer force evaluation

4.1. Introduction

In this chapter the buffer force and the associated frictional force derived in chapter 3 are evaluated performing dynamic analyses of a SDoF dynamic model. Hereby, the validity of the proposed formulas regarding the buffer force and its accompanied internal friction is evaluated. This allows one to trace any, possible mistakes in the assumptions made in chapter 3 regarding the derivation of the idealized buffer force and the corresponding frictional term.

The dynamic model under consideration, consists of a buffer with a mass attached to one end, while the other end is being fixed to an immovable boundary. The configuration of the SDoF oscillator is illustrated in Figure 4.1. The buffer is described by two terms; one concerns the buffer's characteristic force deformation and the other one accounts for its frictional damping generated by friction at the interface of the disc springs.

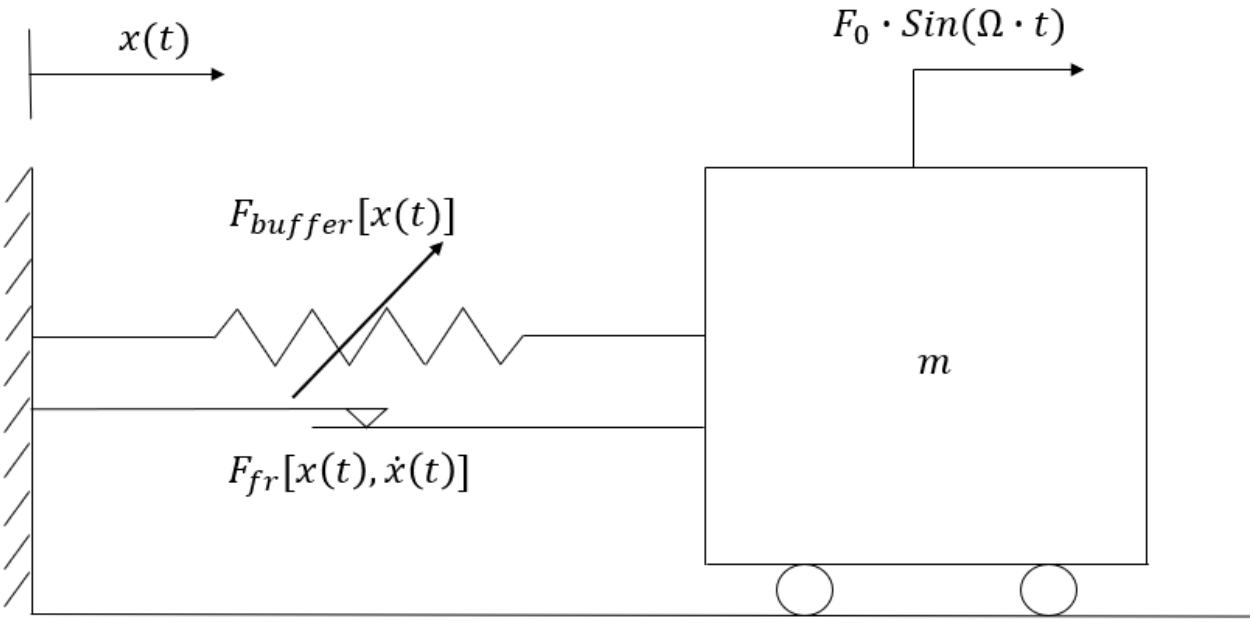

Figure 4.1: SDof oscillator composed of a buffer and a mass excited harmonically

4.2. Dynamic analysis

A number of forced vibration dynamic analyses under harmonic loading are performed in the system and the response of it in terms of mass displacement and buffer force is evaluated. The equation of motion of the system is:

$$m \cdot \ddot{x}(t) + F_{buffer}[x(t)] + (\mu \cdot (n-1)) \cdot \left|F_{buffer}[x(t)]\right| \cdot sign[\dot{x}(t)] = F_0 \cdot \sin(\Omega \cdot t) \quad (4.1)$$

wherein Eq.(4.1), the following quantities are introduced

m is the mass attached to the buffer;

$x(t)$ is the horizontal displacement of the mass;

F_{buffer} is the buffer force as determined in (3.25) of chapter 3;

μ is the friction coefficient of the buffer;

F_0 is the amplitude of the external harmonic load;

Ω is the excitation frequency.

In the upcoming analyses the inputs for the buffer force are the same as in Table 3.1 of chapter 3. The variables of the analyses are:

- The mass
- The excitation frequency and the amplitude of the external harmonic load
- The friction coefficient of the buffer

Regarding the influence of each of these variables in the dynamic response of the system, it is desired to perform a primary analysis for a first check of the buffer's modeling. For that reason, the following assumptions are made:

- The mass of the system is assumed to be equal to $m = 1ton = 1000kg$
- The amplitude of the external force is assumed to be higher than the force corresponding to the stroke of the buffer. Referring to Figure 3.9 the stroke of the buffer is reached at approximately $300N$. Thus, it is adopted $F_0 = 350N$
- The excitation frequency is estimated such that the period of the load is approximately 30s i.e. $\Omega = \frac{1}{5}\frac{rad}{s}$.
- The friction coefficient of the buffer is assumed $\mu = 0{,}02$

The dynamic response of the SDoF oscillator in terms of horizontal displacement of the mass is illustrated in Figure 4.2, drawn with a blue line. The orange line represents the harmonic part of the external loading.

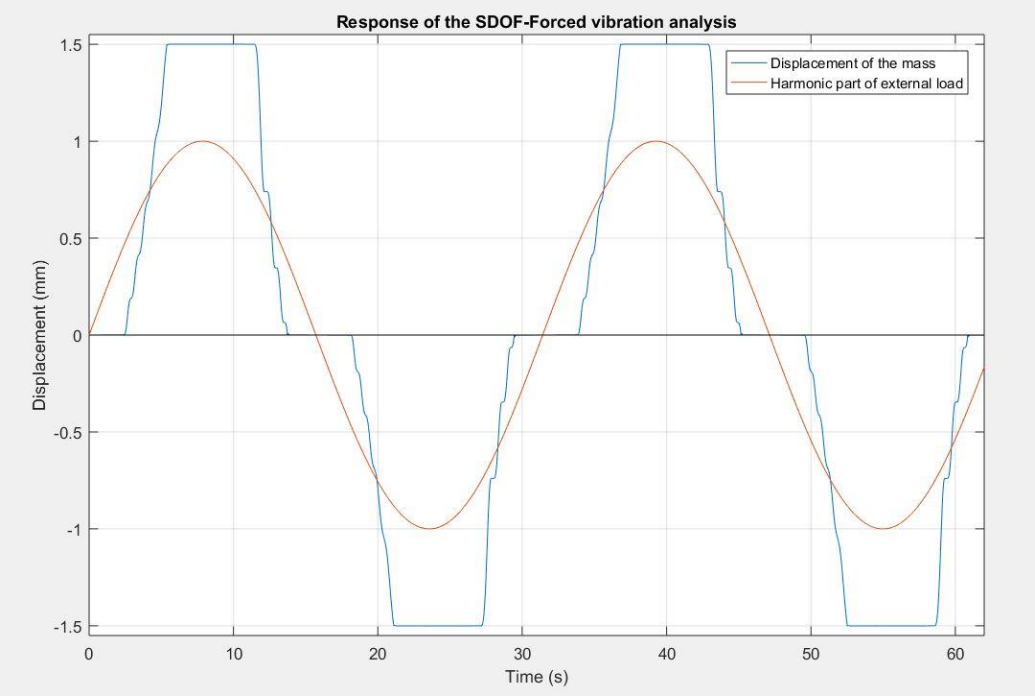

Figure 4.2: Response of the SDoF oscillator in term of displacement of the mass

The displacement of the mass shows the expected behavior. It is expected that the motion of the mass follows the deformation of the buffer. The buffer is rigid, both in tension and compression, for loading less than its prestress or higher than the load corresponding to its stroke. In these regions the mass should be immobile. This is exactly what is shown in Figure 4.2. The external load at $t = 0$ is zero and starts to increase harmonically. The mass is not moving until the external load surpasses the prestress of the buffer and the additional load due to friction. Afterwards the external load continues to increase resulting in motion of the mass. Once the stroke of the buffer ($1{,}5mm$) is reached it cannot be stretched further and the mass stops moving at that position even if higher load is applied. The same behavior is followed in unloading as well as when the buffer is compressed

Moreover, the force-deformation relationship of the buffer is checked. For that reason, the two following tables are filled:

$$Table\left[x(t), F_{buffer}[x(t)]\right] \tag{4.2}$$

$$Table\left[x(t), F_{buffer}[x(t)] + (\mu \cdot (n-1)) \cdot \left|F_{buffer}[x(t)]\right| \cdot sign[\dot{x}(t)]\right] \tag{4.3}$$

The first table refers to the buffer's characteristic force-deformation without taking into account the global friction in the stack of disc springs, whilst the second one accounts for it. The entries of tables (4.2) and (4.3) are plotted in Figure 4.3 in orange and blue respectively.

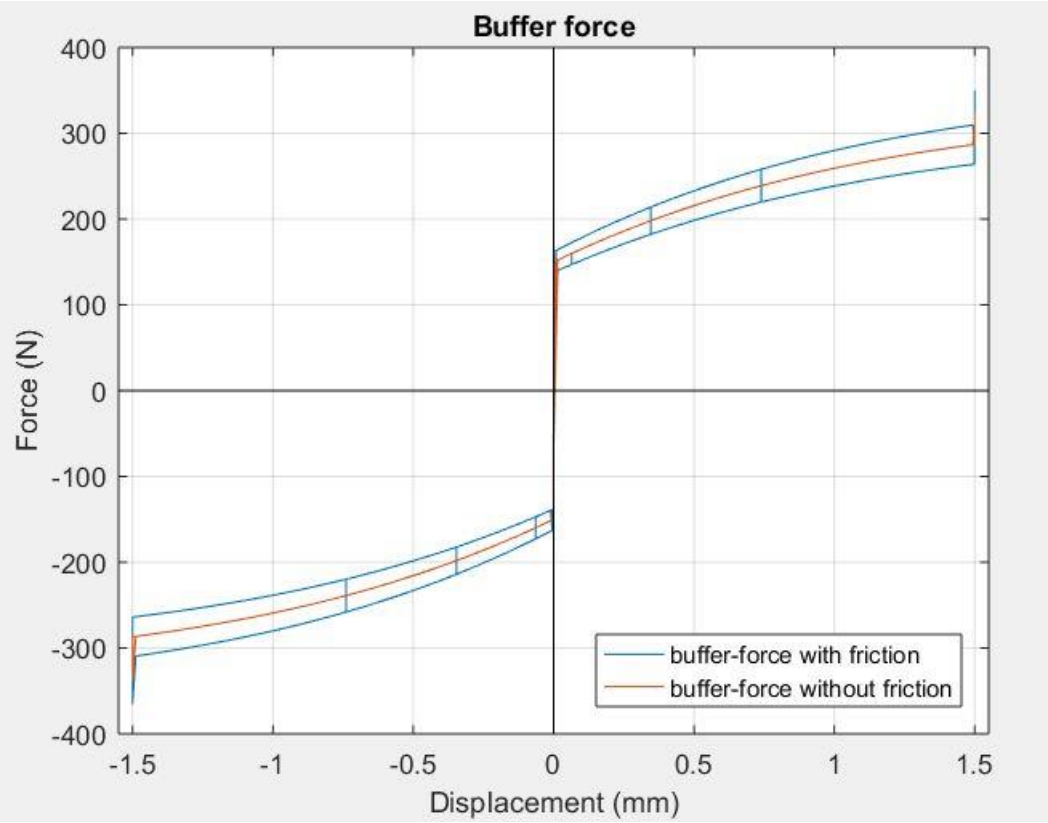

Figure 4.3: Characteristic force deformation diagram of the buffer with friction (blue line) and without friction (orange line) taken into account.

The blue line in Figure 4.3 follows a hysteretic behavior due to the influence of friction as is expected according to the review in the technical documents of the manufacturer (Christian Bauer (3), 2006). The kick shown at the end of the plots in both positive and negative direction results from the state of the buffer after reaching its maximum deformation. There it becomes a rigid component undeformable with the increase of the applied force. The hysteresis of the buffer in Figure 4.3 shows a proper behavior.

With this simple analysis, it is verified the proper consideration for the modeling of the generalized buffer force displacement function (Eq.(3.24)) and its associated frictional force (Eq.(3.29)) in chapter 3.

After the assessment of the buffer's modeling in the SDoF oscillator and before proceeding to the incorporation of it in the dynamic model of the movable bridge-machinery system, a sensitivity analysis is carried out in this model regarding the influence of the four variables mentioned before.

4.2.1. Influence of the amplitude of the external force

In this sub-section the influence of the amplitude of the external force in the dynamic response of the SDoF oscillator is evaluated. The three other variables (mass, frequency of excitation, friction) are kept constant assigning the same values as in the analysis of section 4.2. The displacement of the mass is plotted for different values of the amplitude (F_0) in Figure 4.4.

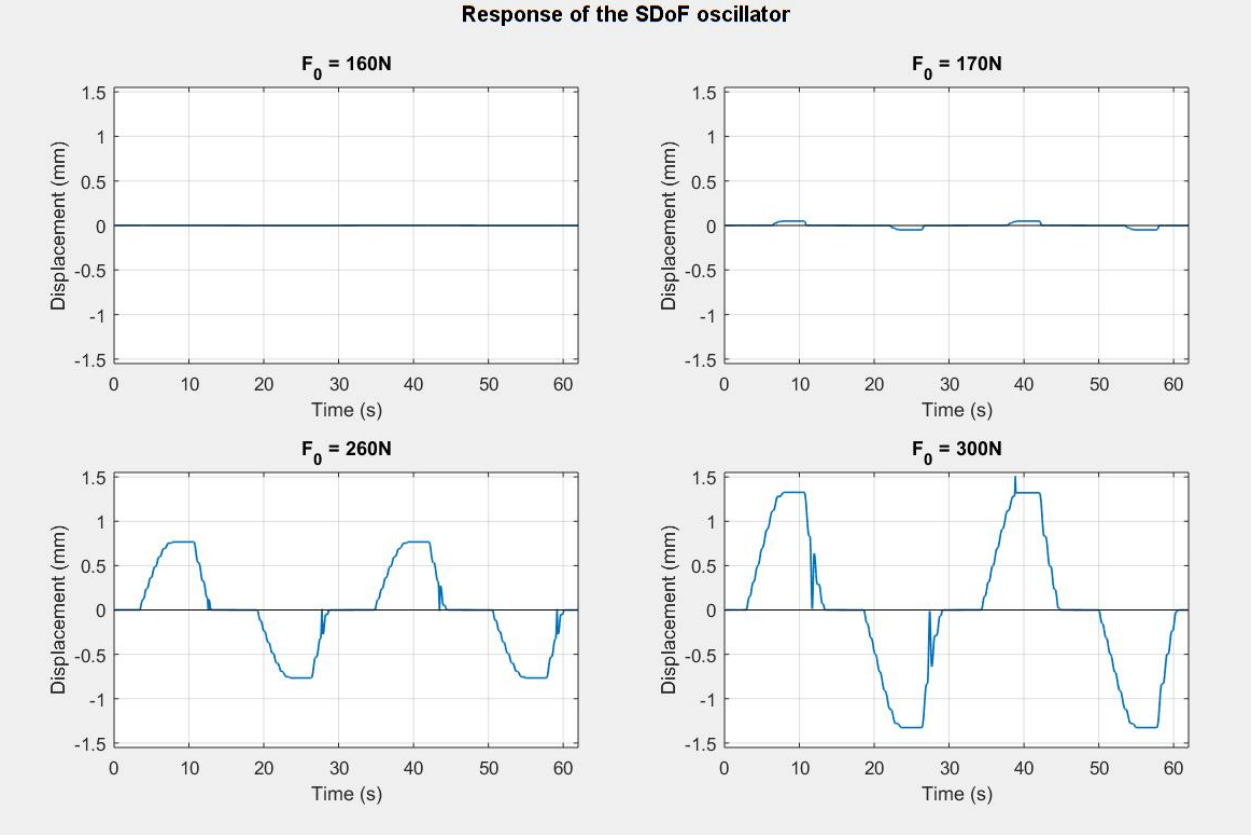

Figure 4.4: Displacement of the mass of the SDoF oscillator for different amplitudes of external loading (F_0)

Until a certain loading level is reached, the mass is at rest (Figure 4.4). Due to friction and the corresponding hysteretic behavior of the disc springs the buffer behaves in a stiffer manner when loading. This in turn, results in a higher load requirement for deformation, than the prestress of the disc springs. This stiffer behavior is also observed at the load needed so as to reach the stroke of the buffer. These observations are also illustrated in the plots of the preliminary analysis (Figure 4.3).

In addition, a horizontal plateau is observed at the peaks of the mass' displacement (Figure 4.4). This behavior can be explained inspecting the hysteretic force-deformation performance of the buffer. For that reason, the response of the system in terms of displacement of the mass and the associated buffer force-displacement diagram are plotted for amplitude of external load $F_0 = 200N$ (Figure 4.5). It is illustrated that unloading the system from maximum load, the buffer behaves rigid in a certain range of unloading, resulting in a vertical plateau in the force deformation diagram, where the force of the buffer is reduced

and at the same time it does not deform (Figure 4.5(Right)). Thus, at that range the displacement of the mass is kept constant at its maximum value.

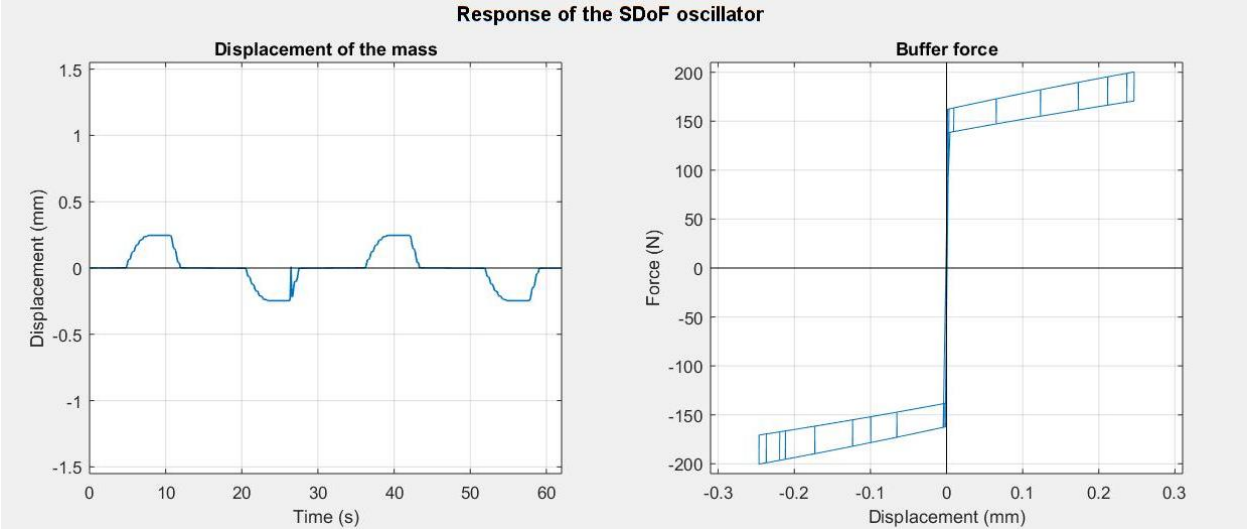

Figure 4.5: Response of the SDoF oscillator in forced vibration analysis under harmonic load ($F_0 = 200N$). Left: Displacement of the mass versus time. Right: Force-displacement diagram of the buffer

4.2.2. Influence of friction

The influence of friction in the dynamic response of the SDoF oscillator is examined here. The three other variables (mass, amplitude of external load, frequency of excitation) are kept constant assigning the same values as in the analysis of section 4.2.

The influence of friction is evaluated carrying out forced vibration analyses and free vibration analyses in the system. In the first case the buffer's force-displacement diagram is plotted (Figure 4.6), whilst in the second case the displacement of the mass is drawn (Figure 4.7). In the free vibration analyses an initial displacement is given to the mass equal to the stroke of the buffer with zero initial velocity.

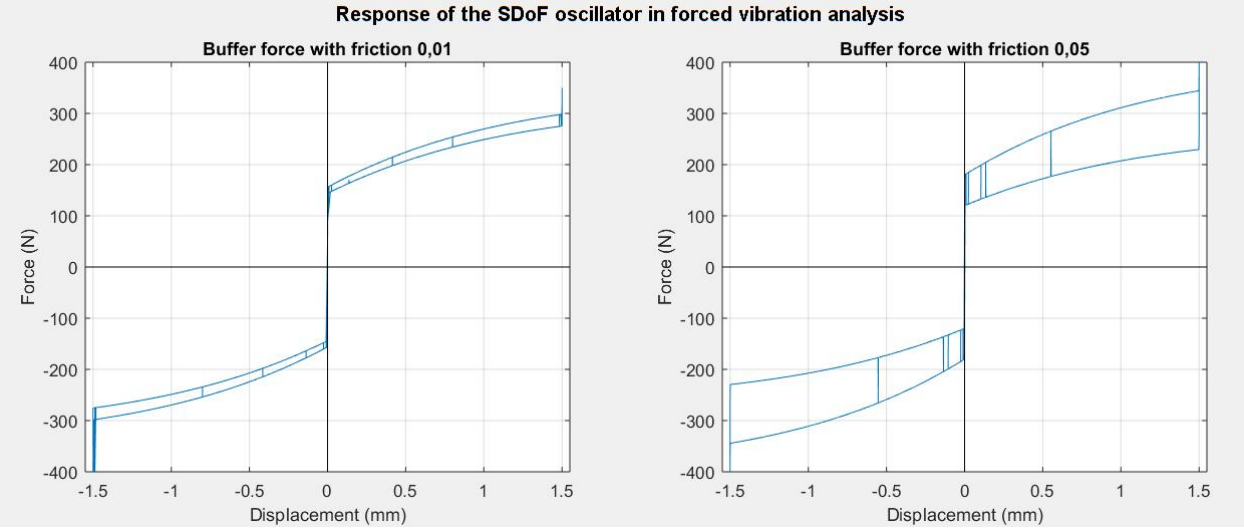

Figure 4.6: Resulting buffer's force-displacement diagram for different friction coefficients in forced vibration analysis.

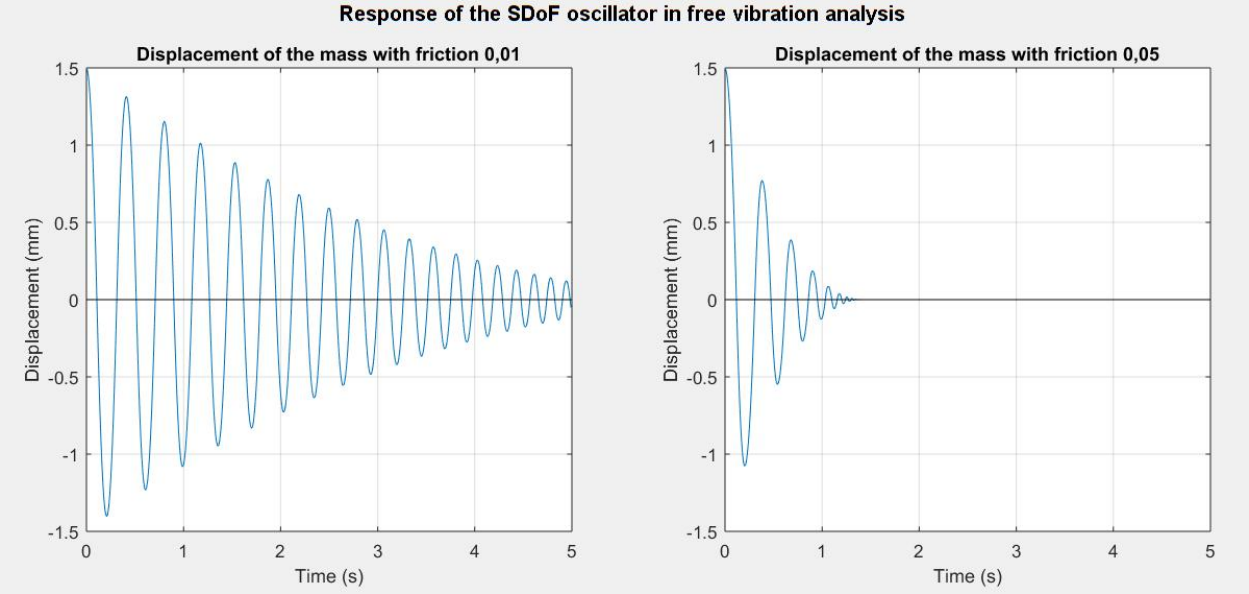

Figure 4.7: Resulting displacement of the mass for different friction coefficients in free vibration analysis.

Having a look at the resulting buffer's force (Figure 4.6), with the increase of the friction coefficient, the hysteresis of the disc springs becomes larger as it is supposed (Ch.3). Moreover, examining the response of the system in free vibration analysis (Figure 4.7), the displacement of the mass decays faster with the increase of friction, which is also anticipated.

4.2.3. Influence of mass

In this sub-section, the influence of the mass in the response of the SDoF oscillator is examined. In the corresponding analyses the mass of the system is increased and its resulting displacement versus time is

plotted. The three other variables (friction, amplitude of external load, frequency of excitation) are kept constant assigning the same values as in the analysis of section 4.2.

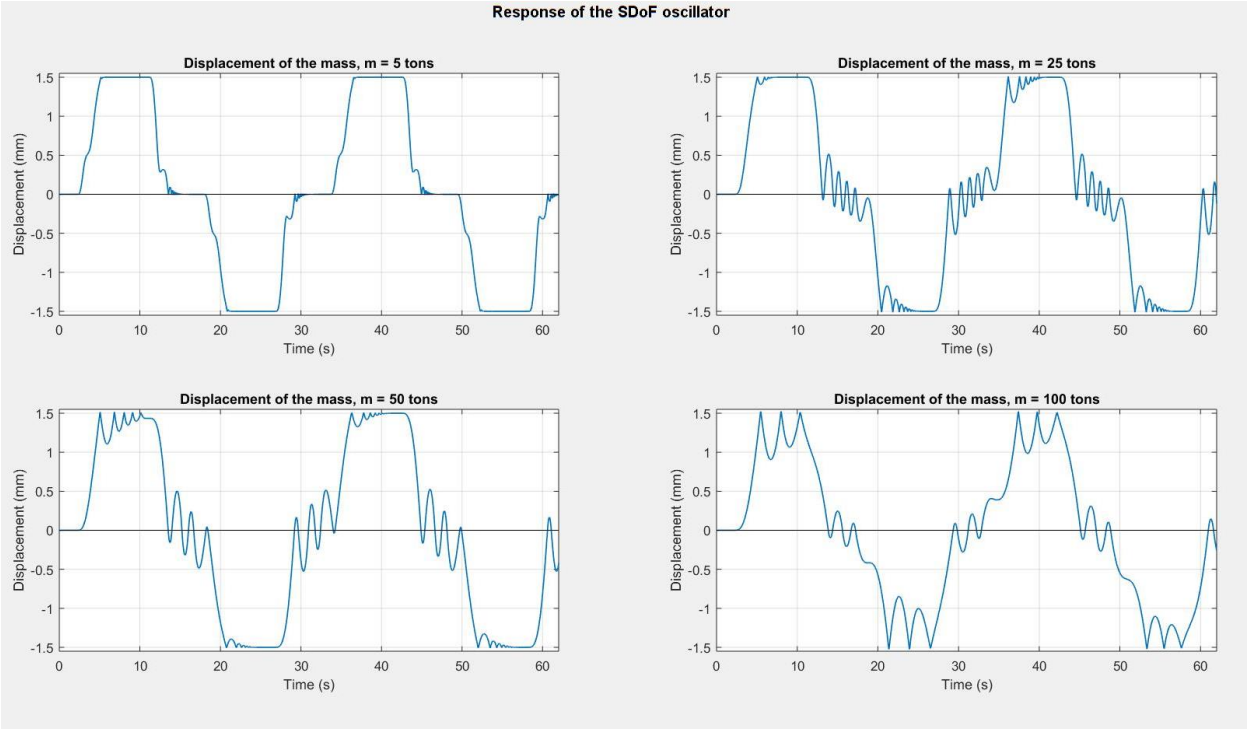

Figure 4.8: Displacement of the mass for different mass magnitudes.

Increasing the mass of the system a short of vibration is generated in the areas where the buffer is rigid (Figure 4.8). Having a closer look, once the mass reaches the maximum displacement, reacts like hitting an obstacle and repels backwards. Since the external loading does not change direction in this stage of motion, it drags the mass and it reaches again the maximum, resulting in repetition of this behavior. This outcome generates the interest to study further this phenomenon. What happens is that the buffer reaches its maximum deformation and cannot be stretched further. However, this case could be also realized, when instead of restricting the deformation of the buffer, limit the displacement of the mass by applying a stop. Influenced by this last interpretation, a literature review is carried out regarding dynamic analyses in impact oscillators.

According to (Budd & Dux, 1994) the phenomenon of infinite number of impacts in a finite time (vibro-impacts) is called chatter. In the same paper, the displacement of the mass versus time shows the same behavior as in the SDoF oscillator that is considered in this chapter. In (Wagg & Bishop, 2001) it is mentioned that if the sequence of impacts are long enough the velocity of the impacting mass tends to zero such that the mass becomes stick to the stop. In case the mass stops vibrate the chatter is complete and the mass has stuck, whilst in case the mass is not stick the chatter phenomenon is incomplete. In the response of the SDoF oscillator, complete chatter is observed for masses (25tons,50tons), whereas for mass equal to (100tons) it is incomplete.

The chatter phenomenon is more apparent while the mass of the system increases keeping all the other inputs the same.

The increase in the "rebound" is supposed that is influenced by the change in the momentum of the mass. To examine this, the change in velocity at the time the mass reaches the first maximum is calculated. Afterwards the associated change in the momentum is calculated and the results are summarized in Table 4.1.

Table 4.1: Change in momentum of the mass when it reaches the maximum at first time, for different mass magnitudes

Mass (ton(s))	Change in momentum (kg·(m/s))
1	-2,02946
5	-4,76568
25	-24,0777
50	-83,3516
100	-178,385

The results of the calculations in Table 4.1 indicate that the increase in the magnitude of the mass results in an increase in the change of momentum the time the mass reaches the maximum displacement at first time. This corresponds to larger impulse and consequently larger "rebound".

To make this statement concrete, a final analysis is carried out with mass equal to 100 tons, while the excitation frequency is reduced to $\frac{1}{10}\ \frac{rad}{s}$. The response of the systems with mass equal to 100 tons and excitation frequencies $\frac{1}{5}\ \frac{rad}{s}$ and $\frac{1}{10}\ \frac{rad}{s}$ respectively is plotted in Figure 4.9.

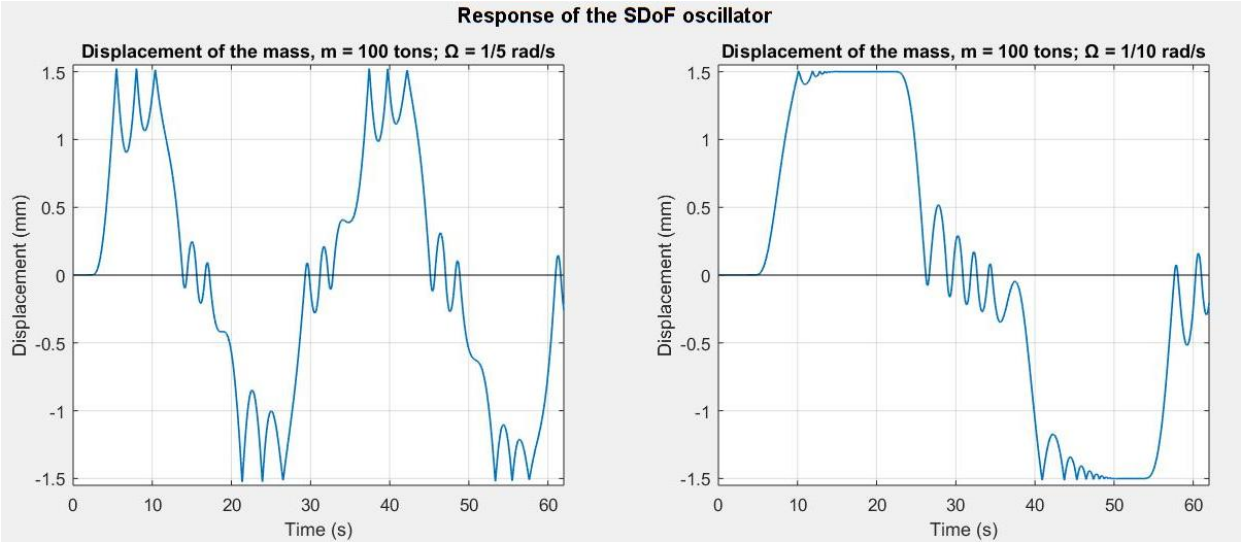

Figure 4.9: Displacement of the mass for mass magnitude 100 tons for different excitation frequency

It is observed that the chatter phenomenon for the same mass is less significant for lower excitation frequency than in the analysis with double frequency of excitation. Here, again the change in momentum when the mass reaches for the first time the maximum displacement is calculated. The result of the

analysis with lower excitation frequency is compared with the last line of Table 4.1, and both are summarized in Table 4.2.

Table 4.2: Change in momentum of the mass when it reaches the maximum at first time, for the same mass magnitude and different excitation frequency

Mass (tons)	Excitation frequency (rad/s)	Change in momentum (kg·(m/s))
100	1/5	-178,385
100	1/10	-48,1323

The last analysis verified the conclusion that the chatter phenomenon in the SDoF oscillator is influenced by the change in the momentum of the mass when it reaches the maximum. The magnitude of the mass influences the change in the momentum however it is not the only factor that does so as it is shown in Figure 4.9.

4.2.4. Influence of the excitation frequency

The last variable to be examined regarding its influence in the response of the SDoF oscillator, is the excitation frequency. In the last analysis of the previous sub-section the external frequency was reduced to half so as to observe its contribution in the change of momentum of the mass and the associated influence in the phenomenon of chatter.

In this sub-section the excitation frequency is decided to be increased and again observe the corresponding displacement of the mass. The three other variables (mass, amplitude of external load, friction) are kept constant assigning the same values as in the analysis of section 4.2.

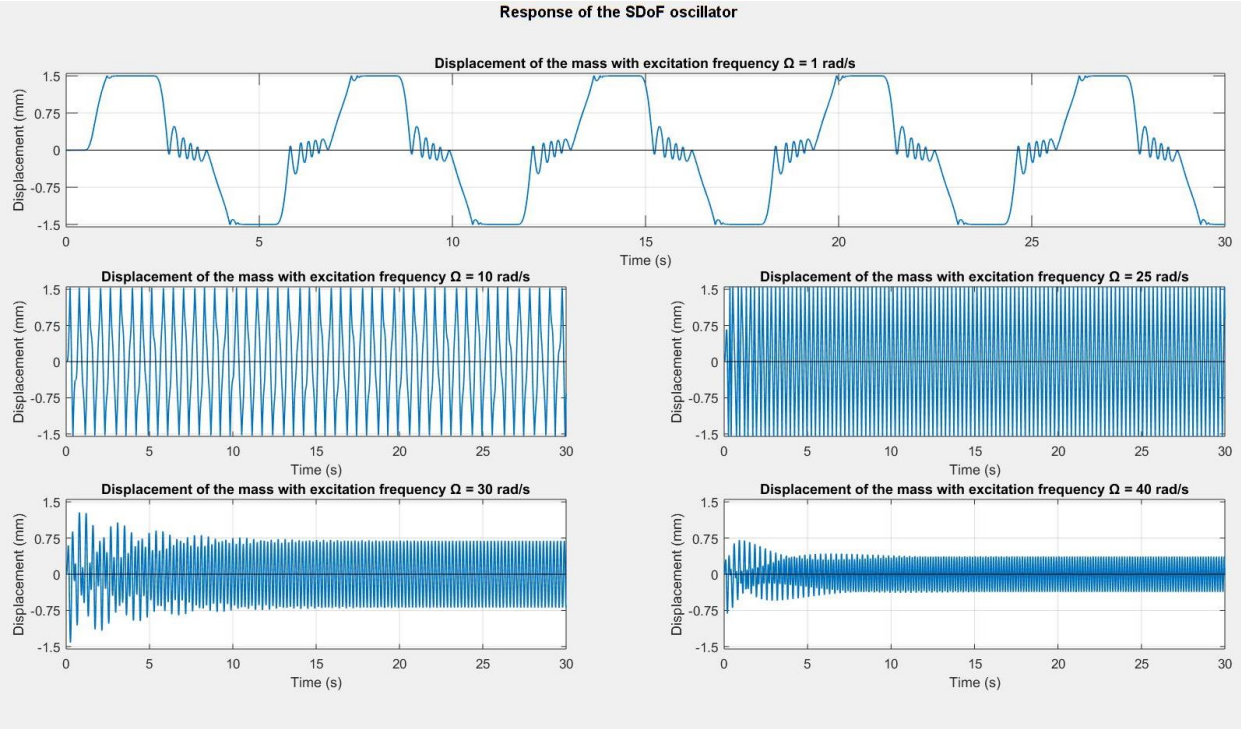

Figure 4.10: Displacement of the mass for different excitation frequencies

With the increase of the frequency of excitation, the period of the forced vibration reduces (Figure 4.10). The amplitude of the displacement is still restricted by the stroke of the buffer in both directions. However, for frequencies higher than 30 rad/s the amplitude of the mass displacement is almost half of the stroke of the buffer and decreases with the increase of the external frequency. This behavior is expected since it is present in every dynamical system, since for high frequencies the response tends to zero.

5. Dynamic model of the bridge-machinery system

5.1. Introduction

In the previous chapters, the methodology of modeling the buffer is discussed and its associated hysteretic behavior due to friction is illustrated. Furthermore, the validity of the proposed modeling approach is evaluated with a simple dynamic model, assessing the dynamic response of the SDoF oscillator including the buffer. This chapter aims to establish the equations of motion of the bridge-machinery system, including the buffer component.

5.2. New lumped mass model

To start with, it is decided to add a degree of freedom in the equations of motion, as described in sub-section 2.4.2, in order to incorporate the buffer. Influenced by the configuration of the system, this degree of freedom is chosen to be the Panama wheel. The mass moment of inertia of a Panama wheel is extremely smaller compared to that of the bridge. Referring to the study performed in chapter 2, the addition of a very small mass has a minor influence on the response of the system in terms of decisive dynamic load at the motor shaft. The new dynamic model of the system is illustrated in Figure 5.1. This model has three degrees of freedom, where $r_1(t)$ is the rotation of the motor, $r_2(t)$ is the rotation of the Panama wheel and $r_3(t)$ is the rotation of the bridge.

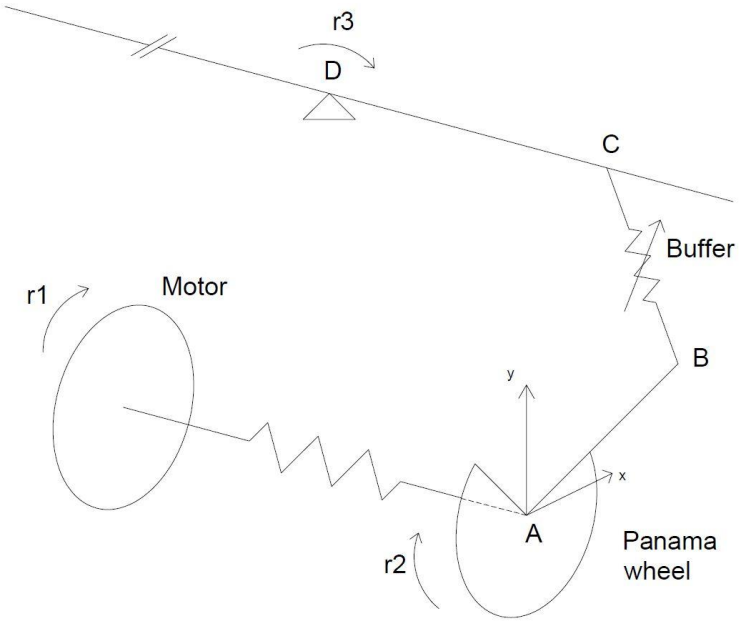

Figure 5.1: Lumped mass model for the system bascule bridge driven by Panama wheel drive

The analysis is performed at the level of the Panama wheel. Hence, all the required quantities of the motor (inertia) and machinery (stiffness, damping) are transferred there using the corresponding transmission factors.

The system under consideration is a highly nonlinear one. Thus, it is preferable to use the Lagrangian formalism for the derivation of the equations of motion. This is an automated technique, easy in use once one succeeds in formulating the kinetic and potential energies of the system.

The Lagrangian equations are given as:

$$\frac{d}{dt}\frac{\partial L}{\partial \dot{q}_s} - \frac{\partial L}{\partial q_s} = Q_s \tag{5.1}$$

where

$L = K - P$: the Lagrange function which is defined as the difference between the kinetic energy and the potential energy of the system under consideration;

K: is the kinetic energy of the system;

P: is the potential energy of the system;

q_s with s = 1,2,3,…: the generalized coordinates of the system (degrees of freedom);

Q_s with s = 1,2,3,…: the generalized forces acting on the system.

5.2.1. Energy of the system

In the first place, the kinetic and potential energies of the system must be written down as functions of the generalized coordinates of the system. Below the kinetic and potential energies of the system are listed.

$$K_{motor} = \frac{1}{2} \cdot J_1 \cdot (\dot{r}_1(t))^2 \tag{5.2}$$

$$K_{panama} = \frac{1}{2} \cdot J_2 \cdot (\dot{r}_2(t))^2 \tag{5.3}$$

$$K_{bridge} = \frac{1}{2} \cdot J_3 \cdot (\dot{r}_3(t))^2 \tag{5.4}$$

$$P_{machinery} = \frac{1}{2} \cdot \widetilde{K}_{12} \cdot (r_2(t) - r_1(t))^2 \tag{5.5}$$

The stiffness of the machinery indicated in formula (5.5) is equal to:

$$\widetilde{K}_{12} = K_1 + C_d \frac{d}{dt} \tag{5.6}$$

This is a fictitious spring stiffness that accounts for the damping of the machinery. The damping coefficient is already defined in Eq.(2.40) in chapter 2.

The potential energy of the buffer is determined taking the integral of the piecewise formula (3.25):

$$P_{buffer} = \int F_{buffer}[s]\, ds \tag{5.7}$$

The potential energy of the buffer is a function of its axial deformation. However, according to the Lagrangian formalism technique, it must be written as a function of the generalized coordinates $r_2(t)$ and $r_3(t)$. To do so, the axial deformation of the buffer is written in terms of the two degrees of freedom $r_2(t)$ and $r_3(t)$, based on the geometry of the system between the bridge and the Panama wheel.

5.2.2. Geometry between the bridge and the Panama wheel

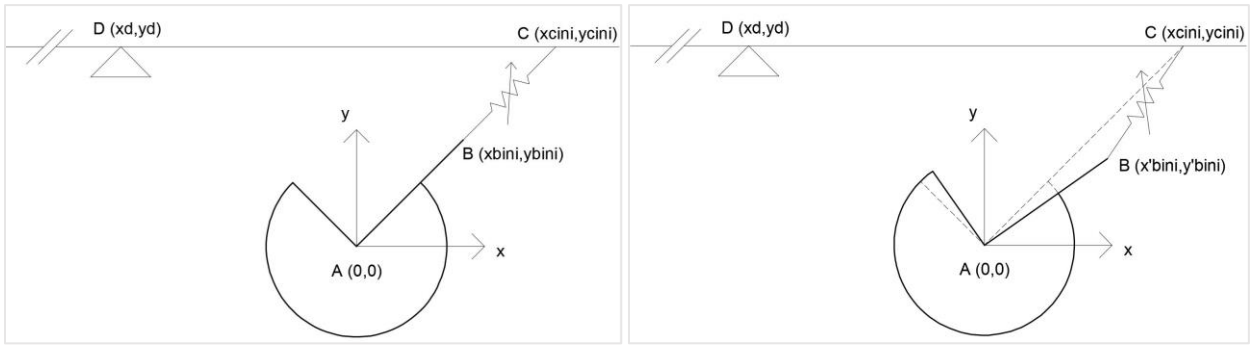

Figure 5.2: Geometry of the system between the bridge and the Panama wheel. Left side: Bridge closed, system out of motion Right side: Bridge closed pre-compression of the buffer removed.

The origin of the coordinate system is decided to be placed at the pivot of the Panama wheel, point A(0,0). Furthermore, three more points are placed in the system:

- Point B, is the interconnection point of the buffer with the crank of the Panama wheel.
- Point C is the interconnection point of the buffer with the bridge.
- Point D is the pivot of the bridge.

Points A and D are constant during motion, whilst points B and C change position.

In Figure 5.2, on the left, the geometry between the bridge and the Panama wheel is illustrated, while the bridge remains closed and the machinery is not in motion. At this position the buffer is compressed to ensure that the bridge remains closed, preventing possible movements as a result of suction caused by wind or flapping due to traffic.

In Figure 5.2, on the right, the geometry is depicted at the time when the pre-compression of the buffer is removed due to the motion of the machinery. At this time the buffer has reached its initial length. From that instant and on, the bridge starts to open. The initial length of the buffer is:

$$l_0 = \sqrt{(x'_{bini} - x_{cini})^2 + (y'_{bini} - y_{cini})^2} \tag{5.8}$$

The coordinates of point B and C are written in respect of the two degrees of freedom in the following equations:

$$x_b(r_2) = AB \cdot \cos(r_2(t)) \tag{5.9}$$

$$y_b(r_2) = AB \cdot \sin(r_2(t)) \tag{5.10}$$

$$x_c(r_3) = DC \cdot \cos(r_3(t)) + x_b \tag{5.11}$$

$$y_c(r_3) = DC \cdot \sin(r_3(t)) + y_b \tag{5.12}$$

Based on these coordinates, the length of the buffer at any time of motion can be determined with the following formula:

$$l(r_2, r_3) = \sqrt{(x_b(r_2(t)) - x_c(r_3(t)))^2 + (y_b(r_2(t)) - y_c(r_3(t)))^2} \tag{5.13}$$

Subtracting the result of formula (5.8) from that of formula (5.13) the axial deformation of the buffer is obtained during motion, in terms of the generalized coordinates r_2 and r_3, which can be seen in formula (5.14).

$$s = l(r_2(t), r_3(t)) - l_0 \tag{5.14}$$

5.2.3. Generalized forces acting on the system

The generalized forces on the system are torques applied at the degrees of freedom.

The torque exerted on the first degree of freedom are generated by the motor. This torque is denoted with the symbol $M_1(t)$. Additionally, since the system is described by a set of statically inditermined equations of motion as mentioned in sub-section 2.4.1. the external generalized forces on the third degree of freedom must be balanced by external generalized forces on the first degree of freedom with the same magnitude but with different sign. The external force is transferred from the level of the bridge to the level of the Panama wheel using the corresponding transmission factor. The transmission factor between the bridge and the Panama wheel changes during motion. Thus, the geometry of the system is recalled to derive a formula for that one.

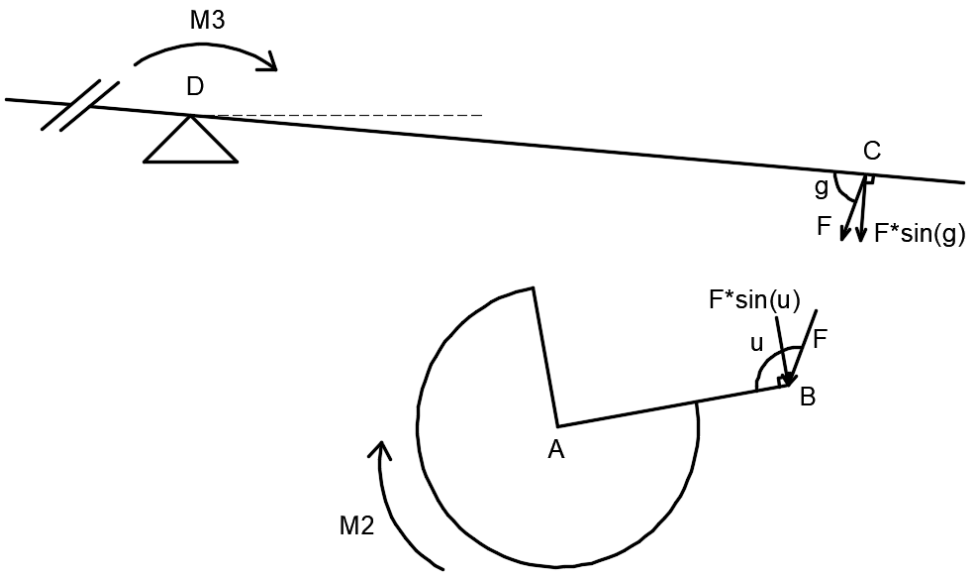

Figure 5.3: Geometry between bridge and Panama wheel at a random instant of motion

In Figure 5.3 the geometry of the system between the Panama wheel and the bridge is represented at a random instant of motion. The force F in Figure 5.3 denoted the force in the buffer. The external torque on the bridge is denoted as M_3 and it is transferred to the Panama wheel following the subsequent process.

Equilibrium around point D yields:

$$M_3 = F \cdot \sin(g) \cdot DC \tag{5.15}$$

Equilibrium around point A gives:

$$M_2 = F \cdot \sin(u) \cdot AB \tag{5.16}$$

By solving equation (5.15) for F and substituting it into (5.16), torque M_3 on the bridge is transferred to the Panama wheel. This results in:

$$M_2 = M_3 \cdot \frac{\sin(u) \cdot AB}{\sin(g) \cdot DC} \tag{5.17}$$

The ratio M_3/M_2 is the transmission factor between the bridge and the Panama wheel, referred as i_{pv} in the formula below.

$$i_{pv} = \frac{sin(g) \cdot DC}{sin(u) \cdot AB} \tag{5.18}$$

In equations (5.15)-(5.18) the two angles u and g change during motion and are calculated based on simple geometric relationships. The quadrilateral formed by the points A, B, C and D is split into individual triangles, where the law of cosines is applied to determine the two angles of interest u and g. This procedure is demonstrated in Figure 5.4.

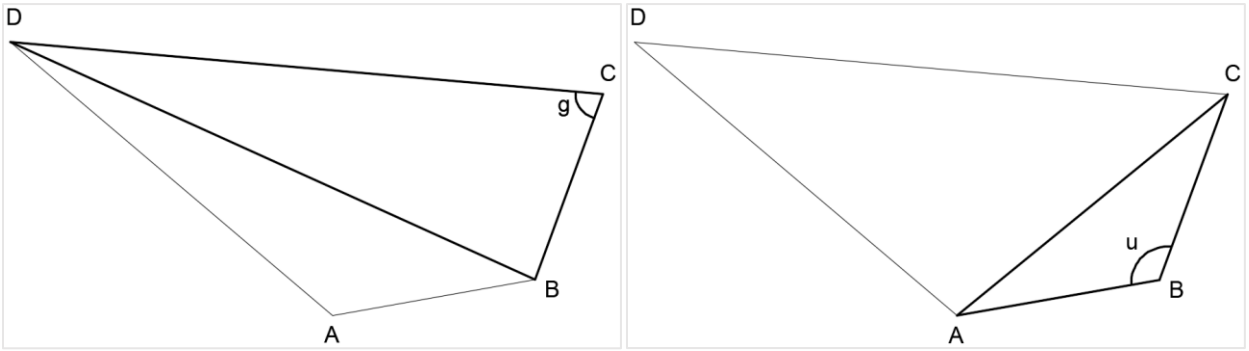

Figure 5.4: Quadrilateral formed during motion

Law of cosines for angle g in the triangle BCD (Figure 5.4 left):

$$g = \cos^{-1}\left(\frac{DC^2 + BC^2 - DB^2}{2 \cdot DC \cdot BC}\right) \tag{5.19}$$

Law of cosines for angle u in the triangle ABC (Figure 5.4 right):

$$u = \cos^{-1}\left(\frac{BC^2 + AB^2 - AC^2}{2 \cdot BC \cdot AB}\right) \tag{5.20}$$

It is reminded that points B and C change during motion, and their coordinates vary with the degrees of freedom $r_2(t)$ and $r_3(t)$. Consequently, the angles g, u and the transmission factor i_{pv} are functions of these two degrees of freedom.

The torques applied on the Panama wheel are only due to friction in the stack of disc springs of the buffer. The formula (3.29) of friction checked in the single degree of freedom model of chapter 4 is now expanded to the case of the Panama wheel. The torque due to friction on the second degree of freedom is indicated in the coming formula (5.21):

$$F_{fr2} = \mu \cdot (n-1) \cdot \left| F_{buffer}[s] \cdot \frac{\partial s}{\partial r_2(t)} \right| \cdot sign(\dot{r}_2(t) - \dot{r}_3(t) \cdot \frac{sin(g) \cdot DC}{sin(u) \cdot AB}) \tag{5.21}$$

In Eq.(5.21) the signum of the velocity difference in both ends of the buffer is used. Since the velocities are calculated in different positions within the structure, they have to be transferred at the same level to determine their actual difference. The mechanical power transmission between the bridge and the Panama wheel yields:

$$M_2 \cdot \dot{r}_2 = M_3 \cdot \dot{r}_3 \tag{5.22}$$

Substituting Eq.(5.17) into Eq.(5.22) results in:

$$\dot{r}_2 \cdot \frac{\sin(u) \cdot AB}{\sin(g) \cdot DC} = \dot{r}_3 \tag{5.23}$$

which can be rewritten:

$$\dot{r}_2 = \dot{r}_3 \cdot \frac{sin(g) \cdot DC}{sin(u) \cdot AB} \tag{5.24}$$

With Eq.(5.24) the velocity of the bridge is transferred to the level of the Panama wheel using the associated transmission factor.

The torques acting on the bridge are originated from wind and also its overweight. It is understood that these loads are dependent on the angle of the bridge (degree of freedom $r_3(t)$). Further attention to the calculation of these loads will be given later on in chapter 6. In the generic equations of motion these torques are combined and indicated with one symbol $M_3(t)$. In addition, a torque due to friction in the stack of disc springs of the buffer is acting on the bridge which is indicated in the coming formula (5.25):

$$F_{fr3} = \mu \cdot (n-1) \cdot \left| F_{buffer}[s] \cdot \frac{\partial s}{\partial r_3(t)} \right| \cdot sign(\dot{r}_3(t) \cdot \frac{sin(g) \cdot DC}{sin(u) \cdot AB} - \dot{r}_2(t)) \tag{5.25}$$

5.2.4. Equations of motion

Until now, all required input of the Lagrangian formalism technique have been established. Before continue with the resulting equations of motion, all prerequisites are summarized first.

- Lagrange function L:

$$L = \frac{1}{2} \cdot J_1 \cdot (\dot{r}_1(t))^2 + \frac{1}{2} \cdot J_2 \cdot (\dot{r}_2(t))^2 + \frac{1}{2} \cdot J_3 \cdot (\dot{r}_3(\mathrm{t}))^2 - \frac{1}{2} \cdot \left(K_1 + C_d \frac{d}{dt}\right) \cdot (r_2(\mathrm{t}) - r_1(t))^2 - \int F_{buffer}[s]\, ds \tag{5.26}$$

- Axial deformation of the buffer as a function of the degrees of freedom:

$$s = \sqrt{(x_b(r_2(t)) - x_c(r_3(t)))^2 + (y_b(r_2(t)) - y_c(r_3(t)))^2} - l_0 \tag{5.27}$$

- Generalized force regarding the degree of freedom $r_1(t)$:

$$Q_1 = -M_3(t) \cdot \frac{\sin(u) \cdot AB}{\sin(g) \cdot DC} + M_1(t) \tag{5.28}$$

- Generalized force regarding the degree of freedom $r_2(t)$:

$$Q_2 = -\mu \cdot (n-1) \cdot \left| F_{buffer}[s] \cdot \frac{\partial s}{\partial r_2(t)} \right| \cdot sign(\dot{r}_2(t) - \dot{r}_3(t) \cdot \frac{sin(g) \cdot DC}{sin(u) \cdot AB}) \tag{5.29}$$

- Generalized force regarding the degree of freedom $r_3(t)$:

$$Q_3 = -\mu \cdot (n-1) \cdot \left| F_{buffer}[s] \cdot \frac{\partial s}{\partial r_3(t)} \right| \cdot sign\left(\dot{r}_3(t) \cdot \frac{sin(g) \cdot DC}{sin(u) \cdot AB} - \dot{r}_2(t) \right) + M_3(t) \tag{5.30}$$

Substituting formulas (5.26) to (5.30) into equation (5.1) and applying the Lagrangian formalism technique, the following equations of motion are obtained:

$$J_1 \cdot \ddot{r}_1(t) + C_d \cdot (\dot{r}_1(t) - \dot{r}_2(t)) + K_1 \cdot (r_1(t) - r_2(t)) = Q_1 \tag{5.31}$$

$$J_2 \cdot \ddot{r}_2(t) + C_d \cdot (\dot{r}_2(t) - \dot{r}_1(t)) + K_1 \cdot (r_2(t) - r_1(t)) + F_{buffer}[s] \cdot \frac{\partial s}{\partial r_2(t)} = Q_2 \tag{5.32}$$

$$J_3 \cdot \ddot{r}_3(t) + F_{buffer}[s] \cdot \frac{\partial s}{\partial r_3(t)} = Q_3 \tag{5.33}$$

6. Application and results

6.1. Introduction

The new set of equations of motion derived in the previous chapter are assessed through application on an existing movable bridge. The bridge examined for this purpose is the movable part of the new Ramspol bridge. All required inputs of the bridge are provided by Rijkswaterstaat. The external wind loads acting on the bridge are calculated according to the rules in the standard NEN 6786:2001 (2001). In the upcoming analyses the torque at the motor shaft is calculated and compared with the corresponding design formulas addressed by the standard NEN 6786:2001 (2001).

6.2. Inputs for the analyses

The new Ramspol bridge (Dutch: nieuwe Ramspolbrug) is estimated to be about 550 meters long, 34 meters wide and on average 13 meters high. It is located on the N50 and links the provinces of Flevoland and Overijssel. The cross section includes 2x2 lanes, a parallel road and a cycle path. The bridge has a movable part which consist of two bascule bridges that work together as one, the West bridge (Dutch: West brug) with a width of 11.2 meters and the East bridge (Dutch: Oost brug) with a width of 22.75 meters. The West bridge is driven by one Panama wheel whilst the East bridge is driven by two. However, the design of both operating mechanisms is identical since the latter is twice in width.

Figure 6.1: Location of Ramspol bridge pinned on the map. (Google Maps, 2018)

Figure 6.2: Side view of Rampsol Bridge, while the bascule bridges are in open position. (Vialis, 2012)

The data of the West bridge are used for the dynamic analysis in this chapter. All required inputs are obtained from technical drawings and technical reports provided by Rijkswaterstaat. The inputs are grouped in three main categories namely, characteristics of the system, geometry between the Panama wheel and the bridge, and properties of the buffer.

The first group of inputs corresponds to the properties of the system regarding inertias, stiffnesses and transmission factors. All this information is collected in Table 6.1.

Table 6.1: Characteristics of the system

Description	Notation	Value	Units
Mass moment of inertia of the motor	J_1	7,385	$kg \cdot m^2$
Mass moment of inertia of the Panama wheel*	J_2	107.052	$kg \cdot m^2$
Mass moment of inertia of the bridge	J_3	45.776.000	$kg \cdot m^2$
Stiffness of the machinery	K_1	7.960.000	$N \cdot m$
Damping ratio	ξ	0,0344	–
Transmission factor of the gearbox	i_{twk}	226,27	–
Transmission factor pinion-Panama wheel	i_{rp}	9,125	–
Transmission factor motor-Panama wheel	$i_{mp} = i_{twk} \cdot i_{rp}$	2064,71	–
Nominal speed of the motor	ω_{nom}	103,2	rad/s

*This value is calculated roughly based on technical drawings

The dimensions and geometry of the bridge required for the analysis are illustrated in Figure 6.3 and Figure 6.4 and collected in Table 6.2 and Table 6.3.

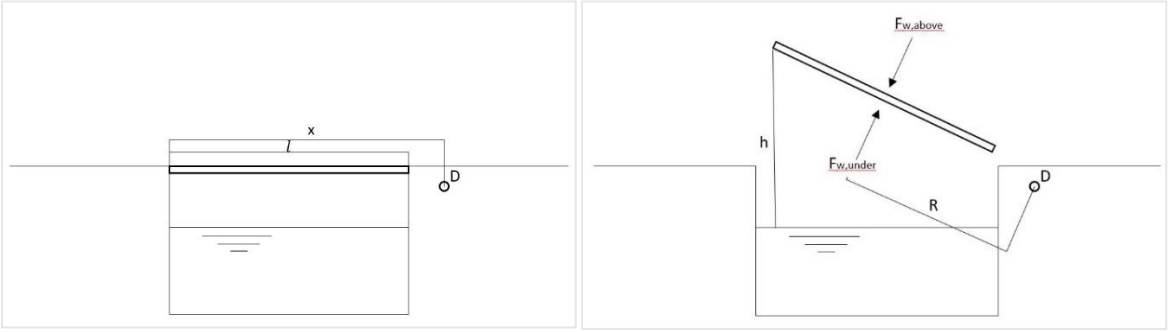

Figure 6.3: Side view impression of bridge configuration. Left: Bridge in closed position. Right: Bridge while open.

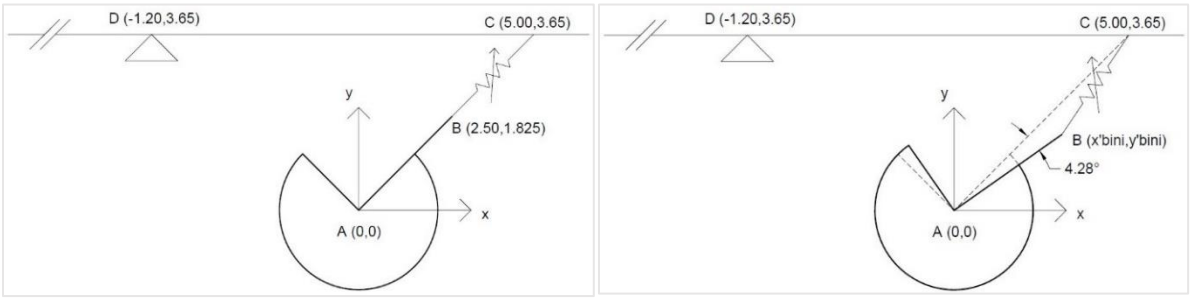

Figure 6.4: Geometry between the pivot of West bridge and the Panama wheel. Left: Initial geometry when the system is out of motion in closed position. Right: Geometry during motion of the system when the buffer has reached its initial length.

Table 6.2: Geometric features of West bridge

Description	Notation	Value	Units
Distance between the tip of the bridge and its pivot (point D)	x	24,675	m
Length of the bridge	l	21,155	m
Width of the bridge	d	11,2	m
Level arm of the external wind load	$R = x - l/2$	14,0975	m
Height of the tip of the bridge with respect to the water level when bridge closed	h_{ini}	15,63	m
Relative rotation of the Panama wheel compared to its initial angle when the buffer has reached its initial length	$r_{st2;ini}$	4,28	degrees

Table 6.3: Coordinates of the four important points between the pivot of the bridge and the Panama wheel when the system is out of motion in closed position

Description	Point	Coordinate X	Coordinate Y	Units
Pivot point of the Panama wheel	A	0	0	m
Connection point of the buffer and the Panama wheel at closed position	B	2,50	1,825	m
Connection point of the buffer and the bridge at closed position	C	5,00	3,65	m
Pivot of the bridge	D	-1,20	3,65	m

Given the angle $r_{st2;ini}$ (Table 6.2), the coordinates of point B when the buffer has its initial length can be determined with formulas (6.1), (6.2). Afterwards, substituting the resulted coordinates in formula (5.8) the initial length of the buffer can be calculated.

$$x'_{bini} = AB \cdot \cos(\tan^{-1}\left(\frac{y_{bini}}{x_{bini}}\right) - r_{st2;ini}) \quad (6.1)$$

$$y'_{bini} = AB \cdot \sin(\tan^{-1}\left(\frac{y_{bini}}{x_{bini}}\right) - r_{st2;ini}) \quad (6.2)$$

The properties of the buffer are collected and mentioned in Table 6.4 and Table 6.5. The buffer of West bridge consists of disc springs with dimensions 250x127x14. The properties of the stack of disc springs required for the analyses are collected and summarized in Table 6.4.

Table 6.4: Properties of the stack of disc springs used in the buffer of West bridge

Description	Notation	Value	Units
Displacement of individual disc spring in flat condition	h_0	0,0056	m
Curve parameter	κ	0,56	$-$
Individual disc spring force in flat condition	F_c	311.000	N
Number of disc springs in parallel	n	3	$-$
Number of disc springs in series	i	14	$-$

Table 6.5: Properties of the West bridge's buffer

Description	Notation	Value	Units
Prestress of the buffer	F_p	311.000	N
Stroke of the buffer	s_{str}	0,0176	m
Factor regarding the linear approximation of the stiff branches*	l_{dsp}	$1 \cdot 10^{-6}$	$-$
Friction of the buffer	μ	$0{,}05 \div 0{,}15$	$-$

*This factor has been selected arbitrary due to its small value

In the aforementioned inputs there are three parameters estimated by the author:

- The mass moment of inertia of the Panama wheel (J_2)
- The factor regarding the linear approximation of the stiff branches (l_{dsp})
- Friction of the buffer (μ)

It can be considered that the factor $l_{dsp} = 1 \cdot 10^{-6}$ is sufficiently small and no further attention concerning its influence in the decisive dynamic loads is required (See Chapter 3). On the contrary the influence of the other two factors (friction of the buffer, inertia of the Panama wheel) is necessary to be assessed in the upcoming analyses.

6.3. External loads and sign conventions

The external loads acting on the system are grouped in sub-section 5.2.3. in two categories:

- Torque generated by the motion of the motor ($M_1(t)$)
- Torque due to wind and overweight of the bridge ($M_3(t)$)

The torque generated by the motion of the motor is describe with the piecewise function of formula (6.3)

$$M_1(t) = \begin{cases} a_{ac} \cdot (J_1 + J_2 + J_3), & 0 \le t \le t_{nom} \\ a_{br} \cdot (J_1 + J_2 + J_3), & t_{br} \le t \le t_{br} + t_{br;dur} \end{cases} \quad (6.3)$$

in which:

a_{ac} is the acceleration of the motor calculated as $a_{ac} = \omega_{nom}/t_{nom}$;

a_{br} is the deceleration of the motor or deceleration of the system due to brake and is calculated as $a_{br} = \omega_{nom}/t_{br}$;

t_{nom} is the time that is needed by the motor to reach its nominal speed;

t_{br} is the time that the motor starts to decelerate or the time the brake is applied;

$t_{br;dur}$ is the duration of the emergency stop.

It must be mentioned that the acceleration and the deceleration of the system can be split into parts. In addition, there is evidence that the torque due to the application of the brake at the motor shaft is not constant during an emergency stop as it is assumed until now in the existing analyses but can be modeled as bilinear. These situations are illustrated in the upcoming chapters (sections (6.6) and (6.7)).

The torque due to the wind and overweight of the bridge is given by:

$$M_3(t) = M_{ov} \cdot \cos\big(r_3(t)\big) + M_{wind}(|r_3(t)|) \quad (6.4)$$

in which:

M_{ov} is the torque due to the overweight of the bridge at closed position and is equal to $318{,}740\ Nm$ for the West bridge;

$M_{wind}(|r_3(t)|)$ is the torque due to wind load acting on the bridge;

$r_3(t)$ is the angle of the bridge. This term is used with absolute value for the calculations of the external torque due to wind, since the wind velocity pressure on the movable bridge is a function of the opening angle which varies in the range (0° ÷ 90°) in the standard NEN 6786:2001 (2001).

The torque due to wind load acting on the bridge is calculated as:

$$M_{wind}(|r_3(t)|) = p_{w;rep}(|r_3(t)|) \cdot l \cdot d \cdot R \tag{6.5}$$

where

$p_{w;rep}(|r_3(t)|)$ is the characteristic value of the wind velocity pressure perpendicular to the affected surface for the bridge and is calculated according to the standard NEN 6786:2001 (2001) and (Antohe, 2016)

$l, d\ and\ R$ are respectively the length of the bridge, the width of the bridge and the level arm of the external wind load with values given in Table 6.2.

The inputs for the calculation of the characteristic wind velocity pressure for the West bridge of Ramspol bridge are summarized in Table 6.6.

Table 6.6: Inputs of Ramspol bridge required for the calculations of wind velocity pressure

Description	Notation	Value	Units
Hourly average wind velocity at 10m above ground level (table 3 NEN 6786:2001 (2001))	U_r	13,7	m/s
Roughness length (table 3 NEN 6786:2001 (2001))	z_0	0,2	m
Height above ground level at which hourly average wind speed U_r is determined	z_{ur}	10	m
Aspect ratio of the bridge (length/width)	l/b	1,88884	$-$
Density of the air	ρ	1,25	kg/m^3
Factor that takes the dimensions of the bridge into account	C_{dim}	0,95	$-$
Dynamic amplification factor for wind	φ_w	1,15	$-$

The height of the tip of the bridge with respect to the water level during motion is given by formula:

$$h(|r_3(t)|) = h_{ini} + x \cdot \sin(|r_3(t)|) \tag{6.6}$$

in which:

h_{ini} is the height of the tip of the bridge with respect to the water level when bridge is closed (Table 6.2)

x is the distance between the tip of the bridge and its pivot, point D (Table 6.2, Figure 6.3)

The sign conventions of the analysis follow those defined by the coordinate system placed at the pinion of the Panama wheel (Figure 6.4) and are the same as illustrated in Figure 2.6. This implies that the accelerations and velocities of the degrees of freedom have negative sign when the bridge opens, while on the other hand deceleration or braking carry a positive sign. The signs of these variables are opposite

when the bridge is closing. In addition to the above, wind load under the bridge has a negative sign (see also Figure 2.8), while wind load above the bridge has a positive sign.

6.4. Stages of the analysis

As mentioned in sub-section 5.2.2., when the bridge is in the closed position the buffer is precompressed. When the system begins its motion, the bridge does not move until the precompression of the buffer is removed. The angle that the Panama wheel has to rotate in order to reach the initial length of the buffer is known beforehand ($r_{st2;ini}$ (Table 6.2)).

Since the bridge does not move until the buffer has reached its initial length the motion of the system can be split into two stages:

Stage 1: Rotation of motor and Panama wheel from initial state until the buffer reaches its initial length. During this stage the bridge does not move. This implies that during this stage the 3rd equation of motion (5.33) does not hold and the 3rd degree of freedom is prescribed zero. The motion of the system is described by the first two equations of motion (5.31), (5.32) with the following initial conditions:

$$r_{1;st1}(0) = \tan^{-1}(\frac{y_{ini}}{x_{ini}}) \ , r_{2;st1}(0) = \tan^{-1}(\frac{y_{ini}}{x_{ini}}) \tag{6.7}$$

$$\dot{r}_{1;st1}(0) = 0 \ , \dot{r}_{2;st1}(0) = 0 \tag{6.8}$$

The initial condition for the angles of the motor and the Panama wheel is the angle that the crank of the Panama wheel (AB line) forms with the horizontal x axis Figure 6.4. The reason behind this is that the equations of motion are linked with the geometry between the Panama wheel and the bridge. The rotation of the Panama wheel is governed by the position of point B in the coordinate system. Therefore, the initial state of (AB line) needs to be input in the equations of motion.

The analysis in this stage stops when the Panama wheel has rotated $4{,}28^{\circ}$ ($r_{st2;ini}$) related to its initial position. The corresponding time (t_{st2}) is calculated solving the following equation in terms of t:

$$r_{2;st1}(t) = \tan^{-1}\left(\frac{y'_{ini}}{x'_{ini}}\right) = r_{st2;ini} \tag{6.9}$$

The response of the system in terms of rotations and rotational velocities of the motor and the Panama wheel at that time (t_{st2}) are used as initial conditions in the next stage of motion.

Stage 2: The motion of the motor and the Panama wheel continues while the bridge starts to move. The motion of the system in this stage is described by the 3 equations of motion (5.31), (5.32), (5.33) and the initial conditions in this stage are:

$$r_{1;st2}(0) = r_{1;st1}(t_{st2}) \, , r_{2;st2}(0) = r_{2;st1}(t_{st2}) \, , r_{3;st2}(0) = 0 \tag{6.10}$$

$$\dot{r}_{1;st2}(0) = \dot{r}_{1;st1}(t_{st2}) \, , \dot{r}_{2;st2}(0) = \dot{r}_{2;st1}(t_{st2}) \, , \dot{r}_{3;st2}(0) = 0 \tag{6.11}$$

The outcome of the two stages of motion described previously are combined using formulas (6.12)-(6.14) to obtain the total response of the dynamic system.

$$r_1(t) = \begin{Bmatrix} r_{1;st1}(t), & 0 \le t \le t_{st2} \\ r_{1;st2}(t - t_{st2}), & t > t_{st2} \end{Bmatrix} \tag{6.12}$$

$$r_2(t) = \begin{Bmatrix} r_{2;st1}(t), & 0 \le t \le t_{st2} \\ r_{2;st2}(t - t_{st2}), & t > t_{st2} \end{Bmatrix} \tag{6.13}$$

$$r_3(t) = \begin{Bmatrix} 0, & 0 \le t \le t_{st2} \\ r_{3;st2}(t - t_{st2}), & t > t_{st2} \end{Bmatrix} \tag{6.14}$$

6.5. Preliminary analysis

A preliminary dynamic analysis for the West bridge is performed using the set of equations of motion (5.31)-(5.33) and the associated inputs (sections 6.2.-6.5) as described previously. The analysis is carried out for opening of the bridge from closed position with external wind load under the bridge. The phases of motion of the system follow those of the motor. Therefore, the phase of motion of the motor for this analysis are summarized in Table 6.7.

Table 6.7: Phases of motor's motion of the preliminary analysis

Description	**Start time (s)**	**End time (s)**	**Duration (s)**	**Acceleration-Deceleration/Brake (rad/s)**
Phase 1: Acceleration of the system from initial state (rest) until it reaches the nominal motor speed	0	12	12	$-103{,}2/12 = -8{,}6$
Phase 2: The system is driven with constant speed, the nominal motor speed	12	72	50	0

The phases of motion, determine the behavior of the external torque $M_1(t)$ (6.3) which is the driving force of the system.

The analysis is performed at the level of the Panama wheel as mentioned in chapter 5. Hence, all inputs regarding the motor (J_1 , $M_1(t)$) and the characteristics of the machinery (K_1 , C_d) are transferred to the level of the Panama wheel using the associated transmission factors.

The results of the analysis in terms of rotations and rotational velocities of the three degrees of freedom are illustrated in Figure 6.5 and Figure 6.6

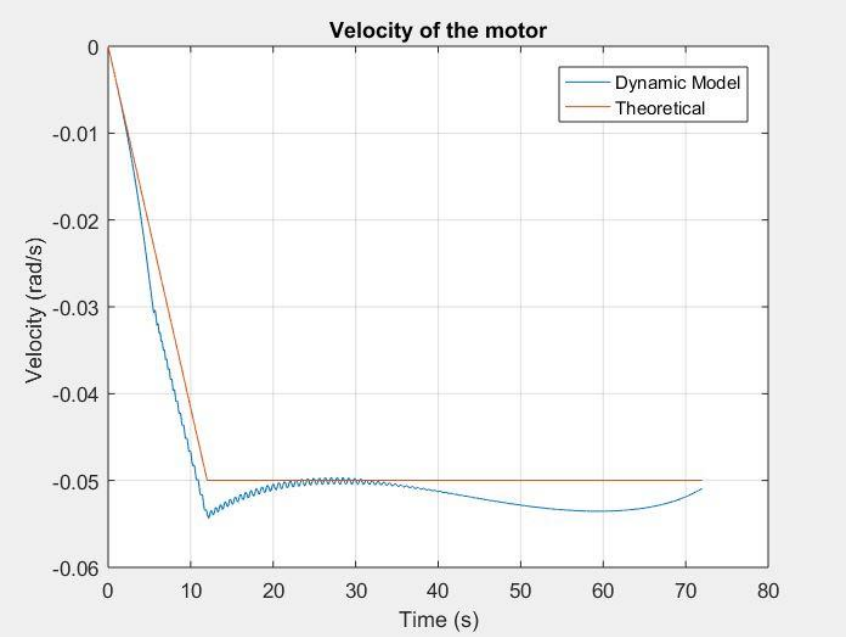

Figure 6.5: Rotational velocity of the motor reduced at the level of the Panama wheel. The blue line represents the velocity as resulted from the analysis with the dynamic model whereas the orange one illustrates the theoretical one as a result of the assumed phases of motor's motion

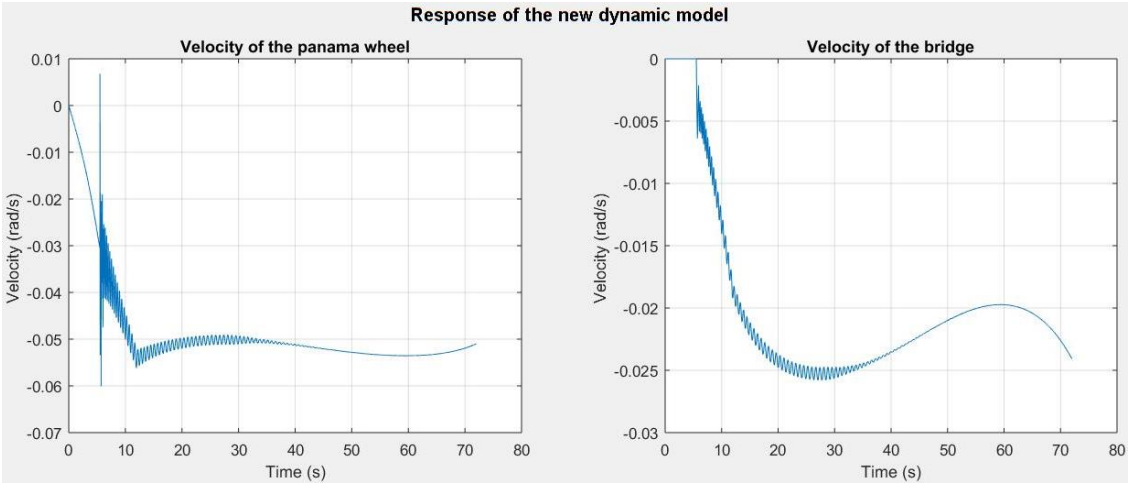

Figure 6.6: Rotational velocity of the Panama wheel (left) and the bridge (right) as resulted from the analysis with the dynamic model

In Figure 6.5 the rotational velocity of the motor resulted from the dynamic analysis is compared with the theoretical one that is expected based on the assumed phases of motion in Table 6.7. The observed

difference is caused due to the influence of nonlinearity in the transmission factor between the bridge and the Panama wheel.

In reality the velocity of the motor is either linearly proportional to the time or constant during the phases of motion. This is achieved by introducing error detection amplifiers in the system. This device compares the input signal of the motor with the feedback of the motor shaft and the error in these two signals is eliminated by a speed controller which speeds up or slows down the motor.

The exact behavior of the motor can be achieved by removing the degree of freedom of it and applying a boundary at that position with prescribed rotational velocity equal to the programed (theoretical) one of the motor. This change in the system does not influence its response in terms of the maximum torques at the motor shaft as it is depicted in sub-section 2.4.1. The updated version of the dynamic model of the bridge-machinery system is mentioned in the upcoming section with the associated results of the dynamic analyses of it.

6.6. Updated dynamic model of the bridge-machinery system

The updated version of the dynamic model of the bridge-machinery system is illustrated in Figure 6.7.

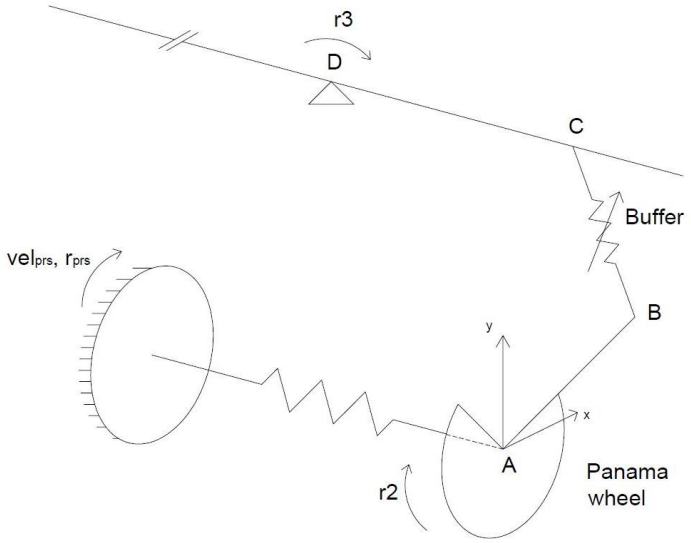

Figure 6.7: Updated dynamic model of the bridge – machinery system

The degree of freedom of the motor is removed and a boundary is attached to the left end of the torsional spring. At this boundary a prescribed velocity is applied which is calculated according to the formula:

$$vel_{prs}(t) = \int a(t)\, dt \tag{6.15}$$

where

$a(t)$ is the acceleration/deceleration of the motor defined by the different phases of motion.

Moreover, the rotation of the boundary can be simply calculated integrating the prescribed velocity (6.15) adding its initial position at $t = 0$ (6.7):

$$r_{prs}(t) = \int vel_{prs}(t)\, dt + \tan^{-1}(\frac{y_{ini}}{x_{ini}}) \tag{6.16}$$

Furthermore, the updated set of equations of motion becomes:

$$J_2 \cdot \ddot{r}_2(t) + C_d \cdot \left(\dot{r}_2(t) - vel_{prs}(t)\right) + K_1 \cdot \left(r_2(t) - r_{prs}(t)\right) + F_{buffer}[s] \cdot \frac{\partial s}{\partial r_2(t)} = Q_2 \tag{6.17}$$

$$J_3 \cdot \ddot{r}_3(t) + F_{buffer}[s] \cdot \frac{\partial s}{\partial r_3(t)} = Q_3 \tag{6.18}$$

with

$$Q_2 = -\mu \cdot (n-1) \cdot \left| F_{buffer}[s] \cdot \frac{\partial s}{\partial r_2(t)} \right| \cdot sign(\dot{r}_2(t) - \dot{r}_3(t) \cdot \frac{sin(g) \cdot DC}{sin(u) \cdot AB}) \tag{6.19}$$

$$Q_3 = -\mu \cdot (n-1) \cdot \left| F_{buffer}[s] \cdot \frac{\partial s}{\partial r_3(t)} \right| \cdot sign\left(\dot{r}_3(t) \cdot \frac{sin(g) \cdot DC}{sin(u) \cdot AB} - \dot{r}_2(t)\right) + M_3(t) \tag{6.20}$$

The updated set of equations of motion is used to perform a dynamic analysis for a complete opening cycle of the bridge. The wind load is assumed acting under the bridge during the whole cycle. The phases of motor's motion are presented in Table 6.8.

Table 6.8: Phases motor's motion in a complete opening cycle of West bridge

Description	**Start time (s)**	**End time (s)**	**Duration (s)**	**Acceleration-Deceleration/Brake (rad/s)**
Phase 1: Acceleration of the system from initial state (rest) until it reaches 30% of the nominal motor speed	0	3,6	3,6	$-(103{,}2 \cdot 0{,}3)/3{,}6 = -8{,}6$
Phase 2: The system is driven with constant creep speed, 30% of the nominal motor speed	3,6	8,6	5	0
Phase 3: Acceleration of the system until it reaches the nominal speed	8,6	17	8,4	-8,6
Phase 4: The system is driven with constant speed, the nominal motor speed	17	73	56	0

Phase 5: Deceleration of the system from the nominal motor speed until it reaches 10% of it	73	83,8	10,8	8,6
Phase 5: The system is driven with constant creep speed, 10% of the nominal motor speed	83,8	88,8	5	0
Phase 6: Deceleration of the system until it stops	88.8	90	1,2	8,6

The aforementioned phases of motor's motion during the complete opening cycle of the bridge are illustrated graphically in Figure 6.8.

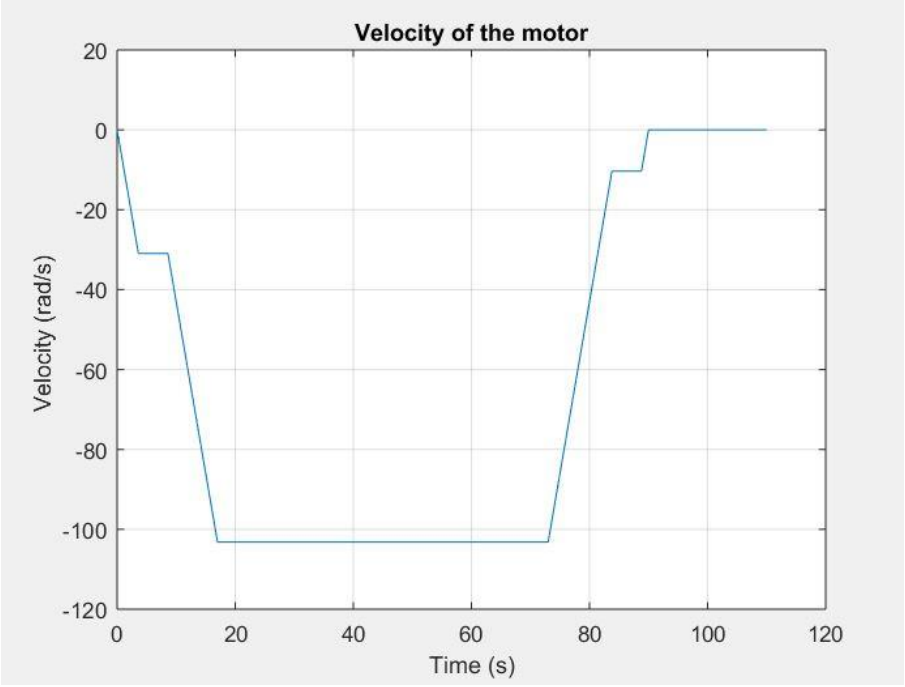

Figure 6.8: Velocity of the motor versus time during the complete opening cycle of the West bridge

The input velocity of the motor shown in Figure 6.8 is reduced at the level of the Panama wheel using the associated transmission factor (i_{mp}) from Table 6.1 and the associated rotation of the boundary is calculated using Eq.(6.16). The resulting prescribed velocity and rotation of the boundary of the updated dynamic model are illustrated in Figure 6.9.

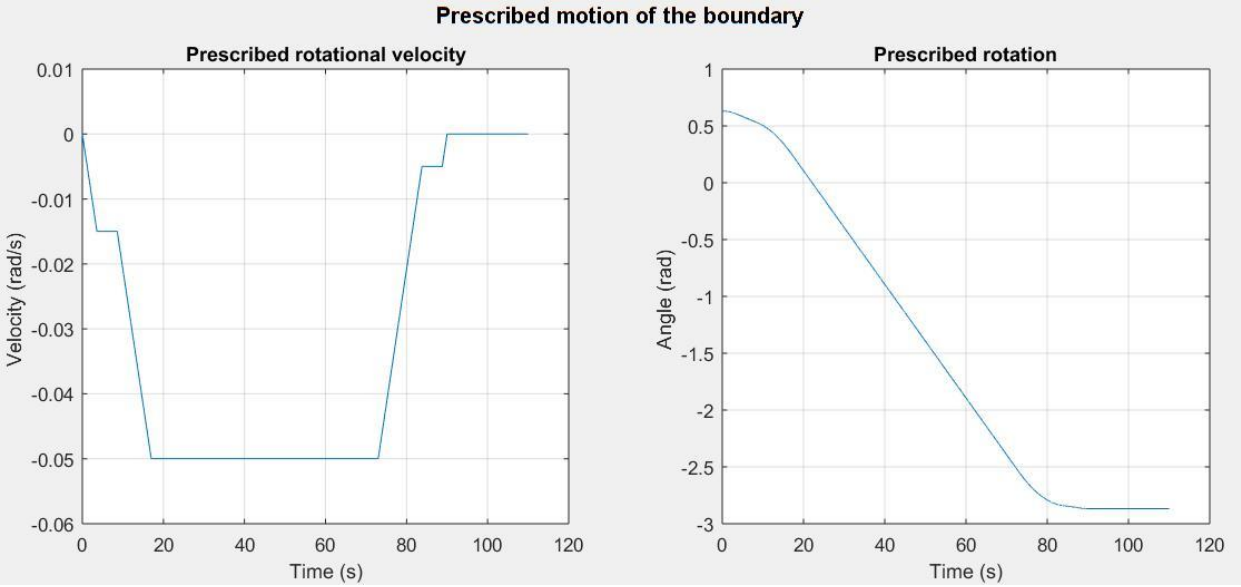

Figure 6.9: Prescribed motion of the boundary of the updated dynamic model during the complete opening cycle of the West bridge

The response of the system in terms of rotations and rotational velocities of the Panama wheel and the bridge are illustrated in Figure 6.10. More specifically the rotation of the Panama wheel is plotted in Figure 6.10 as absolute rotation from its initial condition using the equation:

$$r_{2;abs}(t) = r_2(t) - r_2(0) \tag{6.21}$$

in which:

$r_2(t)$ is the calculated rotation of the Panama wheel resulted from the dynamic analysis;

$r_2(0)$ is the initial condition of the Panama wheel as defined in the dynamic analysis (Eq.(6.7)).

In addition, the transmission between the bridge and the Panama wheel (Eq.(5.18)) and the resulted torque at the motor shaft during the complete opening cycle of the bridge are plotted in Figure 6.11 and Figure 6.13. The latter is calculated using the equation:

$$T(t) = \frac{K_1 \cdot \left(r_{prs}(t) - r_2(t)\right) + C_1 \cdot \left(vel_{prs}(t) - \dot{r}_2(t)\right)}{i_{mp}} \tag{6.22}$$

Using the proposed updated dynamic model, the analysis is performed at the level of the Panama wheel and the torque of interest is at the level of the motor shaft. Therefore, the transmission factor between the motor and the Panama wheel is used in formula (6.22).

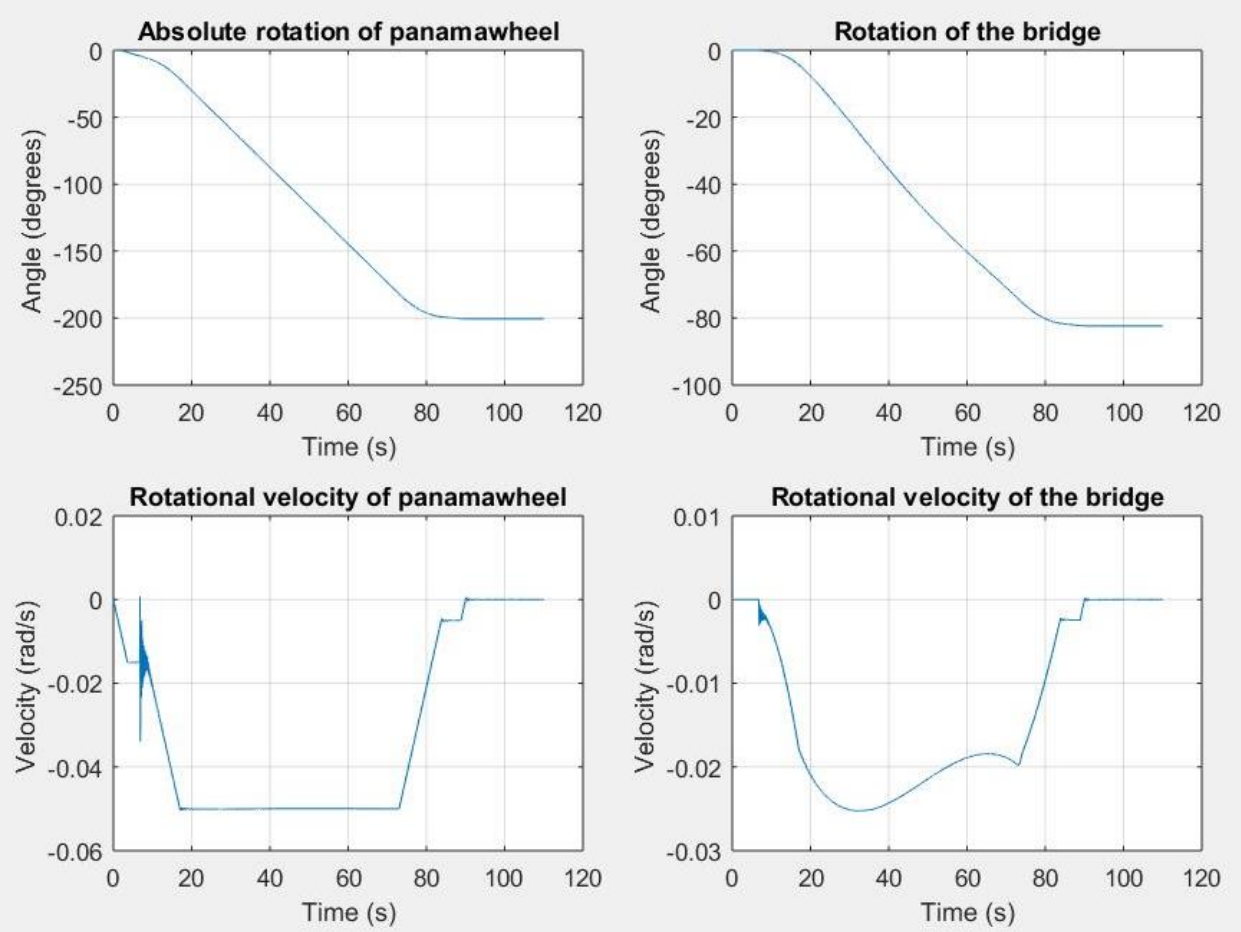

Figure 6.10: Results of the dynamic analysis of a complete opening cycle of the West bridge using the updated dynamic model

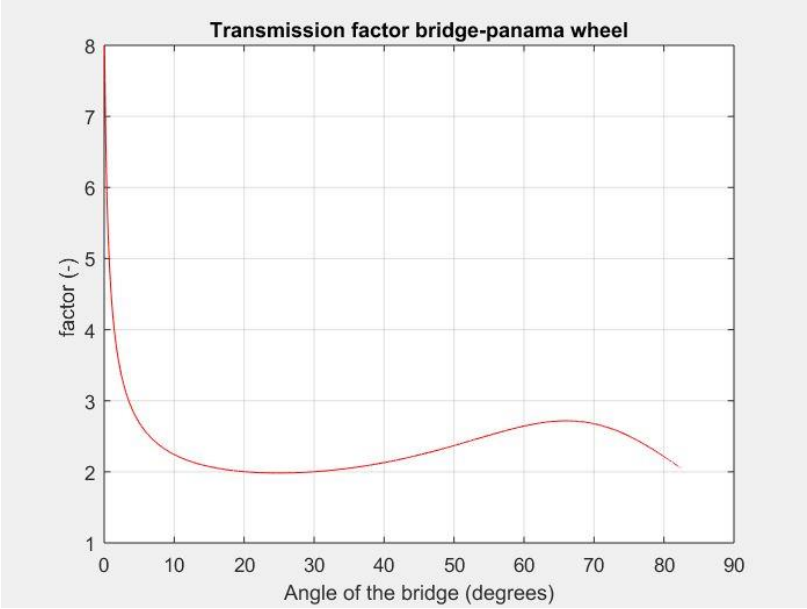

Figure 6.11: Transmission factor between the West bridge and the Panama wheel as a function of the angled of the bridge

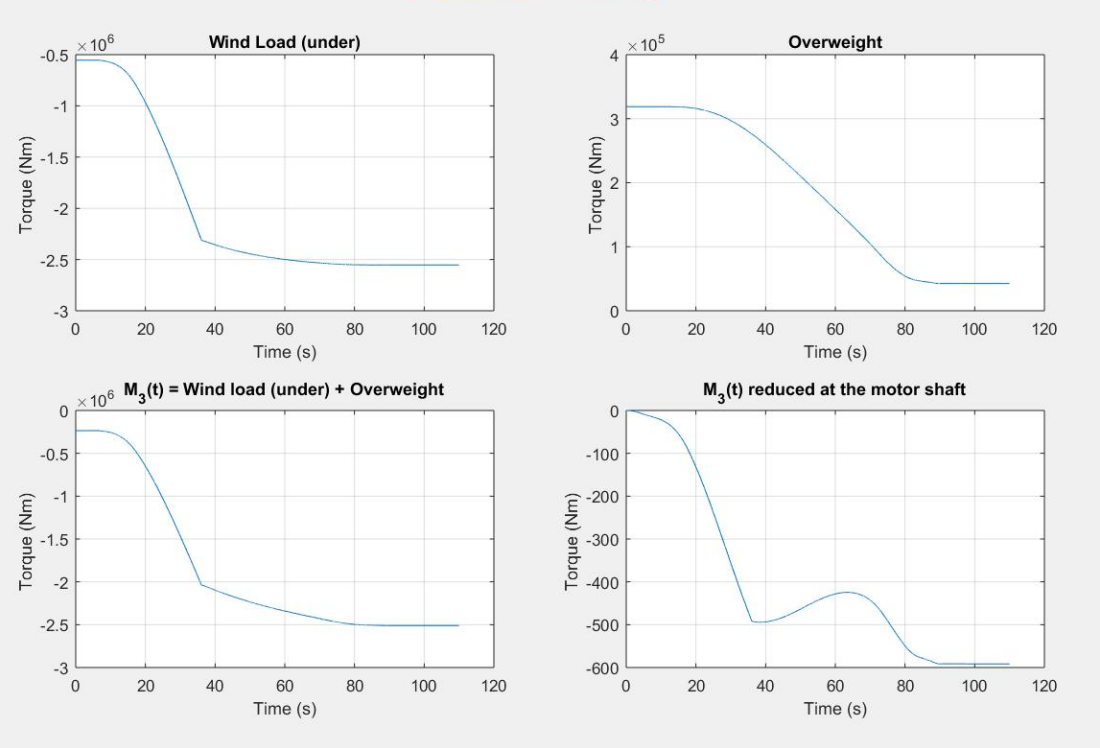

Figure 6.12: External loads on the bridge

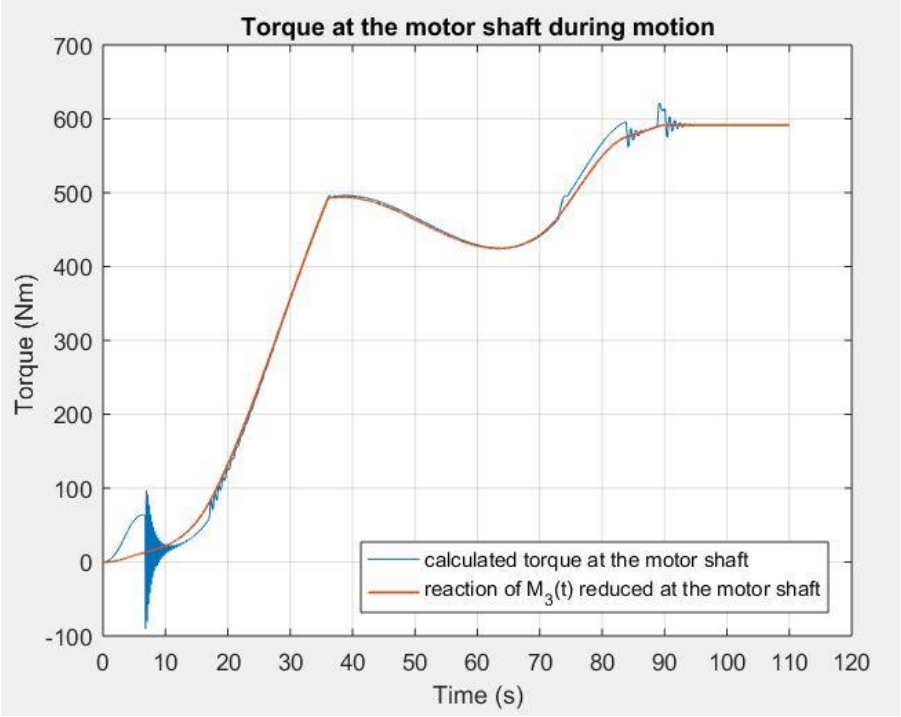

Figure 6.13: Resulting torque at the motor shaft during a complete opening cycle of the West bridge with wind under using the updated dynamic model (blue) and reaction of the total external load on the bridge reduced at the motor shaft (red)

In Figure 6.10 is shown that through the use of the updated dynamic model, the system has the expected behavior in terms of velocity versus time according to the defined phases of motion (Table 6.8). Therefore, using this model in the following chapter, in the dynamic analyses of the West bridge, is justified.

6.7. Results and comparison with existing standard

The content of this section is a series of dynamic analyses carried out based on the updated dynamic model mentioned before. The purpose of this implementation is to calculate the maximum torque at the motor shaft during an emergency stop and compare it with the torque calculated according to the tabulated formulas of the existing standard NEN 6786:2001 (2001).

The loading case of these analyses is braking at full speed with wind load under the bridge without changing direction. The parameters of the upcoming analyses are:

- The friction coefficient of the buffer (μ)
- The time the brake is applied (t_{br})
- The duration of the emergency stop ($t_{br;dur}$)

A step by step description of the process is drawn next. First the magnitude of the friction coefficient is specified. The magnitude of the friction coefficient ranges between 0,05 ÷ 0,15. Afterwards, the time of the brake application is chosen. The system moves with full speed between 17s ÷ 73s. It is decided to perform emergency stops at 30, 40, 50 and 60 seconds. Subsequently, given these two prerequisites and varying the duration of the emergency stop a series of dynamic analyses are performed and the torque at the motor shaft is calculated. The phases of motor's motion in the upcoming analyses are summarized in Table 6.9.

Table 6.9: Phases of motor's motion in an emergency stop at full speed of the system during opening of the bridge

Description	**Start time (s)**	**End time (s)**	**Duration (s)**	**Acceleration-Deceleration/Brake (rad/s)**
Phase 1: Acceleration of the system from initial state (rest) until it reaches 30% of the nominal motor speed	0	3,6	3,6	$-(103{,}2 \cdot 0{,}3)/3{,}6 = -8{,}6$
Phase 2: The system is driven with constant creep speed, 30% of the nominal motor speed	3,6	8,6	5	0
Phase 3: Acceleration of the system until it reaches its the nominal motor speed	8,6	17	8,4	-8,6
Phase 4: The system is driven with constant speed, the nominal motor speed	17	t_{br}	$t_{br} - 17$	0
Phase 5: Emergency stop	t_{br}	$t_{br} + t_{br;dur}$	$t_{br;dur}$	$103{,}2/\ t_{br;dur}$

The next stage is the calculation of the torque at the motor shaft using Eq.(6.22). The maximum torque at the motor shaft stemming from the dynamic analyses is plotted in Figure 6.14. This figure depicts this maximum torque for the extreme values of the friction coefficient (0,05, 0,15) for different braking times varying the duration of the emergency stop.

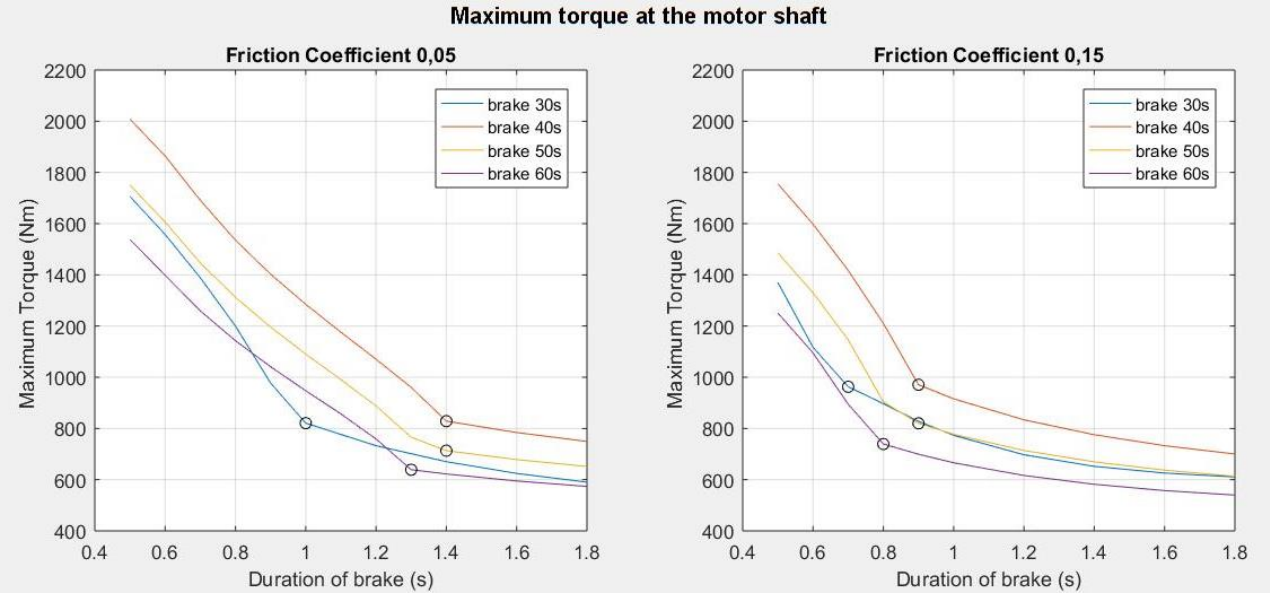

Figure 6.14: Maximum torque at the motor shaft as a function of the duration of the brake for different times of emergency stop. Left: Results for the lower limit of the assumed friction coefficient. Right: Results for the upper limit of the assumed friction coefficient

According to Figure 6.14 the worst-case scenario regarding the maximum torque generated at the motor shaft during an emergency stop is when the brake is applied at 40 seconds. In terms of rotational velocity of the system, the worst-case scenario is when performing emergency stop at full speed. The system rotates at full speed from 17s to 73s. At that timespan one can observe the generated torque at the motor shaft reaching an apex at approximately 37s (see Figure 6.13). It is concluded that, the worst-case scenario regarding the maximum torque generated at the motor shaft during an emergency stop is referring to an emergency stop at full speed of the system beginning at the time that maximum torque is applied at the motor shaft.

Therefore, a series of dynamic analyses is performed applying the brake at the time that maximum torque is applied at the motor shaft during full speed of the system. As can be seen in Figure 6.13 this is the apex reached at time 37s approximately. The resulting maximum torque during the emergency stop is plotted in Figure 6.15 versus the duration of the brake (Figure 6.15 (left)) and versus the braking deceleration (Figure 6.15 (right)) for different values of the friction coefficient of the buffer.

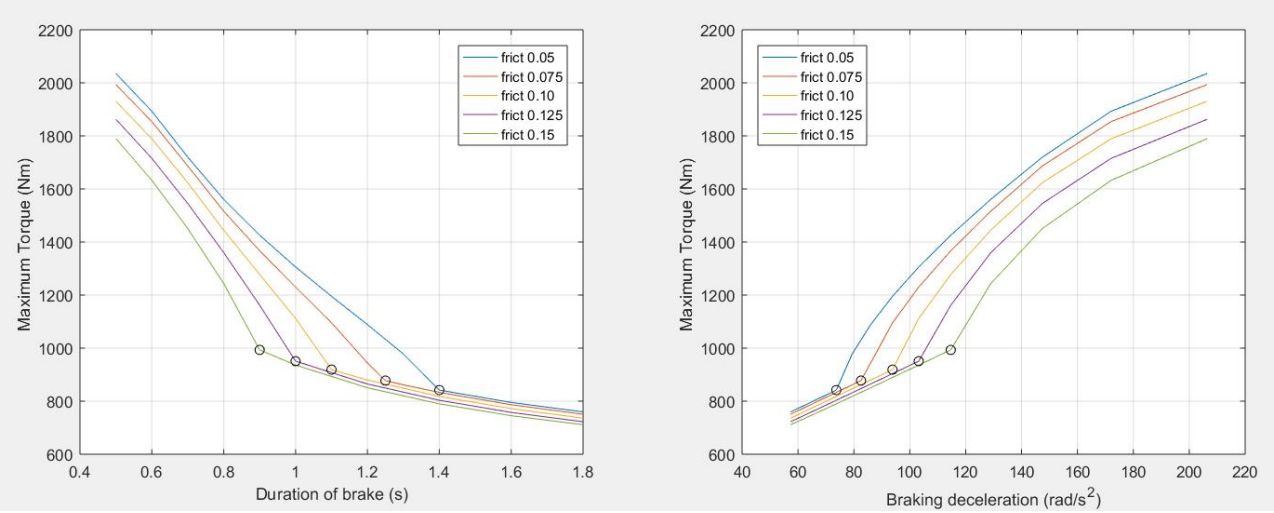

Figure 6.15: Maximum torque at the motor shaft during emergency stop at the 37th sec of motion. The marked points indicate the values where a change in the buffer's state during an emergency stop is observed. Left: Maximum torque against the duration of brake. Right: Maximum torque in contrast with the braking deceleration.

Examining the graphs of Figure 6.14 and Figure 6.15 (left) the relationship of the maximum torque at the motor shaft in relevance with the duration of braking can be observed. As can be seen in these graphs, the lower the duration of the brake, the higher the maximum torque at the motor shaft due to the application of the brake. In general, this behavior is anticipated since the time needed for a system to stop moving is reverse proportional to the required load and the braking deceleration of the system, individually. Specifically for the latter, this can be observed in Figure 6.15 (right).

In addition, the friction of the buffer component influences the response of the system. As the friction coefficient of the buffer increases, the resulting maximum torque at the motor shaft reduces. With the increase of the friction coefficient, more energy is converted to other forms (e.g. heat) resulting in less energy being transferred to the motor shaft during an emergency stop.

To explore in more detail the plotted results of Figure 6.14 and Figure 6.15, the change of the maximum torque with the increase of the duration of the brake (or the braking deceleration) is not constant. However, an abrupt change of it is observed at specific values (marked points in the graphs of Figure 6.14 and Figure 6.15). Given this observation, the state of the buffer corresponding to the resulting maximum torque is monitored. As a result, the state of the buffer changes at the marked points. For durations of brake lower than the ones associated with the marked points, the buffer is fully compressed, whereas for larger durations the buffer is not fully compressed. The opposite holds for the right graph of Figure 6.15. Overall, the stiffer the behavior of the buffer (buffer fully compressed), the larger the change of the maximum torque with the change of the variable of the horizontal axis, as can be seen in both instances of Figure 6.15.

The maximum torque resulted from the dynamic analyses (Figure 6.15) is compared with the formulas of the standard NEN 6786:2001 (2001) (Eq.(2.1) and Eq.(2.3)). For the situations where the buffer is not fully

compressed the percentage deviation (percentage reduction) of the dynamic analysis' outcome as opposed to the result of Eq. (2.1) is calculated (Figure 6.16). On the contrary, when the buffer is fully compressed the validity of the factor 0,4 in the second term of formula (2.3) is examined. This is achieved by substituting the factor 0,4 of formula (2.3) with an unknown variable z and solving the following equation in terms of this variable:

$$T_{max} = M_{s;d} + z \cdot 0{,}9 \cdot \gamma_0 \cdot \sqrt{\omega^2 \cdot \mathrm{K}_1 \cdot J_2} \tag{6.23}$$

in which:

T_{max} is the maximum torque at the motor shaft as resulted from the dynamic analyses.

The results of Eq. (6.23) are plotted in a contour diagram in terms of the duration of the brake and the friction coefficient of the buffer (Figure 6.17)

To use Eq. (2.1) and Eq. (2.3), the external load ($M_{s;d}$) and the transmission factor between the bridge and the Panama wheel (5.18) at the time of the maximum torque are necessary to be determined. Since these two quantities are functions of time, the time associated to the maximum torque at the motor shaft is also estimated.

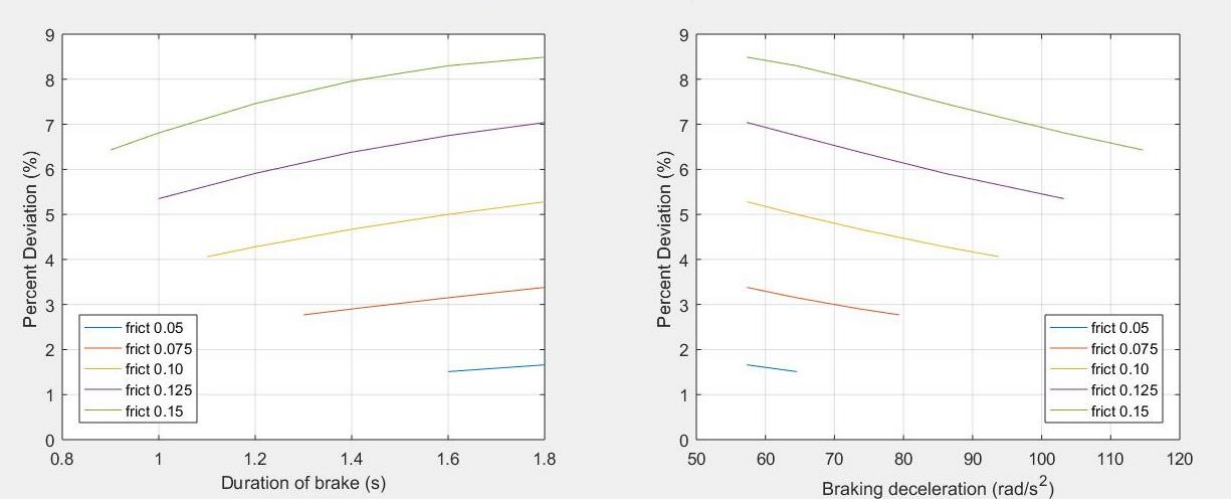

Figure 6.16: Percentage deviation (reduction) of the maximum torque resulted from the dynamic analyses compared with Eq. (2.3) of the standard NEN 6786:2001 (2001) for the case where the buffer is not fully compressed during an emergency stop

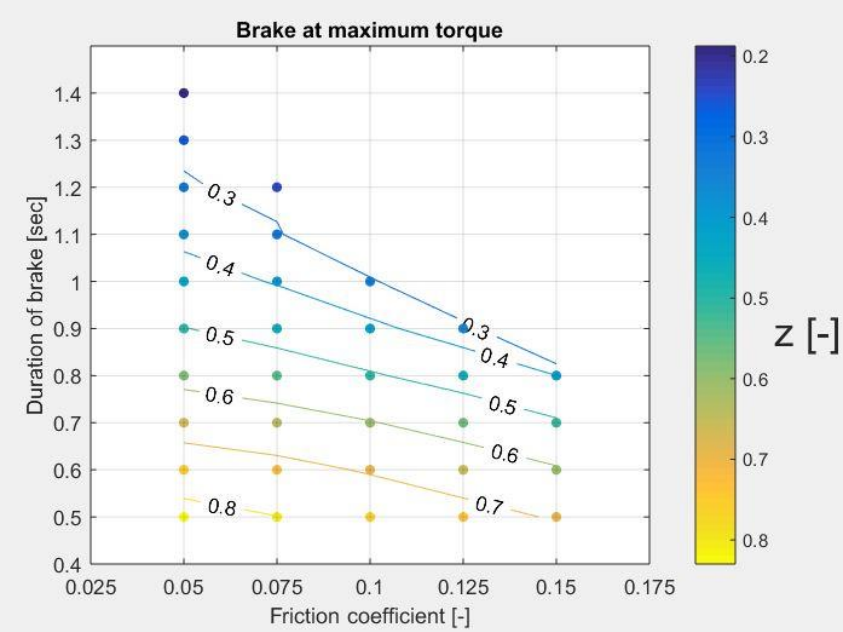

Figure 6.17: Contour plot for the value of the factor 0,4 of Eq.(2.3) so as to calculate the same maximum torque at the motor shaft in case the buffer is fully compressed during an emergency stop as the torque resulted from the dynamic analyses

In reference to Figure 6.16, the maximum torque resulting from the dynamic analysis is lower than that calculated with Eq.(2.1). In particular, for higher values of the buffer's friction coefficient, the percentile deviation of the maximum torque, as a result of the dynamic model, is increased when compared to the value taken from the standard Eq.(2.1).

In Figure 6.17, the dependence of z factor on the duration of the brake and the friction coefficient is illustrated. Consequently, the maximum torque at the motor shaft for the case of fully compressed buffer depends on those parameters, as well. None of those influence factors is taken into account yet in Eq. (2.3) of the standard NEN 6786:2001 (2001).

To sum up, the updated dynamic model is used to perform dynamic analyses for the West bridge, while the calculations aim to determine the maximum torque generated at the motor shaft during an emergency stop. The influence of the friction coefficient of the buffer and its state (fully compressed or not) on the maximum torque is already depicted.

Furthermore, as mentioned in section 6.3 there are evidences that the torque at the motor side due to the application of the brake can be modeled bilinear instead of constant modeling during the whole duration of the emergency stop. When the system is subjected to an emergency stop, a brake is applied at the motor shaft. Two brake shoes come in contact with the motor shaft and generating a torque against its motion due to friction, the braking of the system is accomplished. It is reasonable to assume that the braking torque is not maximum from the time the brake shoes come in contact with the shaft but it takes some time to reach its maximum value.

In the updated dynamic model, the degree of freedom of the motor is removed and the motion of the system is achieved via prescribed motion of the boundary. The braking of the system is modeled as

deceleration of the boundary (Table 6.9). It is decided to model the constant deceleration in Table 6.9 as an associated bilinear one, respecting the two following conditions:

- The maximum of the bilinear deceleration is equal to the constant one (Figure 6.18)
- The change in velocity in both cases remains the same Eq.(6.25)

The aforementioned conditions are illustrated in Figure 6.18 and the associated mathematic relationships are given in Eq.(6.24), Eq.(6.25)

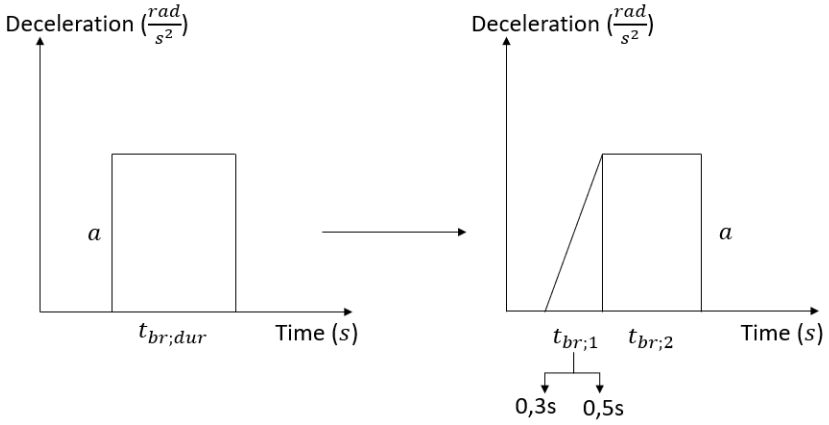

Figure 6.18: Graphic representation of the constant deceleration due to braking (left) and the associated bilinear one (right)

$$a = \frac{103{,}2}{t_{br;dur}} \tag{6.24}$$

$$a \cdot t_{br;dur} = \frac{1}{2} \cdot a \cdot t_{br;1} + a \cdot t_{br;2} \tag{6.25}$$

in which:

$t_{br;dur}$ is the duration of the constant brake;

$t_{br;1}$ is the duration of the linear increasing part in the bilinear case and is assumed to be either 0,3 or 0,5 seconds. The first case is referred as **bilinear1** and the second one is referred as **bilinear2** respectively;

$t_{br;2}$ is the duration of the constant part in the bilinear case and is calculated based on Eq.(6.25)

The total duration of the bilinear case is the summation $t_{br;1} + t_{br;2}$

The bilinear brake is examined for emergency stop when the torque reaches its peak value during full speed of the system. Based on the aforementioned conditions the outcome of the dynamic analyses for the bilinear brake can be compared with the one resulted from the constant one (Figure 6.15) and the associated torques calculated with the formulas of the design standard. The phases of motion of the bilinear case are described in Table 6.10. An impression of the bilinear brake and the resulting rotational velocity of the boundary at that stage is shown in Figure 6.19. The results of the analyses and the

comparison with the constant brake and the standard are shown in Figure 6.20 and Figure 6.21. In these figures the results are plotted in terms of the maximum braking deceleration, since it is the shared component between these two braking models (Figure 6.18).

Table 6.10: Phases of motor's motion for bilinear braking of the system at full speed while the bridge is opening

Description	**Start time (s)**	**End time (s)**	**Duration (s)**	**Acceleration-Deceleration/Brake (rad/s)**
Phase 1: Acceleration of the system from initial state (rest) until it reaches 30% of the nominal motor speed	0	3,6	3,6	$-(103{,}2 \cdot 0{,}3)/3{,}6 = -8{,}6$
Phase 2: The system is driven with constant creep speed, 30% of the nominal motor speed	3,6	8,6	5	0
Phase 3: Acceleration of the system until it reaches its the nominal motor speed	8,6	17	8,4	-8,6
Phase 4: The system is driven with constant speed, the nominal motor speed	17	t_{br}	$t_{br} - 17$	0
Phase 5: Emergency stop: Linear deceleration until it reaches its maximum value	t_{br}	$t_{br} + t_{br;1}$	$t_{br;1}$	$\frac{103{,}2 \cdot (t - t_{br})}{t_{br;dur} \cdot t_{br;1}}$
Phase 6: Emergency stop: Constant maximum deceleration until the systems stops	$t_{br} + t_{br;1}$	$t_{br} + t_{br;1} + t_{br;2}$	$t_{br;2}$	$\frac{103{,}2}{t_{br;dur}}$

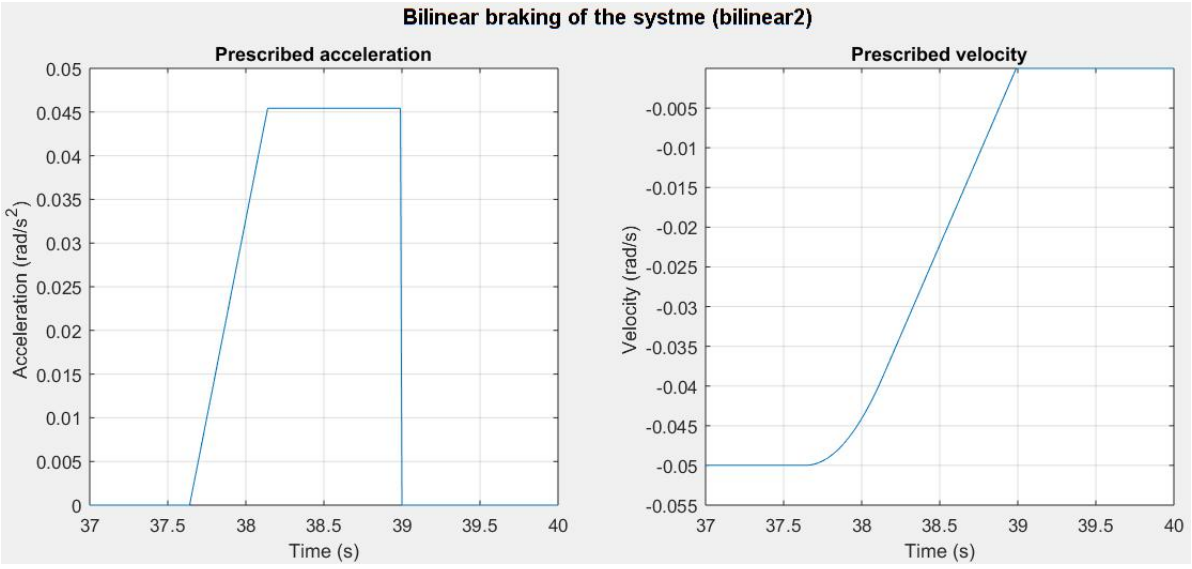

Figure 6.19: Impression of the bilinear braking of the system (left) and the resulting prescribed rotational velocity of the boundary at that phase of motion

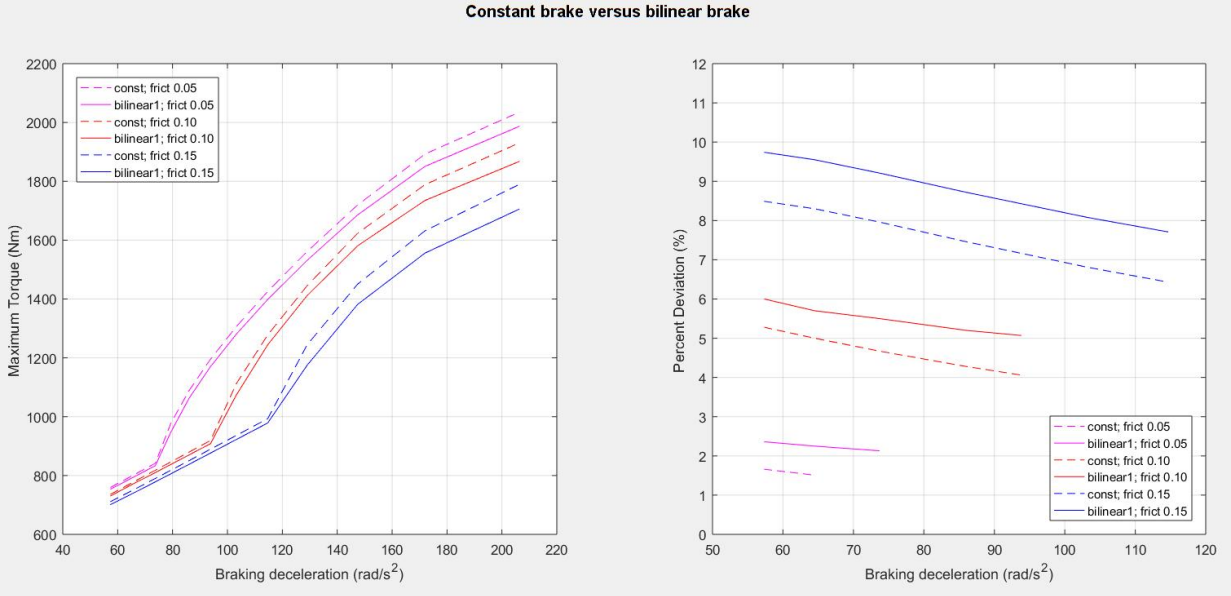

Figure 6.20: Comparison of the maximum torque at the motor shaft calculated with constant and bilinear brake in the dynamic model. In the latter the brake increases linearly for 0,3s. Left: Comparison of the maximum torque calculated with constant brake (dashed line) with the one calculated with bilinear brake (continuous line). Right: Percentage deviation (reduction) of the torque calculated with constant brake (dashed line) or bilinear brake (continuous line) with the formula (2.1) of the standard NEN 6786:2001 (2001) for the case where the buffer is not fully compressed during an emergency stop

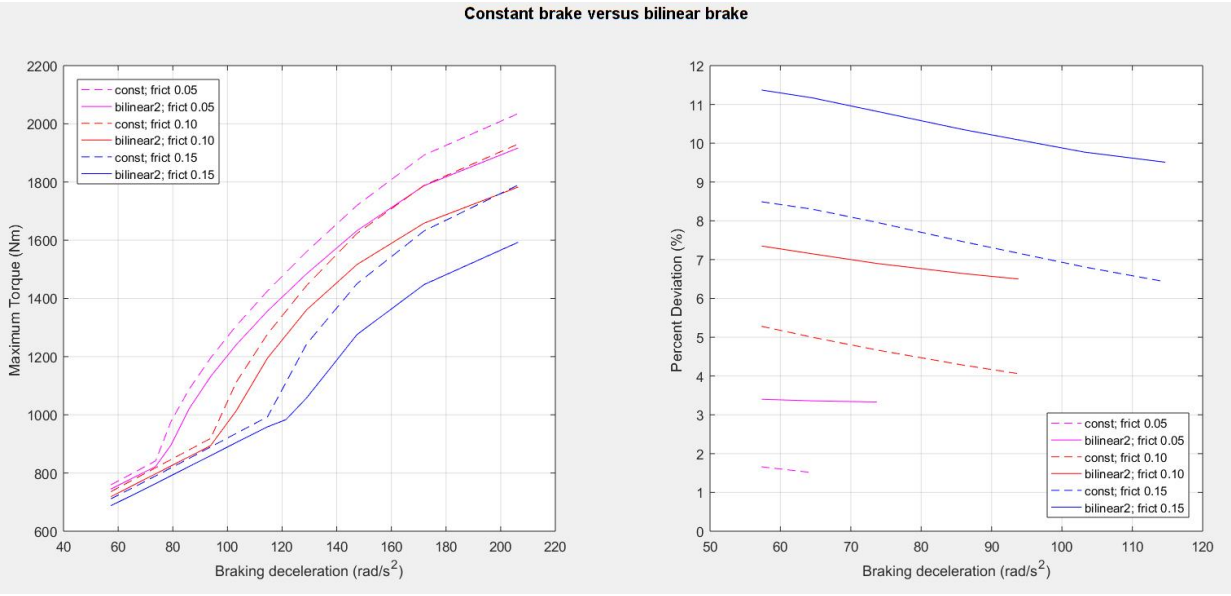

Figure 6.21: Comparison of the maximum torque at the motor shaft calculated with constant and bilinear brake in the dynamic model. In the latter the brake increases linearly for 0,5s. Left: Comparison of the maximum torque calculated with constant brake (dashed line) with the one calculated with bilinear brake (continuous line). Right: Percentage deviation (reduction) of the torque calculated with constant brake (dashed line) or bilinear brake (continuous line) with the formula (2.1) of the standard NEN 6786:2001 (2001) for the case where the buffer is not fully compressed during an emergency stop

Figure 6.20 and Figure 6.21 illustrate that the bilinear braking of the system results in lower maximum torque at the motor shaft than the constant braking. More specifically, the larger the duration of the linear part of the brake, the larger the reduction of the maximum torque is. The resulting maximum torque at the motor shaft from the dynamic analysis with the bilinear braking can be 3 - 11% lower than the one calculated with Eq.(2.1) of the standard NEN 6786:2001 (2001) (case buffer not fully compressed). Moreover, once the buffer becomes fully compressed during braking of the system (on the right-hand side of the kink in the plots of Figure 6.20 and Figure 6.21) the analysis with the bilinear braking illustrates considerable reduction of the maximum torque compared to the resulting one with constant brake.

Last but not least, it is desired to examine the sensitivity of the results with respect to the magnitude of the inertia of the Panama wheel. As it is mentioned in section 6.1 the mass moment of inertia of the Panama wheel is calculated roughly based on technical drawings regarding the drive mechanism of the West bridge. Therefore, a set of dynamic analyses is performed with magnitude of the Panama wheel's inertia half of the calculated value and 1,5 times bigger. The results of the study are summarized in Table 6.11.

Table 6.11:Results of the study of the maximum torque resulting from the dynamic analyses with respect to the magnitude of the Panama wheel's inertia for emergency stop at 40s with friction coefficient of the buffer 0,1

Constant braking of the system for emergency stop at 40s; Friction coefficient of the buffer 0,10			
Duration of brake (s)	$0{,}5 \cdot J_2$	J_2	$1{,}5 \cdot J_2$
	Max. Torque (Nm)	Max. Torque (Nm)	Max. Torque (Nm)
1,6s	757,694	758,8	759,932
1,4s	802,024	803,283	804,54
1,2s	861,216	862,679	864,138
1,0s	1082,88	1084,57	1086,25
0,75s	1497,58	1498,87	1500,14

According to the results summarized in Table 6.11, it is clearly depicted that the results of the dynamic analyses are not sensitive to the magnitude of the inertia of the Panama wheel.

To conclude, the results of the aforementioned dynamic analyses show the influence of the buffer component in the maximum torque generated at the motor shaft during an emergency stop. The worst-case scenario arises when an emergency stop begins at the time that maximum torque is applied at the motor shaft during full speed of the system. As can be seen in Figure 6.13 this is the apex reached at time 37s approximately. The magnitude of the maximum torque during an emergency stop depends on three factors namely: the duration of braking, the friction coefficient of the buffer and the modeling of braking (constant or bilinear). The resulting maximum torque is in inverse proportion to the duration of the brake and/or the friction coefficient of the buffer. The bilinear brake results in lower maximum torques compared to the constant brake.

7. Conclusions and recommendations

This chapter contains the outcome of the research introduced in the previous chapters regarding the effect of the push-pull rod on the dynamic behavior of movable bridges. Firstly, the main conclusions deduced through this research are presented, as were outlined in the research objectives. Following this, recommendations for further research in the field of dynamics of movable bridges are given.

7.1. Conclusions

To start with, the push-pull rod is a component of the machinery that should not be neglected when analyzing the dynamic model of the movable bridge-machinery system. As a result of the dynamic analyses of the system with a set of equation of motion where the buffer is taken into account, the calculated maximum torque generated at the motor shaft during an emergency stop shows remarkable difference when compared with the torque calculated with the formulas of the existing standard NEN 6786:2001 (2001).

The state of the buffer during an emergency stop is crucial with regards to the maximum torque generated at the motor shaft. The buffer can be either fully compressed or not during an emergency stop depending on the load acting on it. Specifically, the buffer is fully compressed when the load acting on it exceeds the load corresponding to its stroke. The two cases regarding the state of the buffer during an emergency stop are distinguished by the kink observed in Figure 6.14 and Figure 6.15. The steep branches correspond to the case the buffer is fully compressed, while the gradual branches refer to the situation where the buffer is not fully compressed.

Given the case where the buffer is not fully compressed during an emergency stop, the maximum potential torque generated at the motor shaft, as derived from the aforementioned dynamic analyses, is 1,5-8% lower than the torque calculated employing the current standard's formulas (Eq.(2.1) NEN 6786:2001 (2001)) (see Figure 6.16). The exact reduction in terms of percentage depends on the friction of the buffer and the duration of the emergency stop.

On the other hand, in the case where the buffer is fully compressed during an emergency stop, a considerable deviation is observed between the maximum torque resulting from the dynamic analyses and the torque calculated with Eq.(2.3) of the standard NEN 6786:2001 (2001). The latter is only dependent on the time the brake is applied and not on the duration of the emergency stop. Contrary to this, the maximum torque obtained from the dynamic analyses has been shown to be dependent on the duration of the braking, resulting thus, in either lower or significantly higher values. However, this formula can be used adequately for the West bridge, by removing the factor 0,4 from its second term and substituting it with a value that can be read from the contour plot in Figure 6.17. This contour plot has been acquired performing a series of dynamic analyses and the factor required to be substituted in Eq.(2.3) is given as a function of the duration of the brake and the friction coefficient of the buffer. Taking the case where an emergency stop lasts more than 0,9 seconds and the friction coefficient of the buffer

is larger than 0,1 the design formula of the standard NEN 6786:2001 (2001) is satisfactory and on the safe side.

In general, the maximum torque resulting from the dynamic analyses is affected by the duration of the brake and the friction coefficient of the buffer. The magnitude of the maximum torque is inversely proportional to those influence factors.

In addition, the modeling of the braking deceleration can influence the maximum torque generated at the motor shaft during an emergency stop. Employing bilinear braking deceleration during an emergency stop, the resulting maximum torques at the motor shaft can be noticeably lower compared to the one derived from the dynamic analysis with constant braking deceleration. The rate of reduction depends on the assumed time required for the braking deceleration to reach its maximum value.

Ultimately, there is no need to take into account the intermediate inertias of the machinery components when applying this dynamic model, since their order of magnitude is negligible when compared to the inertia of the motor and the bridge (see 2.4.2).

7.2. Recommendations

Besides the improvements of the existing dynamic model for the movable bridge-machinery system by incorporating the push-pull rod in the equations of motion, further recommendations are given for future research.

First, it is advised to examine the magnitude of the friction arising from the disc springs in the buffer. This can be accomplished by performing cyclic loading tests in a short scale laboratory model of the buffer and measuring its force deformation behavior. The friction coefficient of the buffer can be derived from the magnitude of the hysteresis in its force-deformation graph.

Another recommendation is to research the time needed for the bridge to stop once the emergency stop procedure has begun. The duration of the emergency stop is of importance as it has an impact on the maximum torque at the motor shaft.

Attention needs be paid also to the modeling of braking, examining in a more detailed manner the bilinear case.

In addition, the dynamic model of the system can be enhanced manifold. Considering the buffer component, it is advised to take into account the possible clearance in the buffer. It might be the case that some disc springs in the buffer have been damaged due to wear. This situation results in the presence of clearance within the buffer component. This in turn, can influence the response of the system in terms of the torque generated at the motor shaft.

Moreover, the bridge can be modeled as a continuous system in the equations of motion. It can be of interest the stress and strain state of the bridge structure during motion of the system. In this case the

existing modeling is not accurate and it is required to model it as a 1D continuous system using Euler-Bernoulli theory or more advanced ones like Rayleigh or Timoshenko theory.

Furthermore, the effect of other system components on its dynamic response could be studied. For instance, the effect of the gearboxes can be analyzed by introducing them into the equations of motion rather than assessing their contribution simply as constant transmission factors.

Accordingly, remodeling of the motor side is strongly suggested. Currently the motor side is modeled by a single rotating degree of freedom and is not attached to a boundary. The result of this is a statically indetermined model as depicted in chapter 2. The research can be focused in the components of the motor side that are not taken yet into account as part of the dynamic model.

In either case, a revision of the existing standard NEN 6786:2001 (2001) is required. This is mainly due to the fact that the design formulas of the standard with regards to the machinery are currently based on a simplified model. Consequently, the design formulas are either conservative, as depicted for the Eq.(2.1), or a rough approximation as shown for the Eq.(2.3) and thus require reformatting.

8. Bibliography

Antohe, D. (2016). Analysis of the influencing factors of dynamic loads acting on the operating systems of beam balanced bascule bridges.

Brennan, M. J., Mace, B. R., & Kovacic, I. (2010). Potential benefits of a non-linear stiffness in an energy harvesting device. *Nonlinear Dynamics, 59*(4), 545-558.

Brolsma, J. U., & Roelse, K. (2011). *Waterway guidelines 2011*. Retrieved from WorldCat.org database. Rijkswaterstaat, DVS.

Budd, C., & Dux, F. (1994). Chattering and Related Behaviour in Impact Oscillators. *Philosophical Transactions: Physical Sciences and Engineering, 347*(1683), 365-389.

Christian Bauer (3). (2006). *The product of load and deflection*. Retrieved from Welzheim, Germany:

Christian Bauer (4). (2006). *Spring characteristics and values for CB disc springs*. Retrieved from Welzheim, Germany:

Coelman, B. H. (1992). *Beweegbare verkeersbruggen*. Voorburg: Ministerie van Verkeer en Waterstaat, Bouwdienst Rijkswaterstaat.

Deutsches Institut für Normung. (2006). Disc Springs – Calculation DIN 2092:2006-03. Berlin, Germany: Author.

Google Maps. (2018). *Ramspolbrug N50.* Retrieved from https://www.google.com/maps/place/Ramspolbrug/@52.5928219,5.6812705,11.34z/data=!4m5!3m4!1s0x47c87eeffee27095:0xd38396df125ceda8!8m2!3d52.6131114!4d5.8413976

Koglin, T. L. (2003). *Movable bridge engineering*. Hoboken :: Wiley.

Nederlands Normalisatie Instituut. (2001). Voorschriften voor het ontwerpen van beweegbare bruggen (VOBB) NEN 6786:2001. Delft, The Netherlands: Author.

Schnorr. (1997). *Disc Springs handy for use*. Retrieved from Sindelfingen:

Van Zantvliet, P. (2015). Analysis of force distribution on operating mechanisms in a bascule bridge.

Vialis. (2012). Ramspolbrug. Retrieved from https://www.vialis.nl/nl/referenties/projecten/detail/ramspolbrug

Wagg, D. J., & Bishop, S. R. (2001). Chatter, Sticking and Chaotic Impacting Motion in a Two-Degree of Freedom Impact Oscillator. *International Journal of Bifurcation and Chaos [in Applied Sciences and Engineering], 11*(1), 57-71.

Wisconsin Department of Transportation. (2017). *Structure Inspection Manual*. Retrieved from Wisconsin: http://wisconsindot.gov/Pages/doing-bus/eng-consultants/cnslt-rsrces/strct/inspection-manual.aspx#p3